WEAK ORGANIC ACID MODIFIED GRANULAR ACTIVATED CARBON AND CERIA NANOMATERIAL EMBEDDED GRAPHENE OXIDE FOR DRINKING WATER FLUORIDE REMOVAL

A Dissertation
Submitted to the Graduate Faculty
of the
North Dakota State University
of Agriculture and Applied Science

By

Umma Salma Rashid

In Partial Fulfillment of the Requirements
for the Degree of
DOCTOR OF PHILOSOPHY

Major Department:
Civil and Environmental Engineering

April 2021

Fargo, North Dakota

North Dakota State University
Graduate School

Title

WEAK ORGANIC ACID MODIFIED GRANULAR ACTIVATED CARBON AND CERIA NANOMATERIAL EMBEDDED GRAPHENE OXIDE FOR DRINKING WATER FLUORIDE REMOVAL

By

Umma Salma Rashid

The Supervisory Committee certifies that this ***disquisition*** complies with North Dakota State University's regulations and meets the accepted standards for the degree of

DOCTOR OF PHILOSOPHY

SUPERVISORY COMMITTEE:

Dr. Achintya Bezbaruah
Chair

Dr. G. Padmanabhan

Dr. Kelly Rusch

Dr. Senay Simsek

Dr. Xuefeng Chu

Approved:

April 13, 2021
Date

Dr. David R. Steward
Department Chair

ABSTRACT

Excess fluoride (F^-) in drinking water leads to detrimental health effects including dental and skeletal fluorosis. More than 260 million people worldwide are affected by excess fluoride (>1.5 mg/L) in their drinking water. In this three-phase study, we have used modified activated carbon and cerium oxide nanomaterials for aqueous fluoride removal. The overarching goal of this research was to develop cost-effective drinking water fluoride removal technologies.

In Phase I, a citric acid (0.3 M) modified granular activated carbon (CAGAC) was effectively used to remove >70% of aqueous fluoride within 60 min. The maximum adsorption capacity of CAGAC was two times (1.65 mg/g) that of unmodified GAC (0.88 mg/g). To address the need for defluoridation technologies adaptable in rural and socio-economically challenged communities, commonly available lime (*Citrus aurantiifolia*) juice was used in lieu of citric acid in Phase II of this research. The lime modified GAC (LGAC) showed an adsorption capacity of 1.63 mg/g. Both CAGAC and LGAC worked effectively over a wide range of pH (4-8) even though the point-of-zero-charge (PZC) was 4.89 for CAGAC and 3.05 for LGAC indicating that the fluoride removal was not controlled by electrostatic interaction alone, both surface adsorption and intra-particle diffusion also took part.

In Phase III, graphene oxide-ceria (GO-CeO_2) nanohybrid was used for fluoride removal as the activated carbon-based systems were slow in kinetics. The nanohybrid exhibited ultra-rapid kinetics for fluoride removal. The equilibrium (85% removal of 10 mg F^-/L) was achieved within 1 minute which is the fastest kinetics for fluoride removal reported so far. The maximum fluoride adsorption capacity of GO-CeO_2 nanohybrid was 8.61 mg/g at pH 6.5 and that increased to 16.05 mg/g at pH 4. The experimental results and characterization data indicated that both electrostatic interaction and surface complexation participated in the fluoride removal process. The oxygen ions

present in CeO_2 lattice were replaced by fluoride ions to make a stable CeF_3 complex. During fluoride removal, the GO sheets acted as electron mediators and helped to reduce Ce^{4+} to Ce^{3+} at the CeO_2 NPs-GO interface, and the additional Ce^{3+} enhanced fluoride removal by the nanohybrid.

ACKNOWLEDGEMENTS

First, I would like to thank the Divine Grace for always being there for me.

I would like to express my sincere gratitude and appreciation to my advisor, Dr. Achintya Bezbaruah, for his continuous support and guidance during my study at NDSU. The completion of my dissertation would not have been possible without his valuable advice, encouragement, and continuous support. Dr. Bezbaruah enriched my thinking process as a researcher and always guided me in the right direction with his immense wisdom and knowledge. His guidance and advice will benefit my future career track and help me to reach my goals. I also want to thank all my dissertation committee members, Dr. G. Padmanabhan, Dr. Kelly Rusch, Dr. Senay Simsek, and Dr. Xuefeng Chu for generously offering their valuable time, suggestion, and guidance during my graduate study. I would like to thank Dr. Sudipta Seal and Dr. Tamil Sakthivel from the University of Central Florida for their continuous support and guidance throughout my study.

I would also like to thank all the members of Nanoenvirology Research Group and Environmental Engineering Lab.

My tenure at NDSU was supported by a grant from the National Science Foundation (NSF Grant# CBET- 1707093, PI: Bezbaruah and fellowship grants from North Dakota Water Resources Research Institute, Department of Civil and Environmental Engineering, College of Engineering, North Dakota State University (Grand Challenges Initiative).

Finally, I would like to thank my parents, my in-laws, my husband, my son, my sibling, my friends, and all other family members for their unconditional support and love.

DEDICATION

To Abba and Amma

TABLE OF CONTENTS

LIST OF TABLES

LIST OF FIGURES

LIST OF APPENDIX TABLES

LIST OF APPENDIX FIGURES

CHAPTER 1: INTRODUCTION AND LITERATURE REVIEW

1.1. Background

Human intake of fluoride within the permissible limit is beneficial for health because it helps to prevent tooth decay and strengthen bones (Chouhan and Flora, 2010). When fluoride enters the human body, it gets absorbed by the blood and quickly distributed throughout the body. A small part of the ingested fluoride is later excreted through urine (Barbier et al., 2010). The major portion of the fluoride is accumulated in calcium-rich areas such as teeth and bones as fluoride is more attracted to calcium phosphate present in bones and teeth (Barbier et al., 2010). Tooth enamel is primarily composed of hydroxyapatite crystals. The microorganisms present on the tooth (enamel) use sucrose to produce lactate. These lactate ions demineralize hydroxyapatite and cause tooth decay (Dey and Giri., 2015). When people drink fluoridated water within the permissible limit, most of the ingested fluoride ions get adsorbed into the apatite crystal by replacing the OH^- ions and form fluorapatite. Fluorapatite is more stable than hydroxyapatite, and lactate ions cannot demineralize it easily. The formation of fluorapatite prevents dental decay (Dey and Giri., 2015). Because of these positive health effects, fluoride is added to the piped drinking water supplied by municipalities across the USA (CDC, 2016). Fluoride treatment of teeth in children is also practiced to protect teeth from dental caries (Horst et al., 2018). However, prolonged exposure to high fluoride concentration can lead to dental and skeletal fluorosis (Gbadebo, 2012), depending on the level of ingested fluoride (Table 1.1).

Table 1.1. Effect of fluoride level on human health (Mohapatra et al., 2009).

Fluoride Concentration (mg/L)	Health Outcome
<0.5	Dental caries
0.5-1.5	Optimum dental health
1.5-4.0	Dental fluorosis
4.0-10.0	Dental and skeleton fluorosis
>10.0	Crippling fluorosis

1.1.1. Health impacts of fluoride

1.1.1.1. Dental fluorosis

Dental fluorosis mainly affects children and is characterized by the yellowing of teeth and pitting and mottling of the enamel (Singh et al., 2016). Dental fluorosis can be mild and severe. Chalky white teeth indicate the mild form of fluorosis, whereas the severe condition is characterized by yellowish-brown pigmentation in the middle of the teeth and severe indentation (Singh et al., 2016). The mild form of dental fluorosis may not be noticeable if the teeth are fully grown before fluoride overexposure. Therefore, if an adult does not show any dental fluorosis symptoms, that does not certainly indicate that his or her fluoride intake is within the permissible limit (Jagtap et al., 2012).

1.1.1.2. Skeletal fluorosis

Excessive consumption of fluoride may cause skeletal fluorosis, and it affects both children and adults. In skeletal fluorosis, fluoride gets accumulated in the joints of the neck, knee, pelvic, shoulder bones and their movement becomes difficult (Harrison, 2005). Skeletal fluorosis diagnosis is difficult at the early stage as it is typically confused with arthritic pains. Early symptoms manifest unpredictable pain, burning sensation, back stiffness, muscle weakness, tingling and prickling in the limbs, chronic fatigue, abnormal metallic element deposits in bones and ligaments (Meenakshi and Maheshwari, 2006). In the second stage of fluorosis, bones become

stiffer, leading to “poker back”, a situation where the whole spine becomes a fixed single column of bone. In this stage, the spine movement becomes restricted and noticeable. In the third stage, skeletal bone deformities, muscle wasting, calcification of ligaments, and neurological deficits are significant problems (Yadav et al., 2019). The advanced stage of skeletal fluorosis is osteoporosis (Jagtap et al., 2012). At this stage, the bone becomes very fragile and may break from a minor fall. A person with skeletal fluorosis loses the ability to move and eventually loses the ability to work. which leads to wage losses (Indu et al., 2007). The problem is more severe in the socio-economically challenged community as the medical cost is not affordable and the wage losses lead to financial hardship.

1.1.1.3. Other effects

The advanced stage of skeleton fluorosis may lead to rare bone cancer, osteosarcoma, and damages to the spine, major joints, muscles, and nervous system. Chronic intake of fluoride may also cause muscle fiber degeneration, low hemoglobin level, excessive thirst, skin rashes, depression, abdominal pain, nausea, reduced immunity, gastrointestinal problem, growth retardation, and DNA structural changes (Meenakshi and Maheshwari, 2006; Gbadebo, 2012). It may also cause damages to the kidney, liver, and brain (Jagtap et al., 2012).

1.1.2. World scenario of fluoride occurrence in water

The World Health Organization (WHO) recommends a threshold of 1.5 mg F^-/L in drinking water, beyond which fluoride can have detrimental effects (WHO, 2004). The US EPA has established a maximum contaminant level (MCL) of 4 mg/L to prevent skeletal fluorosis and a secondary maximum contaminant level (SMCL) of 2 mg/L to protect against dental fluorosis.

The fluoride contamination of groundwater has affected many parts of the world. Around 27 developed and developing nations in the world have excess fluoride in their drinking water.

High fluoride level in groundwater is found in Africa, South America, Asia, and parts of North America (Table 1.2). India, China, Sri Lanka, and Rift valley countries in Africa are identified as the most affected with high groundwater fluoride concentrations. Excess fluoride has affected more than 260 million people worldwide (Amini et al., 2008). Prevalence of dental fluorosis, skeletal fluorosis, kidney damage, low IQ level, and low hemoglobin level in humans have been attributed to excess fluoride in drinking water in the affected areas (Yadav et al., 2019) (Table 1.2).

Table 1.2. Reported fluoride levels in groundwater in affected countries and associated health effects (modified after Mumtaz et al. (Mumtaz et al., 2019)).

Affected Countries	Affected Population	Reported fluoride level (mg/L)	Associated effects
India	66.64 million	0.5-69.7	Dental, Skeleton and Crippling fluorosis, low IQ level, adverse impact on kidney
Tanzania	49.25 million	8.0-12.7	Dental, Skeleton and Crippling fluorosis
Kenya	44.35 million	2.0-20.0	Dental and Skeleton fluorosis
South Africa	41.9 million	13.0	Dental and Skeleton fluorosis
China	26.68 million	21.5	Dental, Skeleton fluorosis, Reduction in Intelligence Quotient

1.1.3. Fluoride occurrence in the USA

In the USA, high groundwater fluoride is reported in New Mexico, Iowa, Ohio, Washington, and Virginia (Fig. 1). The number of children between 12 and 15 years of age with dental fluorosis has increased from 23% in 1986–1987 to about 41% in 1999–2004. In North Dakota, eight counties were identified to have fluoride levels of more than 4 mg/L, and 15 counties have more than 1.5 mg/L.

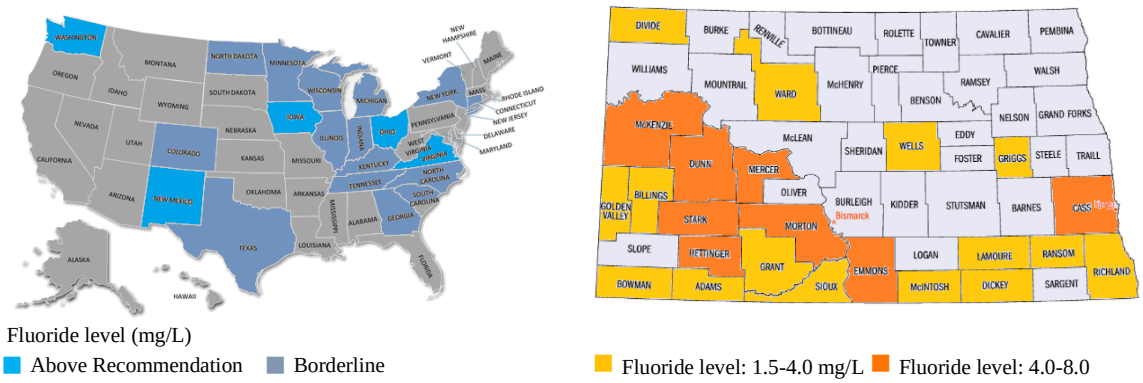

Figure 1.1. (a) The US fluoride concentration map (adapted from Waterlogic, 2019); (b) Areas in the North Dakota with high fluoride level (FAN, 2015).

1.1.4. Sources

Fluorine is the most electronegative element present in the earth's crust. Fluorine is the 24th most available element in the universe (0.00004%) (Budisa et al., 2014), and makes up approximately 0.06-0.09% of the earth's crust (the top 30 km) (Biswas et al., 2017). It is the 13th most abundant element on the earth (Yadav et al., 2019). There are two sources of fluoride in water (1) geogenic and (2) anthropogenic (Damtie et al., 2019). The groundwater fluoride concentration around the world ranges from 0.01 to 48 mg/L (Mumtaz et al., 2015).

The geogenic sources fluoride in groundwater mainly comes from the weathering of different fluoride-bearing minerals which are typically found in igneous, sedimentary, and metamorphic rocks (Jagtap et al., 2012). In these rocks, the fluorine concentration ranges from several hundred to thousands of mg/kg. The average fluorine concentration as the sedimentary rock is 1175 mg/kg, metamorphic rock is 1503 mg/kg, and igneous rock is 1043 mg/kg (He et al., 2013). The release of fluoride from rocks and sediments depends on mineralogical decomposition, changes in sediment chemistry, and geochemistry of water (Yadav et al., 2019). The most common minerals that contribute to the fluoride built-up in groundwater include Na-bearing feldspar (albite), fluorite, fluorspar, cryolite, theorapatite, phosphorite, apatite, topaz, villiaumite, biotite,

hornblende, riebeckite, aegirine, sepiolite, and palygorskite (Yadav et al., 2018). During mineral dissolution, the groundwater fluoride concentration is controlled by the environmental condition of the groundwater with the groundwater parameters such as solubility of other minerals, pH, alkalinity, and concentration of total dissolved solids may the major roles (Yadav et al., 2019). Fluorite (CaF_2) is considered to be the most dominant fluoride mineral phase responsible for groundwater fluoride concentration (Banerjee, 2015). The fluoride content in groundwater depends on the solubility of fluorite during mineral dissolution, whereas the concentration of Ca^{2+} is governed by the solubility of calcite in groundwater (Banerjee, 2015). The dissolutions of calcite and fluorite are inversely proportional to each other, and calcite precipitation enhances the dissolution of fluorite in groundwater (Rafique et al., 2009). Weak alkaline pH, high hydrogen carbonate (HCO_3^-), high sodium (Na^+), average TDS, and low calcium (Ca^{2+}) contents are favorable for increased fluoride content in groundwater (Su et al., 2013). Low calcium content triggers the dissolution of fluorite (Eq. 1.1) and thus increases the groundwater fluoride concentration till fluorite reached the solubility limit (Biswas et al., 2017). At high HCO_3^- content, the fluoride concentration increases in water due to the exchange of Ca^{2+} for Na^+ (Eq. 1.2).

$$CaF_2 \rightarrow Ca^{2+} + 2F^- \quad (1.1)$$

$$CaF_2 + 2NaHCO_3 \rightarrow CaCO_3 + 2Na^+ + 2F^- + H_2O + CO_2 \quad (1.2)$$

The ratio of HCO_3^-/Ca^{2+} affects the dissolution of fluoride, and fluoride dissolution is favorable when the ratio of HCO_3^-/Ca^{2+} is between 0.8-2.3 (Saxena and Ahmed, 2001).

The dissolution of fluoride depends on pH to a great extent. In acidic pH, fluoride is absorbed in clay. However, in alkaline pH, the OH^- tends to replace the fluoride present in fluoride-bearing minerals leading to the dissolution of fluoride in groundwater (Saxena and Ahmed, 2001)

(Eqs. 1.3 and 1.4). Evaporation is another factor that may increase the fluoride level in groundwater.

$$KAl_2[AlSi_3O_{10}]F_2 + 2OH^- \leftrightarrow KAl_2[AlSi_3O_{10}][OH]_2 + 2F^-(Muscovite) \quad (1.3)$$

$$KMg[AlSi_3O_{10}]F_2 + 2OH^- \leftrightarrow KMg[AlSi_3O_{10}][OH]_2 + 2F^- (Biotite) \quad (1.4)$$

Besides geogenic sources, high fluoride level has also been found in anthropogenic sources. Human activities such as discharges of fluoridated municipal water and fluoride chemicals may significantly increase the fluoride concentration in surface waters (Bhatnagar et al., 2011). There are large numbers of industrial sources of fluoride as well. These include semiconductor and integrated circuits manufacturers, aluminum smelters, glass, and ceramic production, hydrofluoric acid plants, and phosphate fertilizer plants (Jagtap et al., 2012). The effluents from these industries have fluoride levels ranging from 10 to 1000 mg/L (Bhatnagar et al., 2011).

1.1.5. Routes of fluoride uptake in human

Drinking water is the major pathway for fluoride to get into the human body. Other sources of fluoride for humans are food, air, cosmetics, and drugs. Higher fluoride concentration is also reported in barley, rice, cassava, taro, and yams (Mumtaz et al., 2015; Biswas et al., 2017). Fluoride level in food items depends on the fluoride content in the soil and irrigation water. So, fluoride level in food items varies depending on the place of cultivation (Jagtap et al., 2012). As fluoride can get accumulated in bones, some canned fishes such as salmon and sardines may contain fluoride (Mumtaz et al., 2015). The tea (*Camellia sinensis*) is another accumulator of fluorine compounds (Chan et al., 2013). The high concentration of fluoride found in tea is because of the phosphate fertilizers used to promote the growth of tea plants (Li et al., 2021; Chan et al., 2013). Long-term use of some drugs such as niflumic acid ($C_{13}H_9F_3N_2O_2$) for the treatment of rheumatoid arthritis, sodium fluoride (NaF) for treatment of osteoporosis, and use of fluoride-based

mouthwash is also associated with human uptake of fluoride (Jagtap et al., 2012). Consumption of different mineral salts such as rock salt and black salt is also another major route for fluoride intake in the human body (Singh et al., 2016; Rustagi et al., 2017). The ingestion of fluoride-containing water, however, remains the primary reason for various health effects reported across the globe.

1.1.6. Defluoridation technologies

It is very important to bring down the fluoride level within the permissible limit not only in drinking water but also in agriculture water as high fluoride level is also detected in food items derived from crops irrigated with water with excessive fluoride. Fluoride concentration in water can be reduced (1) by blending the highly fluoridated water with low-fluoride water from an alternate source, and (2) using defluoridation techniques, If the alternate source is not available then defluoridation is the only practical solution to remove fluoride from water (Meenakshi et., 2006). For other contaminants, water treatment methods target to reduce the contaminant level to zero or below MCL. However, defluoridation technologies always target to bring the fluoride level to the optimum concentration which is needed to get the beneficial effects of fluoride.

Extensive research has been done on various treatment technologies for removing fluoride from water. The main methods are precipitation/coagulation, ion exchange, membrane processes, and adsorption. The treatment type and scale of the system differ between developed and developing countries. In many rural areas, especially in developing countries, precipitation/coagulation and adsorption are the commonly used technology. In developed countries, more efficient and advanced technologies such as reverse osmosis, electrodialysis, and ion-exchange processes are used even for large units which are cost-prohibitive in developing countries. Further, in developing countries, simple, inexpensive, and locally available materials are used at the village, community, or household level for smaller household and community level

treatment (Loganathan et al., 2013). The selection of technologies depends on various factors such as location, cost, ease of technology transfer, and adaptability. The advantages and disadvantages of different treatment methods are discussed in the following sections.

1.1.6.1. Precipitation-coagulation

Precipitation/coagulation is one of the commonly used methods for removing fluoride from drinking water. This process involves the addition of chemicals that leads to the formation of fluoride precipitates. The Nalgonda technique is the best example of this method. It is one of the most widely used defluoridation techniques in India at the household level (Jagtap et al., 2012). It involves the addition of lime, alum, and bleaching powder to the water. This is a two-step process wherein the first step, precipitation occurs due to lime dosing, and in the second step, coagulation occurs due to the addition of alum. Two reactions occur upon alum addition in water: (i) alum reacts with some of the alkalinity and forms insoluble aluminum hydroxide flocs; and (ii) fluoride gets adsorbed on the aluminum hydroxide flocs.

The advantages of the Nalgonda technique include (Meenakshi and Maheshwari, 2006; Jagtap et al., 2012; Yadav et al., 2019): (1) This is a well-established method and most widely used technique at community water units; (2) This technique is simple compared to other techniques as it involves the use of only two chemicals; and (3) It is affordable and involves low operation and maintenance costs. The major disadvantages of the technique are (Meenakshi and Maheshwari, 2006; Jagtap et al., 2012; Yadav et al., 2019): (1) This technique has low fluoride removal efficiency compared to other techniques. It may not be able to remove the fluoride to the WHO limit (1.5 mg/L); (2) It requires a high dosage of chemicals, which makes this technique cost-inefficient; (3) The concentration of sulfate (SO_4^{2-}) may increase or in some cases may exceed the maximum permissible limit of SO_4^{2-} (400 mg/L) in final water due to the use of aluminum sulfate

as the coagulant; (4) There is always a chance of increased aluminum level in the treated water, which can cause dangerous neurological disorders in humans. It may also cause neuro-behavioral, pathophysiological, structural, and biochemical changes in humans; and (5) Formation of toxic sludge which contains aluminum fluoride complex is also common.

1.1.6.2. Membrane process

Different types of membrane processes such as reverse osmosis (RO), nanofiltration (NF), and electrodialysis have been used for defluoridation (Lhassani et al., 2001; Ndiayea et al., 2005; Grzegorzek and Majewska-Nowak, 2018). RO is a physical process in which hydraulic pressure beyond osmotic pressure is applied to the feedwater (with fluoride) to direct it through a semipermeable membrane (0.1 nm pore size) to remove fluoride and other ions from feedwater. In this process, the pressure is applied to the concentrated side of the membrane to overcome the natural osmotic pressure. RO can reject various ions depending on their electric charge and size. RO membranes can remove more than 98% of fluoride and be cleaned and regenerated (Mohapatra et al., 2009). Nanofiltration uses membranes with comparatively larger size pores (1 nm pore size) and provides less resistance to the solvent and solute movement. It can be operated at relatively low pressure. Consequently, less energy is required, and flow is faster compared to RO (Hu and Dickson, 2006; Diawara, 2008). Different types of nanofiltration membranes have been investigated for fluoride removal. All these membranes removed fluoride very effectively from water (Lhassani et al., 2001; Hu and Dickson, 2006; Hoinkis et al., 2011). Hoinkis et al. (2011) used two types of nanofiltration membranes, i.e., NF 90 and NF 270, to remove fluoride from both surface and groundwater and were able to reduce the fluoride level to the WHO limit (from 10 mg/L to 1.5 mg/L for NF 270 and from 20 mg/L to 1.5 mg/L for NF 90). Electrodialysis is the same as RO and NF, except an electric potential is used instead of pressure. Belkada et al. (2018)

used the electrodialysis process to remove fluoride from industrial wastewater (initial concentration 1000 mg/L) and observed significant (98%) removal of fluoride (Belkada et al., 2018).

The main advantages of the membrane process are (Meenakshi and Maheshwari, 2006; Jagtap et al., 2012; Damtie et al., 2019): (1) This process is very effective for defluoridation (up to 98% removal); (2) No chemicals are needed to run the process; (3) Membranes effectively remove suspended solids, organic micropollutants, pesticides, microorganisms, and all inorganic pollutants. Thus, this process ensures good water quality; (4) It does not have any interference from other ions; and (5) The process can work over a wide range of pH.

The major disadvantages of the process include (Jagtap et al., 2012; Yadav et al., 2019): (1) This process is expensive as it requires high capital costs; (2) Skilled labor and high maintenance costs are needed to run the process; (3) Membranes remove all ions from water, including some minerals essential for humans; (4) Reject solution contains highly concentrated fluoride, and the disposal of the reject solution is a big problem; and (5) Membrane fouling is a very common problem in this process.

1.1.6.3. Ion-exchange method

Ion-exchange resins have also been used for defluoridation. The anion-exchange resin containing ammonium functional groups can remove fluoride effectively from water (Eq. 1.5).

$$Matrix - NR^{3+}Cl^{-} + F^{-} \rightarrow Matrix - NR^{3+}F^{-} + Cl^{-} \quad (1.5)$$

Fluoride (F^{-}) ion is more electronegative than chloride (Cl^{-}) ion, and therefore, replaces the chloride ions of the resin. When all the active sites are occupied with fluoride, the resin is backwashed using concentrated sodium chloride (NaCl) solution. The fluoride ions are then replaced by new chloride ions leading to recharge of the resin. Samadi et al. (2014) used a strong

base anion resin to remove fluoride from water and reported a maximum adsorption capacity of 13.7 mg/g at neutral pH (Samadi et al., 2014). Kocakerim et al. (2003) reported the removal of aqueous fluoride (70% for 5 mg/L initial fluoride concentration) using a strongly basic ion-exchange resin, Purolite-250, and regenerated the material with 4% sodium chloride solution (Kocakerim et al., 2003).

The advantages of the ion-exchange process include (Mohapatra et al., 2009; Jagtap et al., 2012; Singh et al., 2016): (1) Ion-exchange process can remove 90-95 % of fluoride from feedwater; and (2) This process does not change the water taste and color. The notable disadvantages of the process are (Jagtap et al., 2012; Yadav et al., 2019): (1) Anion exchange resins are expensive and thus make the process economically not feasible; (2) Although regeneration of the resin is easy, regeneration produces rejects with concentrated fluoride, and the proper disposal of this waste is still a big challenge; and (3) The process is interfered by other anions such as sulfate, phosphate, and bicarbonate.

1.1.6.4. Adsorption

Membrane processes and the ion-exchange processes can remove fluoride from water very effectively, as discussed above. However, high capital and maintenance costs and the generation of highly concentrated fluoride solutions make these processes unsuitable in rural and socio-economically challenged communities. Further, they are not easily available in the local market or via a local vendor. The precipitation/coagulation process is comparatively simple and affordable compared to other techniques but does not have very good fluoride removal efficiency. The adsorption process is the most widely used and attractive technology for fluoride removal in terms of simplicity in design, cost-effectiveness, local availability, and high removal efficiency. Different types of adsorbents from a variety of raw materials have been used for effective

defluoridation. Researchers have investigated activated alumina, aluminum-based adsorbent, carbon-based adsorbent, calcium-based adsorbents, oxides/hydroxides, and layered double hydroxides, nanoparticles, natural minerals, and agricultural waste and biomass-based adsorbents for enhanced defluoridation (Mohapatra et al., 2009; Bhatnagar et al., 2011; Loganathan et al., 2013). The different adsorbents reported for fluoride removal are discussed in detail in the following sections.

1.1.6.4.1. Activated alumina

Activated alumina (AA) is the most widely studied adsorbent for fluoride removal. Farrah et al. (1987) investigated the fluoride adsorption capacity of AA and reported that it depends on the crystallinity and activation process of AA as well as on solution pH and alkalinity (Farrah et al., 1987). Ghorai and Pant. (2005) used granular activated alumina (GAA) for fluoride removal and reported an adsorption capacity of 2.41 mg/g at pH 7.0 (Ghorai and Pant, 2005). The disadvantage of using AA is that its fluoride removal is highly pH-dependent. The pH needs to be on the acidic side (< 7) for effective removal of fluoride (Bhatnagar et al., 2011). It has also been reported that the dissolution of aluminum oxides/hydroxides is unavoidable below pH 6 (Jagtap et al., 2012). Aluminum ions and their fluoride complexes are known to be neurotoxins (Martyn et al., 1989; Strunecka and Patocka, 1999).

1.1.6.4.2. Modified alumina-based adsorbent

Alumina impregnated with different metal oxides or coated alumina is much more effective than AA in removing fluoride from water. Puri and Balani. (2000) used lanthanum hydroxide supported on alumina to remove fluoride, and the adsorption capacity was improved (6.65 mg/g) by two times compared to the bare alumina (3.61 mg/g) (Puri and Balani, 2000). Maliyekkal et al. (2006) coated alumina with manganese oxide (MOCA) and investigated the material for fluoride

removal (Maliyekkal et al., 2006). The adsorption capacity of MOCA was 2.85 mg/g, whereas for AA the adsorption capacity was 1.08 mg/g. A major disadvantage of this metal oxide-modified alumina is the possible toxicity from the metal's leaching.

1.1.6.4.3. Calcium-based adsorbent

Calcium has an excellent affinity for fluoride. Gandhi and Sirisha. (2013) used chalk powder ($CaCO_3$) to remove fluoride from water and observed a maximum adsorption capacity of 3.65 mg/g at pH 5.0 (Gandhi and Sirisha, 2013). Other calcium-based adsorbents such as gypsiferous limestone, calcium aluminate, hydroxyapatite ($Ca_{10}(PO_4)_6(OH)_2$), and magnesium-substituted hydroxyapatite were also explored for defluoridation (Yadav et al., 2018). The maximum fluoride adsorption capacity of these adsorbents was in the range of 1.07-4.7 mg/g at pH 3-11 (Yadav et al., 2018).

1.1.6.4.4. Metal oxides/hydroxides and layered double hydroxides

Oxides and hydroxides of different metals such as Fe, Ce, La, Al, Mn, and Zr are used to remove fluoride from water. The predominant fluoride removal mechanism by these metal oxides is an ion-exchange mechanism, where the hydroxyl ion (OH^-) is replaced by the F^- ion. Granular ferric hydroxide (GFH) was used by Kumar et al. (2009) for enhanced fluoride removal (Kumar et al., 2009). They reported a maximum fluoride adsorption capacity of 7 mg/g over a wide pH range (4-8). Strong interference from phosphate, sulfate, and carbonate was also observed in their study.

Rao and Karthikeyan. (2012) assessed the defluoridation potential of lanthanum oxide (La $(OH)_2$) and reported a maximum adsorption capacity of 2.5 mg/g at pH 3.0-9.5 (Rao and Karthikeyan, 2012). They observed interference from sulfate and carbonate. The fluoride removal efficiency of lanthanum hydroxides (La $(OH)_2$) was also examined by Na and Park. (2010) and the

adsorption capacity was found to be 242.2 mg/g at pH ≤ 7.5 (Na and Park, 2010). No significant interferences from co-existing ions were observed in their study.

The use of bimetallic/trimetallic oxides/hydroxides can remove fluoride more efficiently than mono-oxide/hydroxide (Yadav et al., 2018). Tang and Zhang. (2016) synthesized a Ce-Fe bimetallic oxide with a hierarchical pore structure, which showed a fluoride adsorption capacity of 60.97 mg/g (Tang and Zhang, 2016). This material exhibited good adsorption capacity over a wide range of pH (2.9-10.1), with it being more efficient in acidic pH. The presence of carbonate and bicarbonate significantly decreased the fluoride removal capacity of this bimetallic oxide.

Dou et al. (2011) studied the fluoride adsorption capacity of a granular zirconium-iron oxide (GZI) synthesized by the extrusion method (Dou et al., 2011). They found a maximum adsorption capacity of 9.80 mg/g at pH 7.0. The presence of bicarbonate and phosphate markedly inhibited the fluoride removal capacity of GZI, but sulfate, chloride, and nitrate showed little or no effect on fluoride adsorption. Hussein et al. (2015) assessed the defluoridation capacity of Mg(III)-Al(III)-La(III) triple-metal hydrous oxide produced by the co-precipitation method (Hussain et al., 2015). The material showed 31.75 mg/g at pH 7.0. Biswas et al. (2010) synthesized a hydrated Fe(III)-Al(III)-Cr(III) tri-metal oxide (HIACMO) to investigate the fluoride removal from aqueous solution (Biswas et al., 2010). The maximum fluoride adsorption capacity was found to be 31.89 mg/g at a pH of ~5.6. They investigated the effect of co-existing ions on fluoride removal by using tap water spiked with fluoride and found that with a 4 g/L adsorbent (HIACMO) dose, the fluoride concentration decreased from 10.0 mg/L to 0.43 mg/L.

Kanrar et al. (2016) synthesized a graphene oxide (GO)-incorporated iron-aluminum mixed oxide (HIAGO) composite for enhanced fluoride adsorption (Kanrar et al., 2016). The maximum adsorption capacity varied between 22.13-27.75 mg/g, depending on the solution

temperature. Layered double hydroxides (LDH) have also been studied extensively for fluoride removal. Koilraj and Kaman. (2013) prepared a ZnCr layered double hydroxide ($ZnCr_3$- NO_3-LDH) and found a maximum fluoride adsorption capacity of 31 mg/g (Koilraj and Kannan, 2013). The material exhibited good buffering capacity, and therefore, maintained fluoride removal capacity over a broad pH range (3-10). A significant decrease in fluoride removal was observed in the presence of carbonate, sulfate, and phosphate. Kameda et al. (2015) synthesized Mg-Al LDH by nitrate intercalation (NO_3-Mg-Al LDH) and chlorine intercalation (Cl-Mg-Al LDH). They reported a maximum fluoride adsorption capacity of 62.70 mg/g for NO_3-Mg-Al LDH and 60.80 mg/g for Cl-Mg-Al LDH without initial pH control (Kameda et al., 2015). The presence of chloride and sulfate inhibited fluoride removal by both the adsorbents. An LDH (LALDH-201) was prepared by Cai et al. (2016) by impregnating nanocrystalline Li/Al LDHs (LALDH) inside a commercial polystyrene anion exchanger D201. Their material showed a maximum adsorption capacity of 62.5 mg/g at pH 7.1 (Cai et al., 2016). The fluoride removal efficiency was significantly affected in the presence of phosphate, sulfate, bicarbonate, chlorine, and nitrate.

1.1.6.4.5. Nanoparticles

Different types of nano-based adsorbents have been explored by researchers for enhanced fluoride removal. Patel et al. (2009) investigated the defluoridation capacity of CaO nanoparticles synthesized by the sol-gel method and reported a maximum fluoride adsorption capacity of 163.3 mg/g (Patel et al., 2009). The adsorbent performed well (85-90%) at a pH range of 2-8, but at high pH (>8.0), the fluoride removal adsorption capacity of the adsorbent decreased (70-80%). They did not observe significant interference from sulfate, nitrate, and phosphate. The fluoride ions replaced the hydroxyl ions present in CaO nanoparticles and formed CaF_2 (Patel et al., 2009).

Kumar et al. (2011) synthesized nano-alumina and achieved a maximum fluoride adsorption capacity of 14 mg/g at pH 6.15, which is almost six times higher than the granular activated alumina (Kumar et al., 2011). Change in solution pH strongly impacted the fluoride removal efficiency of nano-alumina with maximum removal observed at pH 6.15. The decrease in fluoride removal capacity in acidic pH was attributed to the formation of HF. The presence of interfering ions (sulfate, phosphate, nitrate, and carbonate) limited the fluoride adsorption capacity of nano-alumina.

Prabhu et al. (2016) prepared nano-sized hydroxyapatite supported on graphene oxide sheets (GOs-nHAP) by in-situ co-precipitation method and evaluated their fluoride scavenging potential (Prabhu et al., 2016). The maximum defluoridation capacity was reported to be 44.06 mg/g over a wide pH range (3-7). The presence of sulfate, chloride, and nitrate did not affect the fluoride adsorption capacity of GOs-nHAP but the presence of bicarbonate significantly decreased the fluoride removal efficiency (from 98% to 70%).

The fluoride adsorption capacity of single-walled carbon nanotubes (SWCNTs) and multi-walled carbon nanotubes (MWCNTs) was investigated (Dehghani et al., 2016). The maximum adsorption capacity of SWCNTs was found to be 2.4 mg/g, and MWCNTs was 2.83 mg/g. MWCNTs have more available internal active adsorption sites compared to SWCNTs, and therefore, exhibited better fluoride adsorption capacity. The acidic pH was more favorable for fluoride adsorption by both species of CNT.

Dhillon and Kumar. (2015) synthesized a new crystalline and hybrid Fe-Ce-Ni nanoporous adsorbent via co-precipitation (Dhillon and Kumar, 2015). Their material exhibited extremely high adsorption capacity (285.7 mg/g) compared to other adsorbents reported in the literature. The fluoride removal efficiency of the Fe-Ce-Ni nanoadsorbent was strongly dependent on solution

pH. Maximum fluoride adsorption (98%) was observed at pH 7, which decreased to 52% when pH was increased to 12 and decreased to 60% when pH decreased to 2. No significant interference was observed in the presence of sulfate, nitrate, bicarbonate but phosphate presence showed a negative impact on fluoride removal by Fe-Ce-Ni nanoadsorbent. The removal mechanism was ion exchange between fluoride ion and the surface hydroxyl group of the Fe-Ce-Ni nanoadsorbent.

Three kinds of ceria (CeO_2) nanomaterials with different morphology (nanorods, octahedron, and nanocube) were prepared hydrothermally by Kang et al. (2017). Change in solution pH showed a sharp impact on fluoride adsorption capacity by the ceria nanomaterials with maximum defluoridation capacity observed at pH 3.0. They reported a maximum adsorption capacity of 71.5 mg/g for CeO_2-Rods, 28.3 mg/g for CeO_2-Octs, and 7.0 mg/g for CeO_2-cubes at pH 3.5. The mechanisms involved in fluoride removal included ion exchange, surface adsorption, and pore filling and were influenced by the presence of Ce^{3+}-O defects.

1.1.6.4.6. Carbon-based adsorbent

Different types of carbon-based materials have been studied for fluoride removal, given that carbon has a high affinity for fluoride. Graphite was used as a fluoride adsorbent by Karthikeyan and Elango. (2008) and adsorption capacity was found to be in the range of 0.16-3.13 mg/g (Karthikeyan and Elango, 2008) at a wide range of pH (4-9). Bicarbonate ion slightly decreased the adsorption capacity, but sulfate, chlorine, and nitrate had a negligible effect on fluoride removal.

Activated carbon (AC) is one of the most widely used adsorbents for fluoride adsorption. Large surface area, high porosity, low cost, ready availability, and high catalytic activities of AC have attracted the researchers to explore the fluoride removal capacity of different types of AC (Loganathan et al., 2013; Mondal and George, 2015). Singh et al. (2017) assessed the fluoride

adsorption capacity of activated carbon prepared from bael (*Aegle marmelos*) shell and found a maximum adsorption capacity of 1.07 at an initial fluoride concentration of 4 mg/L and 2.4 mg/g at an initial fluoride concentration of 8 mg/L (Singh et al., 2017). The point-of-zero-charge (PZC) was found to be 6.3, and the material performed well over a wide pH range (2-10). However, at a low concentration (< 4 mg/L) of fluoride, the adsorption capacity was low (1.07 mg/g), which has limited the practical use of this material.

Zirconium impregnated activated carbon (ZIAC) produced via ultra-sonication was investigated by Mullick et al. (2018) for fluoride scavenging from water (Mullick and Neogi, 2018). They reported a maximum fluoride adsorption capacity of 5 mg/g at pH 4.0. The fluoride removal efficiency decreased from 75% to 42% when pH increased from 4 to 10. Fluoride was removed by an ion-exchange mechanism where hydroxyl ion presents in ZIAC was replaced by fluoride ions. The presence of interfering ions (sulfate, bicarbonate, nitrate, and chlorine) showed negligible or no effect on fluoride adsorption. The same research group used Mg-Mn-Zr impregnated activated carbon synthesized via the sonochemical method for defluoridation (Mullick and Neogi, 2019). The triple metal impregnated AC showed a maximum sorption capacity of 26.27 mg/g. The point-of-zero-charge of the material was reported as 11.9, and so the adsorbent worked effectively at a wide range of pH (2-10).

Ramos et al. (1999) prepared an aluminum impregnated coconut (*Cocos nucifera* L) shell-based activated carbon for fluoride adsorption (Ramos et al., 1999). They reported that the solution pH impacted the impregnation of aluminum onto the activated carbon. The optimum pH for the successful aluminum impregnation was found to be 3.5. Their material exhibited maximum fluoride adsorption of 1.07 mg/g at pH 3.0. Change in solution pH also affected the fluoride removal efficiency with maximum adsorption was observed at pH 3.0.

Ravulapalli and Kunta (2017) investigated the fluoride adsorption capacity of activated carbon prepared from the barks of the fig tree (*Ficus racemosa*) (Ravulapalli and Kunta, 2017). They treated the activated carbon with nitric acid to increase its fluoride removal efficiency. The nitric acid-treated AC showed a maximum adsorption capacity of 1.65 at pH 7.0. Adsorption of fluoride on the AC was strongly dependent on the solution pH. With the increase of pH from 1 to 7, the removal efficiency increased from 68% to 88% and then decreased to 78% when pH increased from 7 to 11. Significant interference was observed from phosphate and bicarbonate ions; however, nitrate and chloride ions exhibited negligible interference in fluoride adsorption.

Fluoride removal by $KMnO_4$-modified activated carbon derived rice (*Oryza sativa*) straw via steam pyrolysis was reported by Daifullah et al., 2007 (Daifullah et al., 2007). The adsorbent removed > 70% fluoride from aqueous solution with initial fluoride concentration < 5 mg/L. The maximum adsorption capacity was found to be 15.9 mg/g at pH 2.0. The fluoride removal capacity of the adsorbent was significantly affected by solution pH. Fluoride adsorption capacity decreased from 15.9 mg/g to 1.5 mg/g when pH increased from 2 to 10. The removal mechanism was dominated by ion exchange.

Ma et al., 2009 developed coated granular activated carbon (GAC) with MnO_2 (GAC-MnO_2) (Ma et al., 2009). The adsorption capacity of the GAC-MnO_2 (2.24 mg/g at pH 5.2) was at least three times higher than that of the uncoated GAC (0.75 mg/g). Both surface adsorption and intra-particle diffusion were participating the fluoride adsorption process by GAC-MnO_2.

Vences-Alvarez et al. (2015) compared the fluoride removal efficiency of GAC and lanthanum oxyhydroxide impregnated GAC (GAC-La) (Vences-Alvarez et al., 2015). The fluoride adsorption capacity of GAC-La (9.96 mg/g at pH 7.0) was five times higher than the unmodified GAC (1.99 mg/g). The lanthanum oxyhydroxides increased the –OH active sites in the adsorbent

and so more fluoride was removed by the ion-exchange process. The presence of co-existing anions (chloride, phosphate, sulfate, and nitrate) at low concentrations (≤ 30 mg/L) did not impact the fluoride adsorption capacity of GAC-La. However, high concentrations (> 30 mg/L) of co-existing anions decreased the fluoride removal efficiency noticeably. Fluoride adsorption by GAC-La was dominated by an ion-exchange mechanism where –OH present in $La(OH)_3$ was replaced by fluoride.

1.2. Scope of the research

Fluoride contamination of drinking water is a global problem. Both urban and rural communities are affected by excess fluoride in water. Specifically, in rural and socio-economically challenged communities, fluoride removal from drinking water remains a big challenge due to the lack of cost-effective and appropriate technology.

Among all the fluoride removal technologies, adsorption is the most effective and adaptable technology in rural, remote, and socio-economically challenged communities. Out of all adsorbents reported in the literature, activated carbon is one of the most widely used adsorbents for removing both organic and inorganic contaminants (Li et al., 2002; Bhatnagar et al., 2011). However, the unmodified activated carbon exhibits low adsorption capacity for inorganic pollutants (Mugisidi et al., 2007). Surface modification is necessary to increase the fluoride adsorption capacity of activated carbon. Different types of surface modifiers such as nitric acid, sulfuric acid, metal, and metal oxide have been used to enhance the fluoride removal efficiency of activated carbon (Section 1.1.6.4.6). These modifiers can increase the defluoridation capacity of activated carbon significantly. However, not all of these modifiers are locally available; they are difficult to handle (because they are corrosive), not environment friendly, and involve complicated preparation and modification process, and hence, not suitable for rural communities. Developing

an activated carbon surface modifier suitable for rural communities is still a big challenge. Raw materials for such modifiers or the modifiers themselves should be locally available, easy to prepare, and environment friendly.

It is also worth noting that all the reported adsorbents suffer from slow adsorption kinetics (contact time of 30-180 minutes) (Yadav et al., 2018). The adsorbents need to be in contact with the adsorbate (fluoride) for a long time to reach equilibrium. The slow adsorption kinetics limit the use of these adsorbents in high throughput defluoridation system. Therefore, developing a new adsorbent for rapid and efficient removal of fluoride is felt necessary.

The first part of this study focuses on developing cost-effective and adaptable carbon-based defluoridation techniques, especially for rural and remote communities. The second part of the study focuses on developing a rapid and efficient nano-based technique applicable both in rural and urban communities.

1.3. Research objectives

The overarching objectives of this research are:

(1) To develop cost-effective and adaptable carbon-based defluoridation techniques, especially for rural and remote communities.

(2) To develop a rapid and efficient nano-based technique applicable both in rural and urban communities.

As discussed earlier (Section 1.2), unmodified activated carbon cannot remove fluoride effectively and surface modification is necessary to increase fluoride removal capacity. To develop an activated carbon surface modifier suitable for rural communities, we have used analytical grade citric acid ($C_6H_8O_7$). Citric acid (CA) is a weak organic acid found naturally in different citrus fruits, which are readily available in rural and remote areas. After synthesizing CA-modified

granular activated carbon, we have used the same methodology to modify the surface of granular activated carbon with the juice of citrus fruit (*Citrus aurontifolia* or Lime).

Carbon-based adsorbents have been reported by others to have very slow adsorption kinetics compared to metal oxide-based adsorbents (Yadav et al., 2018). Therefore, for rapid and efficient removal of fluoride, we are using graphene oxide-ceria (GO-CeO_2) nanohybrid, a metal oxide-based adsorbent.

The specific objectives of this research are:

(1) Develop a citric acid-modified granular activated carbon (CAGAC) for defluoridation and investigate the fluoride removal mechanism by CAGAC.

(2) Develop Lime (*Citrus aurontifolia*) juice modified granular activated carbon (LGAC) for enhanced defluoridation and compare the fluoride removal efficiency and mechanism of LGAC with that of CAGAC.

(3) Evaluate GO-CeO_2 nanohybrid for the removal of aqueous fluoride and elucidate the fluoride adsorption mechanism involved.

1.4. Dissertation organization

These are five (5) chapters in this dissertation. Most of the chapters are written in a journal paper style, and some tables, figures, and equations are repeated in multiple chapters for ease of reading. *Chapter 1* is an overview of the global and national fluoride problems, the health impact of fluoride, currently available technology and materials for fluoride removal, the need for this research, and research objectives. *Chapter 2* to *Chapter 4* are presented in journal paper format. *Chapter 2* is a journal paper already published in *Chemosphere* in 2020 (Rashid and Bezbaruah, 2020), *Chapter 3* contains a manuscript which ready to be submitted to a peer-reviewed journal (Rashid et al., 2021). *Chapter 4* is a manuscript that is submitted to a journal (Rashid et al., 2021).

Each chapter has an introduction, materials and methods, results and discussions, and conclusions. *Chapter 2* focuses on the fluoride removal from the aqueous solution using citric acid modified granular activated carbon (CAGAC). *Chapter 3* explores the fluoride removal capacity of lime (*Citrus aurontifolia*) modified granular activated carbon (LGAC). *Chapter 3* also compares fluoride removal efficiency between CAGAC and LGAC. *Chapter 4* presents the findings from the fluoride removal study using graphene oxide-ceria (GO-CeO_2) nanohybrid and discusses the mechanisms of rapid removal of fluoride by the nanohybrid. Finally, *Chapter 5* presents the general conclusions and the scope for future works. Appendices are added to this dissertation to present additional data related to Chapters 2-4. Appendix A is for Chapter 2. Appendix B is for Chapter 3. Appendix C is for Chapter 4.

1.5. References

Amini, M., Mueller, K., Abbaspour, K.C., Rosenberg, T., Afyuni, M., Moller, K.N., Sarr, M., Johnson, C.A., 2008. Statistical modeling of global geogenic fluoride contamination in groundwaters. Environmental Science & Technology 42, 3662-3668.

Annouar, S., Mountadar, M., Soufiane, A., Elmidaoui, A., Sahli, M.A.M., 2004. Defluoridation of underground water by adsorption on the chitosan and by electrodialysis. Desalination 165, 437-437.

Banerjee, A., 2015. Groundwater fluoride contamination: A reappraisal. Geoscience Frontiers 6, 277-284.

Barbier, O., Arreola-Mendoza, L., Del Razo, L.M., 2010. Molecular mechanisms of fluoride toxicity. Chemico-Biological Interactions 188, 319-333.

Belkada, F.D., Kitous, O., Drouiche, N., Aoudj, S., Bouchelaghem, O., Abdi, N., Grib, H., Mameri, N., 2018. Electrodialysis for fluoride and nitrate removal from synthesized photovoltaic industry wastewater. Separation and Purification Technology 204, 108-115.

Bhatnagar, A., Kumar, E., Sillanpaa, M., 2011. Fluoride removal from water by adsorption-A review. Chemical Engineering Journal 171, 811-840.

Biswas, G., Kumari, M., Adhikari, K., Dutta, S., 2017. A Critical Review on Occurrence of Fluoride and Its Removal through Adsorption with an Emphasis on Natural Minerals. Current Pollution Reports 3, 104-119.

Biswas, K., Gupta, K., Goswami, A., Ghosh, U.C., 2010. Fluoride removal efficiency from aqueous solution by synthetic iron(III)-aluminum(III)-chromium(III) ternary mixed oxide. Desalination 255, 44-51.

Budisa, N., Kubyshkin, V., Schulze-Makuch, D., 2014. Fluorine-Rich Planetary Environments as Possible Habitats for Life. Life, 4, 374-385.

Cai, J., Zhang, Y., Pan, B., Zhang, W., Lv, L., Zhang, Q., 2016. Efficient defluoridation of water using reusable nanocrystalline layered double hydroxides impregnated polystyrene anion exchanger. Water Research 102, 109-116.

CDC (Centers for Disease Control and Prevention), 2016. Community Water Fluoridation, Available at: https://www.cdc.gov/fluoridation/faqs/community-water-fluoridation.html, Accessed Date: April, 2021.

Chan, L., Mehra, A., Saikat, S., Lynch, P., 2013. Human exposure assessment of fluoride from tea (Camellia sinensis L.): A UK based issue? Food Research International 51, 564-570.

Chouhan, S., Flora, S.J.S., 2010. A Indian Journal of Experimental Biology 48, 666-678.

Daifullah, A.A.M., Yakout, S.M., Elreefy, S.A., 2007. Adsorption of fluoride in aqueous solutions using KMnO4-modified activated carbon derived from steam pyrolysis of rice straw. Journal of Hazardous Materials 147, 633-643.

Damtie, M.M., Woo, Y.C., Kim, B., Hailemariam, R.H., Park, K.D., Shon, H.K., Park, C., Choi, J.S., 2019. Removal of fluoride in membrane-based water and wastewater treatment technologies: Performance review. Journal of Environmental Management 251.

Dehghani, M.H., Haghighat, G.A., Yetilmezsoy, K., McKay, G., Heibati, B., Tyagi, I., Agarwal, S., Gupta, V.K., 2016. Adsorptive removal of fluoride from aqueous solution using single- and multi-walled carbon nanotubes. Journal of Molecular Liquids 216, 401-410.

Dey, S., & Giri, B., 2015. Fluoride Fact on Human Health and Health Problems: A Review. Med Clin Rev. 2:2. doi: 10.21767/2471-299X.100011.

Dhillon, A., Kumar, D., 2015. Development of a nanoporous adsorbent for the removal of health-hazardous fluoride ions from aqueous systems. Journal of Materials Chemistry A 3, 4215-4228.

Diawara, C.K., 2008. Nanofiltration process efficiency in water desalination. Separation and Purification Reviews 37, 303-325.

Dou, X., Zhang, Y., Wang, H., Wang, T., Wang, Y., 2011. Performance of granular zirconium-iron oxide in the removal of fluoride from drinking water. Water Research 45, 3571-3578.

Farrah, H., Slavek, J., Pickering, W.F., 1987. Fluoride interactions with hydrous aluminium oxides and alumina. Aust. J. Soil Res. 25, 55–69.

Fluoride Action Network (FAN), 2015. State Fluoride Database, available at http://fluoridealert.org/researchers/states/north-dakota/, Accessed Date: March 2021.

Gandhi, N., Sirisha, D., 2013. Adsorption of fluoride from aqueous solution by using chalk powder. World J. Pharm. Pharm. Sci. 2, 3897-3914.

Gbadebo, A.M., 2012. Groundwater fluoride and dental fluorosis in southwestern Nigeria. Environmental Geochemistry and Health 34, 597-604.

Ghorai, S., Pant, K.K., 2005. Equilibrium, kinetics and breakthrough studies for adsorption of fluoride on activated alumina. Separation and Purification Technology 42, 265-271.

Grzegorzek, M., Majewska-Nowak, K., 2018. Fluoride removal from aqueous solutions with the use of electrodialysis with monovalent permselective anion-exchange membranes. Desalination and Water Treatment 128, 285-297.

Harrison, P.T.C., 2005. Fluoride in water: A UK perspective. Journal of Fluorine Chemistry 126, 1448-1456.

He, J., An, Y.H., Zhang, F.C., 2013. Geochemical characteristics and fluoride distribution in the groundwater of the Zhangye Basin in Northwestern China. Journal of Geochemical Exploration 135, 22-30.

Hoinkis, J., Valero-Freitag, S., Caporgno, M.P., Patzold, C., 2011. Removal of nitrate and fluoride by nanofiltration - a comparative study. Desalination and Water Treatment 30, 278-288.

Horst, J. A., Tanzer, J. M., Milgrom, P. M., 2018. Fluorides and Other Preventive Strategies for Tooth Decay. Dental clinics of North America, 62(2), 207–234.

Hu, K., Dickson, J.M., 2006. Nanofiltration membrane performance on fluoride removal from water. Journal of Membrane Science 279, 529-538.

Hussain, Z., Li, D., Li, X., Kang, J., 2015. Defluoridation by a Mg-Al-La triple-metal hydrous oxide: synthesis, sorption, characterization and emphasis on the neutral pH of treated water. Rsc Advances 5, 43906-43916.

Indu, R., Krishnan, S., Shah, T., 2007. Impacts of Groundwater Contamination with Fluoride and Arsenic: Affliction Severity, Medical Cost and Wage Loss in Some Villages of India. International Journal of Rural Management 3(1), 69-93.

Jagtap, S., Yenkie, M.K., Labhsetwar, N., Rayalus, S., 2012. Fluoride in Drinking Water and Defluoridation of Water. Chemical Reviews 112, 2454-2466.

Kameda, T., Oba, J., Yoshioka, T., 2015. Recyclable Mg-Al layered double hydroxides for fluoride removal: Kinetic and equilibrium studies. Journal of Hazardous Materials 300, 475-482.

Kanrar, S., Debnath, S., De, P., Parashar, K., Pillay, K., Sasikumar, P., Ghosh, U.C., 2016. Preparation, characterization and evaluation of fluoride adsorption efficiency from water of iron-aluminium oxide-graphene oxide composite material. Chemical Engineering Journal 306, 269-279.

Karthikeyan, M., Elango, K.P., 2008. Removal of fluoride from aqueous solution using graphite: A kinetic and thermodynamic study. Indian Journal of Chemical Technology 15, 525-532.

Kim, S.H., Kim, K., Ko, K.S., Kim, Y., Lee, K.S., 2012. Co-contamination of arsenic and fluoride in the groundwater of unconsolidated aquifers under reducing environments. Chemosphere 87, 851-856.

Kocakerim, M.M., Boncukcuoglu, R., Kocadagistan, B., Yartasi, A., Kosklu, A., 2003. Kinetics of fluoride removal from drinking water by ion exchange method. Fresenius Environmental Bulletin 12, 1394-1399.

Koilraj, P., Kannan, S., 2013. Aqueous fluoride removal using ZnCr layered double hydroxides and their polymeric composites: Batch and column studies. Chemical Engineering Journal 234, 406-415.

Kumar, E., Bhatnagar, A., Ji, M., Jung, W., Lee, S.H., Kim, S.J., Lee, G., Song, H., Choi, J.Y., Yang, J.S., Jeon, B.H., 2009. Defluoridation from aqueous solutions by granular ferric hydroxide (GFH). Water Research 43, 490-498.

Kumar, E., Bhatnagar, A., Kumar, U., Sillanpaa, M., 2011. Defluoridation from aqueous solutions by nano-alumina: Characterization and sorption studies. Journal of Hazardous Materials 186, 1042-1049.

Lhassani, A., Rumeau, M., Benjelloun, D., Pontie, M., 2001. Selective demineralization of water by nanofiltration application to the defluorination of brackish water. Water Research 35, 3260-3264.

Li, L., Quinlivan, P.A., Knappe, D.R.U., 2002. Effects of activated carbon surface chemistry and pore structure on the adsorption of organic contaminants from aqueous solution. Carbon 40, 2085-2100.

Li, T., He, J., Zhou, Z., Chen, R., Tang, Y., Wang, D., Feng, Z., Liu, Y., Tian, B., Ma, L., Sun, M., 2021. The Effect of Phosphate Fertilizer on Fluoride Accumulation in Tea Leaves Based on Ecological Environment Analysis. IOP Conference Series: Earth and Environmental Science 696, 012024.

Loganathan, P., Vigneswaran, S., Kandasamy, J., Naidu, R., 2013. Defluoridation of drinking water using adsorption processes. Journal of Hazardous Materials 248, 1-19.

Ma, Y., Wang, S.-G., Fan, M., Gong, W.-X., Gao, B.-Y., 2009. Characteristics and defluoridation performance of granular activated carbons coated with manganese oxides. Journal of Hazardous Materials 168, 1140-1146.

Martyn, C.N., Osmond, C., Edwardson, J.A., Barker, DJP., Harris, E.C., Lacey, R.F., 1989. Geographical relation between alzheimers-disease and aluminum in drinking-water. Lancet; 1: 59-62.

Maliyekkal, S.M., Sharma, A.K., Philip, L., 2006. Manganese-oxide-coated alumina: A promising sorbent for defluoridation of water. Water Research 40, 3497-3506.

Meenakshi, Maheshwari, R.C., 2006. Fluoride in drinking water and its removal. Journal of Hazardous Materials 137, 456-463.

Mohapatra, M., Anand, S., Mishra, B.K., Giles, D.E., Singh, P., 2009. Review of fluoride removal from drinking water. Journal of Environmental Management 91, 67-77.

Mondal, P., George, S., 2015. A review on adsorbents used for defluoridation of drinking water. Reviews in Environmental Science and Bio-Technology 14, 195-210.

Mugisidi, D., Ranaldo, A., Soedarsono, J.W., Hikam, M., 2007. Modification of activated carbon using sodium acetate and its regeneration using sodium hydroxide for the adsorption of copper from aqueous solution. Carbon 45, 1081-1084.

Mullick, A., Neogi, S., 2018. Acoustic cavitation induced synthesis of zirconium impregnated activated carbon for effective fluoride scavenging from water by adsorption. Ultrasonics Sonochemistry 45, 65-77.

Mullick, A., Neogi, S., 2019. Ultrasound assisted synthesis of Mg-Mn-Zr impregnated activated carbon for effective fluoride adsorption from water. Ultrasonics Sonochemistry 50, 126-137.

Mumtaz, N., Pandey, G., Labhasetwar, P.K., 2015. Global Fluoride Occurrence, Available Technologies for Fluoride Removal, and Electrolytic Defluoridation: A Review. Critical Reviews in Environmental Science and Technology 45, 2357-2389.

Na, C.K., Park, H.J., 2010. Defluoridation from aqueous solution by lanthanum hydroxide. Journal of Hazardous Materials 183, 512-520.

Ndiayea, P.I., Moulin, P., Dominguez, L., Millet, J.C., Charbit, F., 2005. Removal of fluoride from electronic industrial effluent by RO membrane separation. Desalination 173, 25-32.

Patel, G., Pal, U., Menon, S., 2009. Removal of Fluoride from Aqueous Solution by CaO Nanoparticles. Separation Science and Technology 44, 2806-2826.

Prabhu, S.M., Elanchezhiyan, S.S.D., Lee, G., Khan, A., Meenakshi, S., 2016. Assembly of nano-sized hydroxyapatite onto graphene oxide sheets via in-situ fabrication method and its prospective application for defluoridation studies. Chemical Engineering Journal 300, 334-342.

Puri, B.K., Balani, S., 2000. Trace determination of fluoride using lanthanum hydroxide supported on alumina. Journal of Environmental Science and Health Part a-Toxic/Hazardous Substances & Environmental Engineering 35, 109-121.

Rafique, T., Naseem, S., Usmani, T.H., Bashir, E., Khan, F.A., Bhanger, M.I., 2009. Geochemical factors controlling the occurrence of high fluoride groundwater in the Nagar Parkar area, Sindh, Pakistan. Journal of Hazardous Materials 171, 424-430.

Ramos, R.L., Ovalle-Turrubiartes, J., Sanchez-Castillo, M.A., 1999. Adsorption of fluoride from aqueous solution on aluminum-impregnated carbon. Carbon 37, 609-617.

Rao, C.R.N., Karthikeyan, J., 2012. Removal of Fluoride from Water by Adsorption onto Lanthanum Oxide. Water Air and Soil Pollution 223, 1101-1114.

Rashid, U.S., Bezbaruah, A.N., 2020. Citric acid modified granular activated carbon for enhanced defluoridation. Chemosphere 252, 126639.

Rashid, U.S., Koep, S., Bezbaruah, A.N., 2021. *Citrus aurantiifolia* Juice Modified Granular Activated Carbon for Drinking Water Defluoridation. Ready to Submit in Chemosphere.

Rashid, U.S., Das, T.K., Sakthivel, T.S., Seal, S., Bezbaruah, A.N., 2021. GO-CeO_2 Nanohybrid for Ultra-Rapid Fluoride Removal from Drinking Water. Under Review in Science of The Total Environment.

Ravulapalli, S., Kunta, R., 2017. Defluoridation studies using active carbon derived from the barks of Ficus racemosa plant. Journal of Fluorine Chemistry 193, 58-66.

Rustagi, N., Rathore, A. S., Meena, J. K., Chugh, A., & Pal, R. (2017). Neglected health literacy undermining fluorosis control efforts: A pilot study among schoolchildren in an endemic village of rural Rajasthan, India. Journal of family medicine and primary care, 6(3), 533–537.

Samadi, M.T., Zarrabi, M., Sepehr, M.N., Ramhormozi, S.M., Azizian, S., Amrane, A., 2014. Removal of Fluoride Ions by Ion Exchange Resin: Kinetic And Equilibrium Studies. Environmental Engineering and Management Journal 13, 205-214.

Saxena, V.K., Ahmed, S., 2001. Dissolution of fluoride in groundwater: a water-rock interaction study. Environmental Geology 40, 1084-1087.

Singh, J., Singh, P., Singh, A., 2016. Fluoride ions vs removal technologies: A study. Arabian Journal of Chemistry 9, 815-824.

Singh, K., Lataye, D.H., Wasewar, K.L., 2017. Removal of fluoride from aqueous solution by using bael (Aegle marmelos) shell activated carbon: Kinetic, equilibrium and thermodynamic study. Journal of Fluorine Chemistry 194, 23-32.

Strunecka, A., Patocka, J., 1999. Pharmacological and toxicological effects of aluminofluoride complexes. Fluoride 32, 230-242.

Su, C.L., Wang, Y.X., Xie, X.J., Li, J.X., 2013. Aqueous geochemistry of high-fluoride groundwater in Datong Basin, Northern China. Journal of Geochemical Exploration 135, 79-92.

Tang, D., Zhang, G., 2016. Efficient removal of fluoride by hierarchical Ce-Fe bimetal oxides adsorbent: Thermodynamics, kinetics and mechanism. Chemical Engineering Journal 283, 721-729.

USEPA (U.S. Environmental Protection Agency), 2009. National Primary Drinking Water Regulations. Available at: https://www.epa.gov/ground-water-and-drinking-water/national-primary-drinking-water-regulations#Inorganic, Accessed date: February 2021.

Waterlogic, 2019. Water Fluoridation in the USA. Avaialable at: https://www.waterlogic.com/en-us/resources/fluoride-level-map/, Accessed date: February 2021.

WHO, 2004. Guidelines for drinking-water quality. Volume 1 recommendations, 3rd edn. World Health Organization, Geneva.

Yadav, K.K., Gupta, N., Kumar, V., Khan, S.A., Kumar, A., 2018. A review of emerging adsorbents and current demand for defluoridation of water: Bright future in water sustainability. Environment International 111, 80-108.

Yadav, K.K., Kumar, S., Pham, Q.B., Gupta, N., Rezania, S., Kamyab, H., Yadav, S., Vymazal, J., Kumar, V., Tri, D.Q., Talaiekhozani, A., Prasad, S., Reece, L.M., Singh, N., Maurya, P.K., Cho, J., 2019. Fluoride contamination, health problems and remediation methods in Asian groundwater: A comprehensive review. Ecotoxicology and Environmental Safety 182.

CHAPTER 2: CITRIC ACID MODIFIED GRANULAR ACTIVATED CARBON FOR ENHANCED DEFLUORIDATION[1]

2.1. Introduction

Fluoride (F^-) is an anionic constituent found naturally in groundwater. The most common source of groundwater fluoride is weathering of fluoride bearing minerals such as fluorite, fluorospar, cryolite, theorapatite, phosphorite, apatite, topaz, villiaumite, sepiolite, and palygorskite present in rocks (Yadav et al., 2018). Drinking water is the major pathway for fluoride to the human body (Meenakshi & Maheshwari, 2006). Intake of fluoride within the permissible limit is beneficial for human health in the production and maintenance of healthy teeth and bones (Biswas et al., 2017). However, prolonged exposure to excess fluoride can lead to dental and skeletal fluorosis (Gbadebo, 2012). Chronic intake of fluoride may also lead to muscle fiber degeneration, low hemoglobin level, excessive thirst, skin rashes, depression, growth retardation, and DNA structural changes (Gbadebo, 2012; Meenakshi & Maheshwari, 2006).

The world health organization (WHO) recommends a threshold of 1.5 mg F^-/L in drinking water (WHO, 2004). The USEPA has established a maximum contaminant level (MCL) of 4 mg/L to prevent skeletal fluorosis and a secondary maximum contaminant level (SMCL) of 2 mg/L to protect against dental fluorosis [1](USEPA, 2009). Fluoride above the permissible limit is found in groundwater in many areas of the world including large parts of Africa, China, India, Sri Lanka,

[1] This chapter has been published as a peer-reviewed paper in *Chemosphere* (2020).
Rashid, U.S., Bezbaruah, A.N., 2020. Citric acid modified granular activated carbon for enhanced defluoridation. *Chemosphere* 252, 126639.

The material in this chapter was co-authored by Umma Rashid and Dr. Achintya Bezbaruah. Umma had primary responsibility for conceptualizing the study and developing the methodology. Umma designed and conducted all batch experiments, analyzed all the data, and investigated the results. Umma also drafted and revised all versions of this chapter. Dr. Achintya served as superviser, proofreader and checked all the results and analysis conducted by Umma.

and some parts of the USA. More than 260 million people worldwide use drinking water with fluoride exceeding the WHO limit (Amini et al., 2008).

Because of the use of contaminated irrigation water, fluoride has been found in crops like barley and rice (e.g., about 2 mg kg^{-1}), and roots including taro, yams, and cassava (Biswas et al., 2017; Mumtaz et al., 2015). Some canned fish such as salmon, and sardines may also be the sources of fluoride in humans (Mumtaz et al., 2015). High fluoride levels (10-10,000 mg/L) have also been found in the industrial wastewater from glass and ceramic production, semiconductor manufacturing, electroplating units, coal-fired power stations, beryllium extraction plants, brick, and iron works, and aluminum smelters (Bhatnagar et al., 2011).

Advanced technologies including membrane and ion exchange are used to effectively (>98%) remove fluoride in drinking water to bring the level within WHO limit (Yadav et al., 2018). Adsorption processes are attractive and very extensively used. Such systems are easy to design, cost-effective, and typically have good removal efficiency (Bhatnagar et al., 2011). Activated carbon (AC) is used as an adsorbent for a wide variety of organic contaminants due to its large surface area, high porosity, and high catalytic activity (Li et al., 2002). However, AC has a very low removal capacity for inorganic pollutants such as fluoride (Mugisidi et al., 2007). Surface modification is required to improve fluoride removal by AC. Various types of modifiers such as sulfuric acid (H_2SO_4), nitric acid (HNO_3), metals, and metal oxides have been used to modify activated carbon for enhanced defluoridation (Brunson & Sabatini, 2016; Daifullah et al., 2007; Getachew et al., 2015; Ma et al., 2009; Ramos et al., 1999; Ravulapalli & Kunta, 2017; Yadav et al., 2018). However, these modifiers are not suitable for use in rural communities as they are not locally available, involve complicated preparation and handling processes, and there are

possibilities of additional toxicity being introduced to the treated water (e.g., from leaching of metal).

Developing an alternate AC surface modifier was felt necessary, and such a modifier should be easy to handle, prepare and the required raw materials should be locally available. It has been reported in the literature that citric acid (CA) is an effective modifier for AC to improve removal of contaminants such as copper (Chen et al., 2003), aniline (Zhou et al., 2014), lead (Wang et al., 2013), uranium (Zou & Zhao, 2012) and methylene blue (Xu et al., 2016). Citric acid introduces an additional carboxylic functional group onto the AC surface. Citric acid is a commercially (retail) available weak organic acid which is widely used in food industries, specifically for food preservation. When CA is heated, it will dehydrate to yield a reactive anhydride which can react with hydroxyl group present in AC to form carboxylated AC. In this study, we have developed citric acid modified granular activated carbon (CAGAC) and investigated its fluoride capacity under environmentally relevant conditions and proposed the possible removal mechanisms. The desorption of fluoride from spent (saturated with fluoride) CAGAC over an extended period of time was studied.

2.2. Materials and methods

2.2.1. Materials

Granular activated carbon (Black Diamond®, Commercial grade, Marineland, VA), citric acid ($C_6O_7H_8$, ACS grade, BDH), sodium hydroxide (NaOH, ACS grade, BDH), hydrochloric acid (HCl, EMD Millipore), sodium sulfate (Na_2SO_4, Sigma-Aldrich), sodium fluoride (NaF, Spectrum), sodium chloride (NaCl, EMD Millipore), potassium nitrate (KNO_3, Sigma-Aldrich), sodium bicarbonate ($NaHCO_3$, Sigma-Aldrich), potassium dihydrogen phosphate (KH_2PO_4, EMD Millipore), and natural organic matter (NOM) [Suwannee River NOM, reverse osmosis (RO)

isolation, International Humic Substances Society (IHSS) (Denver, Colorado)] were used as received unless otherwise specified.

2.2.2. Preparation of citric acid modified granular activated carbon

Commercial grade granular activated carbon (GAC, 4 g) was mixed with 0.3 M citric acid (CA, 25 mL) in a 125 mL flask and mixed for 45 min with a magnetic stirrer to ensure that GAC was impregnated with CA. The CA-impregnated GAC was dehydrated at 50 °C for 24 h and then kept in a hot air oven at 100 °C for another 24 h. When heated, CA dehydrates to yield a reactive anhydride which reacts with the hydroxyl groups present on the GAC surface to form carboxylated GAC (Wang et al., 2013) (Fig. A1, Appendix A). The citric acid modified granular activated carbon (CAGAC) was washed with DI water several times to remove excess CA and then dried at 100 °C for 24 h. The dried CAGAC was stored in glass bottles at room temperature (22±2 ^{o}C) for future use.

2.2.3. Characterization of GAC and CAGAC

The concentration of carboxylic functional group in CAGAC was determined as per Karnitz et al. (Karnitz et al., 2007) and Gurgel et al. (Gurgel et al., 2008). Briefly, 100 mg modified samples were treated with 100 mL of 0.01 M NaOH in a 250 mL beaker and stirred in a magnetic stirrer for 1 h; the content was filtered and the filtrate (25 mL) was titrated with HCl (0.01 M) solution to determine –COOH concentration (Eq. 2.1).

$$C_{COOH} = \left[\frac{(C_{NaOH} * V_{NaOH}) - (4 * C_{HCl} * V_{HCl)}}{M}\right] \quad (2.1)$$

In Eq. 1, C_{COOH} is the concentration of carboxylic functions per gram of GAC (mM/g), C_{NaOH} is the concentration of NaOH used (mM), C_{HCl} is the concentration of HCl used (mM), V_{NaOH} is the volume of NaOH (L), V_{HCl} is the volume of HCl used in titration (L), and M is the mass (g) of CAGAC.

The XPS analysis was done with powdered samples packed into small wells of 3 mm diameter and 3 mm deep. High-resolution scans were made for C, O, and F. The settings were; Pass energy = 50 eV, Dwell Time = 50 ms, Step size = 0.1 eV for a total of 10 scans per sample. The flood gun was also turned on during the analysis to prevent the accumulation of charges in the samples.

Nitrogen adsorption-desorption isotherms studies were conducted at -196 ^{o}C using a Quantachrome Nova-e surface area analyzer. Before the measurements, the samples were outgassed at 120 ^{o}C in a vacuum for 6 h. The Brunauer-Emmett-Teller (BET) method was utilized to calculate the specific surface area. The pore-size distributions were derived from the adsorption branch of the isotherms using the Barrett-Joyner-Halenda (BJH) method. The total pore volume was estimated from the amount adsorbed at a relative pressure of $P/P_0 = 0.95$.

2.2.4. Batch studies

Batch studies were conducted to find out the fluoride removal efficiency of CAGAC under different environmental conditions (pH, temperature, and the presence of coexisting ions and compounds) using an initial fluoride concentration (C_0) of 10 mg/L.

Fluoride stock solution (1000 mg/L) was prepared by dissolving 2.21 g of oven-dried (100 ^{o}C) NaF in 1000 mL DI water. The stock solution was diluted with DI water to get the required fluoride concentration in the test solution. All experiments (except the temperature study) were performed at room temperature and a pH of 6.5-7.0 in batch reactors (40 mL glass vials with caps fitted with silicon septa) using 20 mL of 10 mg/L F^- solution and 400 mg CAGAC. The initial pH of the solution was adjusted using 0.1 M HCl or 0.1 M NaOH; no buffer was used, and additional pH adjustment was not done during the experiment. Controls were run with unmodified GAC and the blanks (only fluoride solution, no GAC). The reactors were rotated for 24 h in a custom-made

end-over-end shaker at 28 rpm to minimize mass transfer resistance. After 24 h, the reactors were taken out and centrifuged, and the supernatant was analyzed for fluoride using a UV-VIS spectrophotometer (Hach, Model DR 5000, Method 8029). Separate calibration for fluoride was done for each batch. The removal efficiency (% removal) of fluoride was calculated as $(C_0 - C_e)/C_e$*100% (where C_0 is the initial and C_e is equilibrium fluoride concentration).

For kinetics studies, three different initial fluoride concentrations were used (5, 10, and 20 mg/L). Sacrificial reactors were withdrawn at predetermined time intervals (0, 15, 30, 60, 120, 240, and 480 min) and fluoride in the bulk solution was measured. Isotherm studies were conducted using multiple initial fluoride concentrations (5-100 mg/L) and the bulk solution fluoride concentration was measured at 24 h. Similarly, the effect of pH was evaluated by changing the initial pH in the range of 2 to 10 using 0.1 M HCl or NaOH, and the bulk solution fluoride concentration was measured after 24 h. The possible interferences by the co-existing ions and compounds on fluoride removal by CAGAC were investigated using different concentrations (0, 10, 100 mg/L) of sulfate (SO_4^{2-}), phosphate (PO_4^{3-}), bicarbonate (HCO_3^-), and nitrate (NO_3^-). The fluoride adsorption performance of CAGAC was evaluated at different temperatures (4-45 ^oC) in an environmental chamber (Walk-in Environmental Chamber, Darwin Chambers Company, USA). The data from this study were used to determine the thermodynamic parameters [Gibbs free energy (ΔG^o), change in enthalpy ($\Delta H°$), and change in entropy (ΔS^o)].

2.2.5. Quality control and statistical analysis

All experiments were conducted in triplicates and the average values are reported here along with the standard deviations. One-way ANOVA analysis was done to determine statistically significant differences in data sets and Tukey's pairwise comparison was used to identify the data that were significantly different.

2.3. Results and discussions

2.3.1. Characterization of GAC and CAGAC

The amount of carboxyl group on the surface increased by 47% when GAC (initial 1.26 ± 0.01 mM of carboxyl group/g of GAC) was functionalized to get CAGAC (post-treatment 1.85 ± 0.03 mM of carboxyl group/g of CAGAC) indicating the successful introduction of carboxyl group on the GAC surface. The BET surface area, however, was reduced by 14% (from 359.1 to 306. 8 m^2/g) when GAC was functionalized. Similarly, the BJH pore volume also decreased (from 0.2554 to 0.1938 cm^3/g) during the functionalization. Citric acid (CA) molecules have a small molecular diameter and can easily enter pores of GAC, and, so, the reductions in surface area and pore volume were observed. However, the BJH pore radius of the modified CAGAC (1.569 nm) was slightly higher than the unmodified GAC (1.563 nm). This increase can be attributed to the solubilization and washing off of impurities by CA during modification. Others reported similar changes in surface area, pore volume, and pore radius in biochar modified with citric acid (Chen et al., 2003; Xu et al., 2016).

XPS analyses indicate that the carbon (C) content was 95.52% and oxygen (O) was 4.48% in unmodified GAC and that changed to 90.70% C and 9.07% O in the CAGAC. The higher O1s/C1s after the modification indicates that the amount of oxygen-containing functional group increased on the surface of CAGAC due to the introduction of CA (Xu et al., 2016).

2.3.2. Optimal citric acid dose for GAC modification

Optimization of initial citric acid (CA) concentration needed for GAC surface modification was done based on fluoride removal by CAGAC. Different types of CAGAC were prepared with eight different concentrations of CA (0-1.0 M). The fluoride removal efficiency increased with the increase of CA concentration till 0.3 M (Fig. A2, Appendix A) beyond which there was no

significant improvement in fluoride removal. Fluoride removal efficiency increased from 30% (0 M CA) to 60% for 0.1 M CA-modified GAC, and then there was a significant improvement to 70% between 0.2 and 0.3 M CA ($p = 0.000$). Beyond 0.3 M CA, the fluoride removal efficiency remained unchanged (70%). Based on this experiment we decided that the optimum concentration of CA to modify GAC for enhanced fluoride removal is 0.3 M.

2.3.3. Kinetic studies

CAGAC exhibited significantly more aqueous fluoride removal compared to unmodified GAC for all three fluoride concentrations (5, 10, 20 mg F^-/L, $p = 0.000$; Fig. 2.1). The fluoride removal efficiencies of 83% (C_0 = 5 mg/L) and 70% (C_0 = 10 and 20 mg/L) were achieved within 4 h and remained unchanged after that. However, the unmodified GAC removed <30% fluoride in the first 15 min and remained unchanged after that for all three concentrations. Most fluoride removal by CAGAC was achieved in the first 1 h (77% for C_0 = 5 mg/L and 59% for 10 and 20 mg/L).

The data from the kinetic studies were fitted onto pseudo-first-order and pseudo-second-order models to find out the mechanism of adsorption and potential rate-controlling steps such as mass transport and chemical reactions. The batch kinetic experimental data were fitted to. The data fitted the pseudo-second-order model (Eq. 2.2) better ($R^2 = 0.999$, Table A1, Appendix A).

$$\frac{t}{q_t} = \frac{1}{k_2 q_e^2} + \frac{t}{q_e} \tag{2.2}$$

To make sure that the reaction followed pseudo-second-order, we compared the model predicted and experimentally found equilibrium adsorption capacities. The pseudo-second-order model predicted equilibrium adsorption capacities ($q_{e,cal}$) are in agreement (1.2-5.5% variation) with the experimental values ($q_{e,exp}$) (see Supplementary Material). In contrast, the values of $q_{e,\,cal}$

estimated from the pseudo-first-order model are markedly different (43.9-67.4% variation) from the experimental $q_{e,exp}$ values.

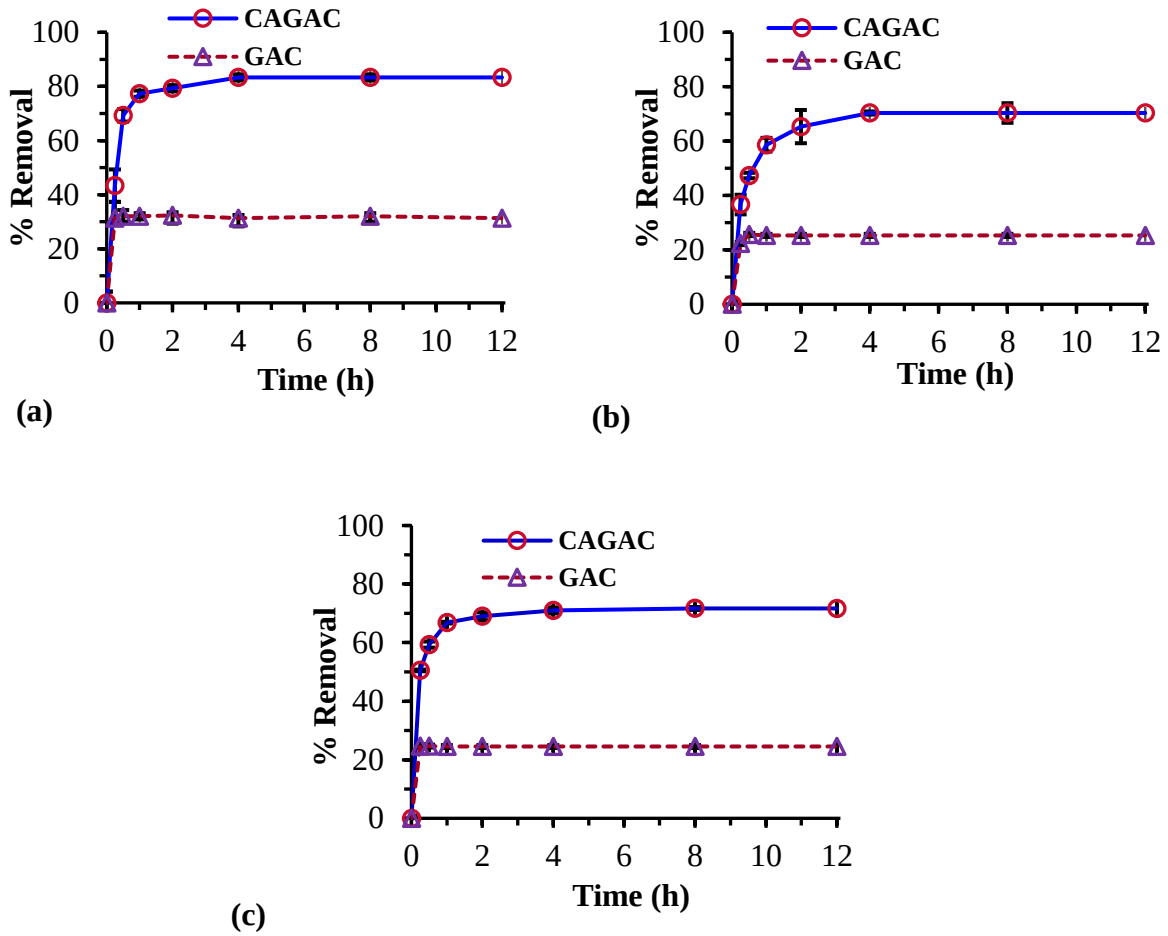

Figure 2.1. Removal of fluoride by GAC and CAGAC when the initial fluoride concentration (C_0) was (a) 5 mg/L; (b) 10 mg/L; and (c) 20 mg/L. The fluoride removal kinetic was fast in the first 30 min, then slowed down to reach equilibrium in 4 h in each case. The data points are connected with straight lines for ease of reading only and they do not represent trendlines. The vertical error bars indicate ± standard deviations.

In a pseudo-second-order reaction, the rate-limiting step is chemisorption involving valence forces through sharing or exchange of electrons between the sorbent and the sorbate (Sun et al., 2013). The adsorption of fluoride onto a porous solid (adsorbent) typically takes place via three distinct pathways (after (Fan et al., 2003)): (1) diffusion or transport of fluoride from bulk solution to the external surface of the adsorbent (external mass transfer), (2) gradual uptake of

fluoride onto the adsorbent's external surface and (3) transfer of adsorbed fluoride into the internal surfaces of the porous solids (intra-particle diffusion).

To elucidate the mechanism of fluoride removal by CAGAC and to find out if diffusion is the rate-controlling step, the experimental data were fitted into the intra-particle diffusion model (Eq 2.3, K_p is the intra-particle diffusion rate in mg g^{-1} $min^{-0.5}$).

$$\text{Adsorption capacity } \left(\frac{\text{mg}}{\text{g}}\right) \text{ at time t,} \qquad q_t = K_p t^{0.5} \tag{2.3}$$

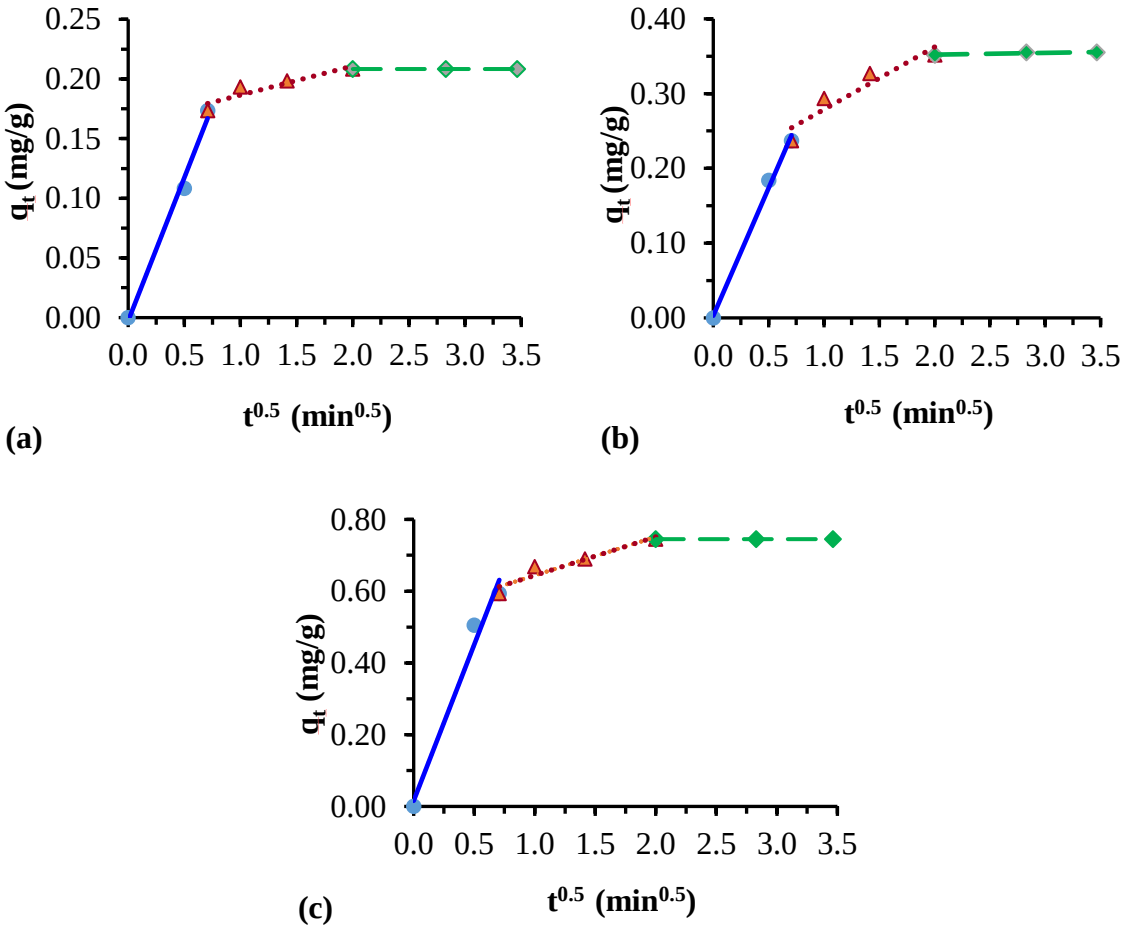

Figure 2.2. Plots for the intra-particle diffusion kinetic equation for fluoride adsorption onto CAGAC for an initial fluoride concentration (C_0) of (a) 5 mg/L; (b) 10 mg/L; (c) 20 mg/L. Here, q_t is the adsorption (mg fluoride per g CAGAC) capacity at time t. Multi-linearity was observed in the plots which indicate that intra-particle diffusion is not the only rate-determining step for fluoride removal.

If intra-particle diffusion is the only rate-determining step then the plot of q_t vs $t^{0.5}$ will pass through the origin (Weber & Morris, 1963). In this work, however, the plot of q_t vs $t^{0.5}$ has shown multi-linearity for all the concentrations of fluoride (Fig. 2.2). This indicates three distinct steps in the fluoride adsorption process: (1) The initial sharp linear portion (solid line) indicates the external mass transport across the boundary layer; (2) The second step (dotted line) is the gradual adsorption where intra-particle diffusion is rate-limiting; (3) the third step (dashed line) indicates the equilibrium stage where intra-particle diffusion slows down (Ma et al., 2009). If the gradual adsorption line (step 2) passes through the origin when extended, then intra-particle diffusion is the rate-limiting step (Ma et al., 2009). However, with the data from the current study, the line does not pass through the origin indicating that the fluoride adsorption onto CAGAC is controlled by both intra-particle diffusion and surface adsorption (Ma et al., 2009).

2.3.4. Adsorption isotherm

The maximum adsorption capacity (experimental) of CAGAC was found to be 1.65 mg/g whereas GAC showed an adsorption capacity of 0.88 mg/g only (Fig. 2.3). Based on comparison with other activated carbon-based material reported in the literature (Table 2.1.), it can be seen that CAGAC has better or similar fluoride adsorption capacity compared to activated carbon treated with the other acids (0.39-1.65 mg/g, Table 2.1). Metal impregnated/modified activated carbon showed better fluoride adsorption capacity than CAGAC. However, these metal modifiers are not locally available in small/rural communities, involve a complicated preparation process, and there are possibilities of additional toxicity from leaching of metal and, therefore, not suitable for use (Mondal & George, 2015).

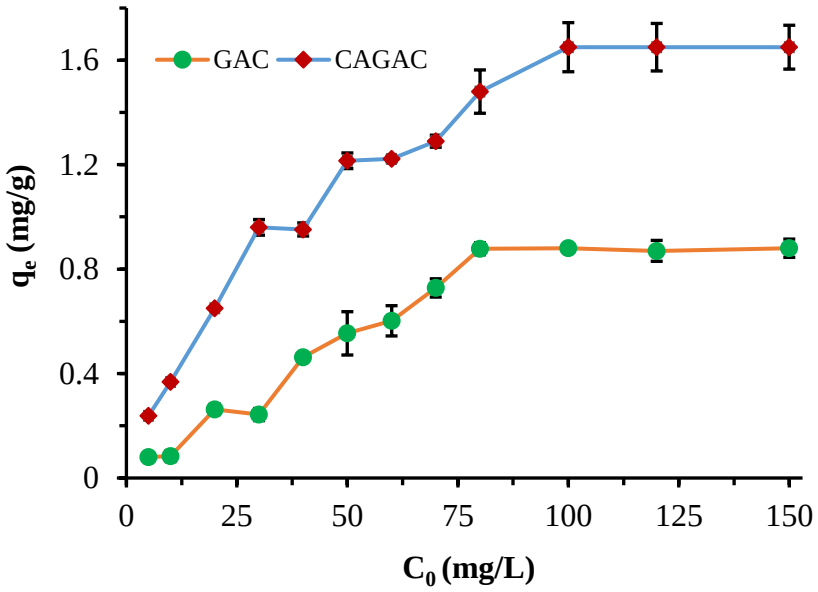

Figure 2.3. Adsorption isotherm study with CAGAC. The Maximum fluoride adsorption capacity of CAGAC was found to be 1.65 mg/g, whereas GAC has a maximum adsorption capacity of 0.88 mg/g only. The vertical error bars indicate ± standard deviations.

Adsorption isotherms for fluoride onto CAGAC were further investigated to understand the mechanisms. Freundlich and Langmuir isotherms were used. The Freundlich equation applies to heterogeneous sorption where sorption is multisided (Eq. 2.4). Whereas, the Langmuir isotherms assume homogenous surface, monolayer coverage, and the sorption of each sorbate molecule onto the surface has equal sorption activation energy (Eq. 2.5). Another very important parameter of Langmuir isotherm is the dimensionless constant R_L (Eq. 2.6), which can reveal if the adsorption is favorable or not.

$$q_e = K_F C_e^{\frac{1}{n}} \tag{2.4}$$

$$q_e = \frac{bq_m C_e}{1 + bC_e} \tag{2.5}$$

$$R_L = \frac{1}{1+bC_0} \tag{2.6}$$

In Eqs. 4-6, q_e (mg/g) is the equilibrium adsorption capacity, K_F (mg/g) is the Freundlich affinity coefficient, C_e (mg/L) is the fluoride concentration at equilibrium, 1/n is Freundlich

linearity constant, q_m (mg/g) is the maximum adsorption capacity, b is the Langmuir constant related to the affinity of the binding sites for fluoride ions, C_0 is the initial fluoride concentration.

Table 2.1. Comparison of fluoride removal by different activated carbon-based adsorbents.

Material	q_m (mg/g)	Treatment/ Modifier Used	pH	Interfering Ions	Source
AC modified with acids only					
H_2SO_4-AC	0.39-0.45	H_2SO_4	2.0	NR	(Getachew et al., 2015)
AIC-300 carbon	1.07	Aluminum	3.5	NR	(Ramos et al., 1999)
ABC	1.15	H_2SO_4	6	NR	(Yadav et al., 2013)
HNO_3-ACBFR	1.2-1.65	HNO_3	7.0	PO_4^{3-}, HCO_3^-	(Ravulapalli & Kunta, 2017)
CAGAC	**1.65**	Citric Acid	6.5	No interference	**This work**
GAC[a]	0.88	No acid used	6.5	Not tested	**This work**
AC modified with metals					
ZICNSC	1.83	Zirconium	7.6	NR	(Alagumuthu & Rajan, 2010a)
ZIGNSC	2.32	Zirconium	3	HCO_3^-	(Alagumuthu & Rajan, 2010b)
GAC-MnO_2	2.24	Manganese oxide	5.2	NR	(Ma et al., 2009)
Metal salt-GAC	1.57-11.1	Aluminum Sulfate, Aluminum Chloride, Iron Nitrate, Iron Chloride	NR	NR	(Brunson & Sabatini, 2016)
ZIWSC	6.38	Zirconium	3	NR	(Rajan & Alagumuthu, 2013)
$KMnO_4$-GAC	15.5	$KMnO_4$	2	NR	(Brunson & Sabatini, 2016; Daifullah et al., 2007)

H_2SO_4-AC = H_2SO_4 treated activated charcoal prepared from banana peel and coffee husk; **AlC-300 Carbon** = Aluminum impregnated carbon; **ABC** = Activated bagasse carbon; **GAC-MnO_2**= Manganese oxide-coated granular activated carbon; **Metal-GAC** = Metal amended granular activated carbon; **HNO_3-ACBFR** = Nitric acid-treated active Carbon derived from the Barks of *Ficus racemosa* (Common name: small cluster fig); **ZIGNSC** = zirconium-impregnated groundnut shell carbon; **ZIWSC** = zirconium-impregnated walnut shell carbon; **ZICNSC** =zirconium-impregnated cashew nut shell carbon; **NR** = pH/Interference study was not reported in the paper;
[a]Used as the control.

In this study, the value of 1/n in Freundlich was between 0 and 1 which indicates favorable adsorption (Table 2.2). While R_L between 0 and 1 tells us that the adsorption process is favorable, $R_L > 1$ indicates unfavorable adsorption. In this study, the value of R_L for Langmuir isotherm was less than one and greater than 0 ($1>R_L>0$) for different initial fluoride concentrations (5-100 mg/L) indicating that fluoride adsorption onto CAGAC is favorable. Both Langmuir and Freundlich isotherms have similar R^2 values and it is difficult to conclude which isotherm describes the experimental data better. Also, Langmuir and Freundlich isotherm cannot distinguish between physical and chemical adsorption. So, Dubinin-Radushkevich (D-R) isotherm (Eq. 2.7) was used to further analyze the adsorption data. The D-R isotherm does not assume a homogenous surface or a constant adsorption potential like Langmuir isotherm.

$$q_e = q_m \exp(-B\varepsilon^2) \tag{2.7}$$

In Eq. 7, q_m is the maximum adsorption capacity, B a constant related to the adsorption energy (mol^2/kJ^2), and, ε is the potential energy of the surface [$\varepsilon = RT \ln\left(1 + \frac{1}{C_e}\right)$]; R is the gas constant (kJ mol^{-1} K^{-1}), C_e is the fluoride concentration at equilibrium and T is the absolute temperature. The constant B gives the free energy E (kJ mol^{-1}, $E = \frac{1}{\sqrt{2B}}$) for the transfer of 1 mol of solute from infinity to the surface of adsorbent (Onyango et al., 2004).

To generate the necessary data for the D-R isotherm, a set of batch adsorption studies were conducted at different temperatures (4-45 ^oC). An initial F^- concentration of 10 mg/L was used in this study. The plot of lnq_e vs ε^2 for F^- sorption onto CAGAC (Fig. 2.4) indicated that the D-R isotherm has a better R^2 value compared to Langmuir and Freundlich isotherms. The mean free energy E was found to be 10.45 kJ mol^{-1} (Table 2.2). The magnitude of E is useful for estimating

Table 2.2. Adsorption isotherm parameters associated with fluoride adsorption onto CAGAC.

Langmuir Isotherm			**Freundlich Isotherm**			**D-R Isotherm**	
b	R^2	R_L	K_F	1/n	R^2	E (kJ mol^{-1})	R^2
0.104	0.959	0.09-0.66	0.349	0.357	0.956	10.45	0.983

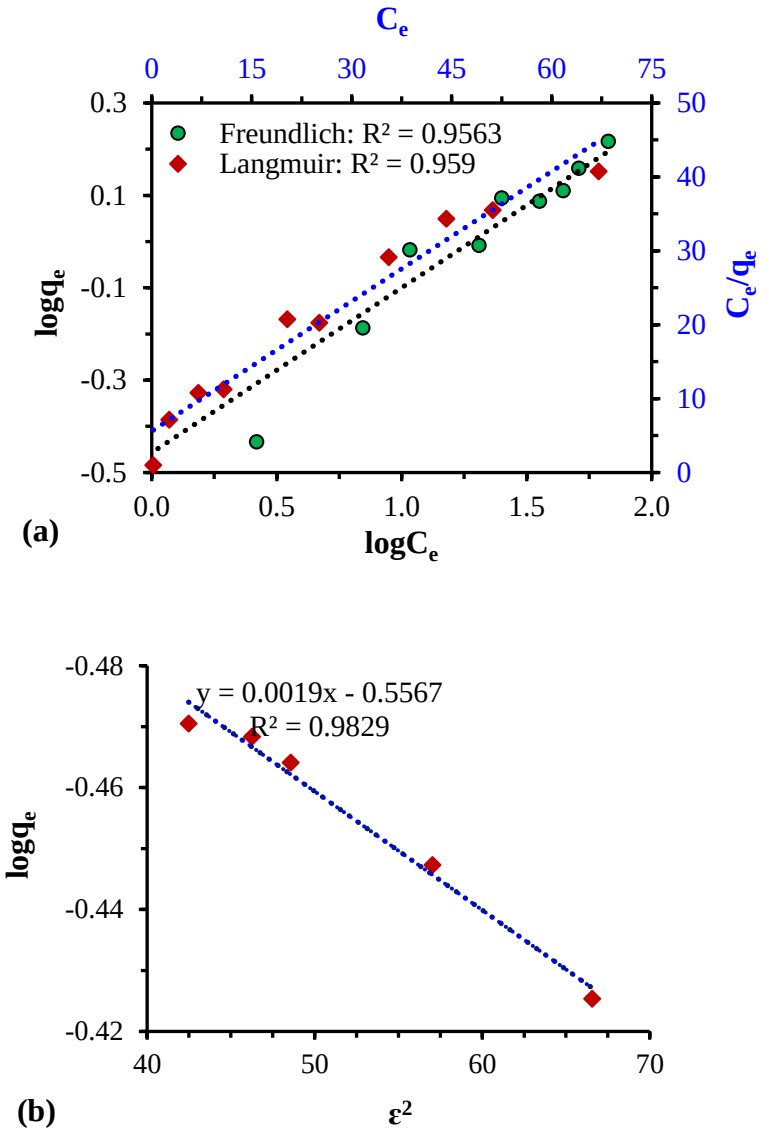

Figure 2.4. (a) Freundlich ($\log q_e$ vs. $\log C_e$) and Langmuir (C_e/q_e vs. C_e), and (c) D-R isotherms models fitted with the experimental data. The dotted lines represent the best-fits [Black: Freundlich; Blue: Langmuir in (a)]. Here, q_e is the equilibrium adsorption capacity, C_e is the fluoride concentration at equilibrium, and Ɛ is the potential energy of the surface.

the type of adsorption. If E < 8 kJ mol^{-1} then the mechanism of adsorption is "physisorption", for E > 16 kJ mol^{-1}, the mechanism of adsorption is "chemisorption", and for 8 ≤ E ≤ 16 kJ $mole^{-1}$, the adsorption mechanism is ion exchange (Basar, 2006; Daifullah et al., 2007; Ravulapalli & Kunta, 2017; Tahir & Rauf, 2006). The value of E for F^- adsorption onto CAGAC was found to be 10.45 kJ mol^{-1} indicating that the mechanism of adsorption is ion exchange.

2.3.5. Effects of pH

The initial pH of the solution plays an important role in controlling adsorption at the water-adsorbent interface. The effect of pH on fluoride adsorption was determined by varying pH from 2 to 10 while keeping other parameters unchanged. A wide range of pH was used in this study to investigate the F^- removal mechanisms although a pH as low as 2 or as high as 10 is atypical in water and wastewater samples. Fluoride removal was almost 100% at pH 2 but got reduced as the pH increased (59% at pH 10, Fig. 2.5a). The point-of-zero-charge (PZC) of CAGAC was determined to be 4.89 (Fig. 2.5b) meaning that the net surface charge is zero at that pH, and the adsorbent surface is positively changed at pH below the PZC and negatively changed above the PZC. If pH < PZC, the adsorption of fluoride is favorable via electrostatic force and if pH > PZC, then it is not favorable (Singh et al., 2017). In this study, at pH < PZC, the fluoride removal efficiency increased with the decrease of pH (Fig. 2.5a), and the fluoride removal was achieved possibly via a two-step ligand exchange reaction (Eq 8-10, (Daifullah et al., 2007)) mechanism:

$$-COH + H^+ \leftrightarrow -COH_2^+ \tag{2.8}$$

$$-COH_2^+ + F^- \leftrightarrow -CF + H_2O \tag{2.9}$$

Net reaction:

$$-COH + F^- + H^+ \leftrightarrow -CF + H_2O \tag{2.10}$$

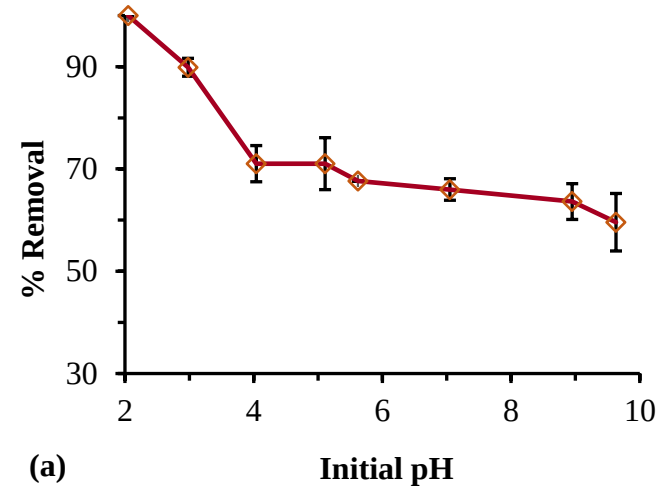

(a)

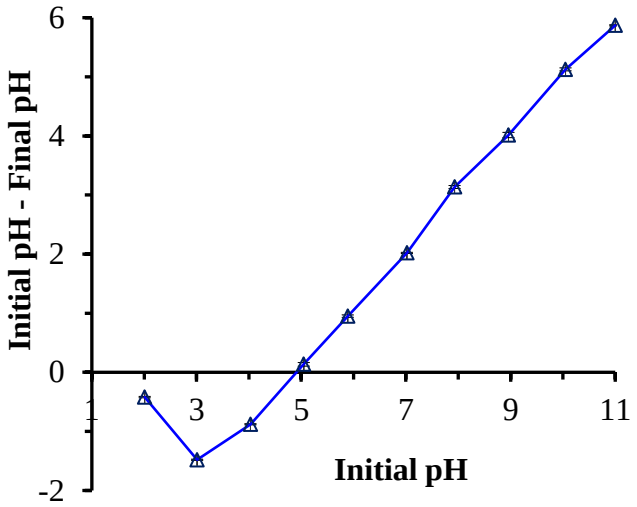

(b)

Figure 2.5. (a) Effect of initial solution pH on fluoride adsorption onto CAGAC; (b) Point-of-zero-charge of CAGAC was found to be 4.89. The Highest removal was obtained at pH = 2. The data points are connected with straight lines for ease of reading only and they do not represent trendlines. The vertical error bars indicate ± standard deviations.

However, at pH > PZC there is no major decrease in fluoride removal efficiency (Fig. 2.5a) even though as per the PZC theory it should have been markedly reduced. This might have happened because the hydroxyl groups (OH^-) present on the CAGAC surface acted as ion exchangers and helped in the removal of fluoride (Eq. 11) (Mullick & Neogi, 2018; Wang &

Reardon, 2001). Fluoride is highly electronegative compared to OH^- and can replace the OH^- ion at the exchange site.

$$-COH + F^- \leftrightarrow -CF + H_2O \quad (2.11)$$

Alternatively, the negative change on the adsorbent surface at pH > PZC might have attracted sodium ions (Na^+), and Na^+ might have taken up fluoride from the solution (Ma et al., 2009) leading to the formation of an electric double layer (Eq. 12).

$$GAC - OH^-_{(solid)} + Na^+_{(aq)} + F^-_{(aq)} \leftrightarrow GAC - OH^-Na^+F^-_{(solid)} \quad (2.12)$$

The fluoride removal efficiency decreased to 63% when pH was raised to 9 and it decreased further to 59% at pH 10. This decrease can be attributed to the presence of excessive OH^- ions that competed with fluoride for adsorption sites on the CAGAC. These two ions (F^- and OH^-) can outcompete each other under the right environmental conditions because of their comparable charge (F^- = -1, OH^- = -1) and ionic radii (F^- = 0.133 nm, OH^- = 0.110 nm) (Gao et al., 2009).

2.3.6. Effects of co-existing ions

Contaminated groundwater contains other anions which can compete with fluoride in the adsorption process. Studies were carried out in the presence of potential interfering anions (NO_3^-, PO_4^{3-}, HCO_3^-, and SO_4^{2-}). Three different concentrations of each interfering ion (0, 10, and 100 mg/L) were independently tested with the initial fluoride concentration of 10 mg/L. No significant difference (p = 0.441-0.928) in fluoride adsorption was observed in the presence of up to 10 mg/L for all anions (Fig. 2.6a). At high concentration (100 mg/L), HCO_3^- did not impact but SO_4^{2-}, PO_4^{3-} and NO_3^- negatively impacted fluoride adsorption. PO_4^{3-} ion had a marked effect on fluoride removal and the removal efficiency decreased by 15% (from 70% removal with no PO_4^{3-} to 55% at 100 mg PO_4^{3-}-P/L). Similarly, the presence of 100 mg/L SO_4^{2-} decreased the fluoride

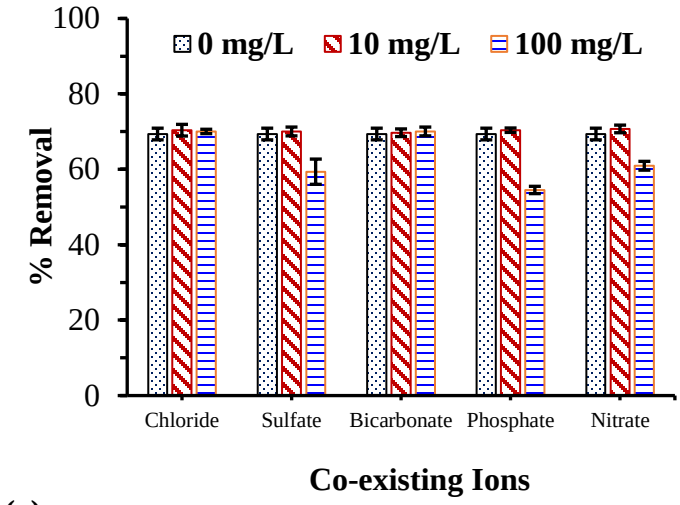

(a)

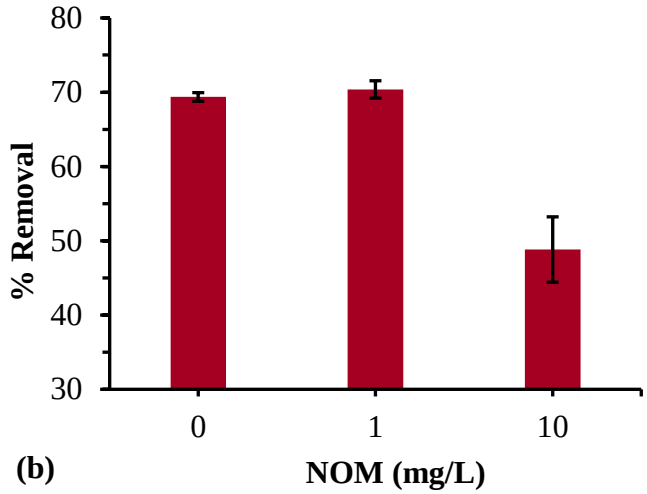

(b)

Figure 2.6. (a) Effect of co-existing ions on fluoride adsorption onto CAGAC. No significant interferences in fluoride removal were observed at environmentally relevant concentrations of the ions. The order of interference: $PO_4^{3-} > SO_4^{2-} > NO_3^-$. (b) Effect of NOM on fluoride adsorption onto CAGAC. There was no significant effect on fluoride removal at environmentally relevant concentrations of NOM. The vertical error bars indicate ± standard deviations.

removal efficiency by 11% and the decrease was 9% for NO_3^-. The typical concentration of PO_4^{3-} in groundwater is 0.001-3 mg/L (Thakur & Mondar, 2017; Zhao et al., 2010) and NO_3^- is 0.01-42 mg/L (Sailo & Mahanta, 2014; Thakur & Mondar, 2017). It is highly unlikely to have PO_4^{3-} and NO_3^- concentrations of 100 mg/L in groundwater and thus won't affect the fluoride removal efficiency. Additionally, the typical concentration of SO_4^{2-} in groundwater is 0.81-60 mg/L (Bhagawan et al., 2019; Sailo & Mahanta, 2014). So, SO_4^{2-} will also have a minimal effect on

fluoride removal efficiency. The order of interference was $PO_4^{3-} > SO_4^{2-} > NO_3^-$. The presence of trivalent PO_4^{3-} and divalent SO_4^{2-} might have introduced strong columbic repulsive forces which might have led to decreasing fluoride adsorption by the active sites (Amalraj & Pius, 2017). In addition, the degree of interference may also be related to the charge to radius ratio of the anions (PO_4^{3-} (3/3.40) > SO_4^{2-} (2/2.40) > NO_3^- (1/2.81) (Chigondo et al., 2018)). The higher the ratio, the more that specific anion will compete with fluoride for active sites (Zhao et al., 2010).

2.3.7. Effect of natural organic matter (NOM)

Natural organic matter (NOM) is found in all drinking water sources. It is a complex mixture of compounds formed from the breakdown of plants and animals present in the environment. The effect of NOM on the adsorption of fluoride onto CAGAC was investigated using Suwannee River NOM. The initial fluoride concentration was fixed at 10 mg/L whilst three different concentrations of NOM (0, 1, and 10 mg/L) were used. The presence of NOM at low concentration did not have any effect on fluoride removal (Fig. 2.6b). However, at high concentration (10 mg/L) the removal efficiency decreased by 20%. NOM consists of low molecular weight organic species such as carboxylic acid, amino acid, and proteins, and large molecular weight species such as humic and fulvic acid (Belin et al., 1993). At high concentrations, the negatively charged molecules (carboxylic acid and phenolic functionalities) present in NOM can compete with the fluoride for active sites on the adsorbent surface (Daifullah et al., 2007). The typical NOM concentration in groundwater is <1 mg/L (Metsamuuronen et al., 2014), and so fluoride removal by CAGAC will not be affected by the presence of NOM in groundwater.

2.3.8. Thermodynamic parameters

Thermodynamic studies were conducted to find out the feasibility of the fluoride adsorption process. Three relevant parameters, changes in (1) standard free energy (ΔG^o), (2)

standard enthalpy (ΔH^o), and (3) standard entropy (ΔS^o) were estimated based on the test data (Eq. 2.13−2.14 (Wang et al., 2017)):

$$lnK_0 = \frac{\Delta S^0}{R} - \frac{\Delta H^0}{RT} \quad (2.13)$$

$$\Delta G_o = -RTlnK_0 \quad (2.14)$$

In Eqs. 13-14, R is the universal gas constant (8.314 J/mol K), T is the absolute temperature in degree Kelvin (^oK) and K_0 is the thermodynamic equilibrium constant. The values of ΔH^o were calculated from the slope and ΔS^o from the intercept of Van't Hoff's plot (lnK_0 vs. 1/T), and ΔG^o was calculated (Table 2.3). The positive values of ΔH^o indicate that the adsorption of fluoride onto the CAGAC surface is endothermic in nature (Ravulapalli & Kunta, 2017). The negative values of $\Delta G°$ for all three temperatures indicate the spontaneous adsorption process (Mullick & Neogi, 2018). The value of $\Delta G°$ decreases with the increase of temperature which indicates that the adsorption process is more spontaneous at high temperature (Amalraj & Pius, 2017). The positive value of $\Delta S°$ represents the increase in disorder and randomness of the process at the solid/solution interface (Mullick & Neogi, 2018). Similar thermodynamic patterns were also reported for other adsorbents (aluminum hydroxide coated activated carbon, nitric acid modified activated carbon) used for fluoride removal (Amalraj & Pius, 2017; Ravulapalli & Kunta, 2017).

Table 2.3. Thermodynamic parameters associated with fluoride adsorption onto CAGAC.

ΔH^o (kJ mol^{-1})	**ΔS^o (kJ mol^{-1})**	**ΔG^o (kJ mol^{-1})**			
		283 ^{o}K	**293 ^{o}K**	**303 ^{o}K**	**313 ^{o}K**
6.549	0.029	-1.658	-1.948	-2.238	-2.528

2.3.9. Desorption study

For an adsorbent to be effective, it is very important that the adsorbed fluoride does not easily desorb out of the adsorbent over time. Desorption of fluoride from CAGAC over time was studied using fluoride saturated CAGAC over a 6-month period. Batches of CAGAC were

saturated with fluoride (400 mg CAGAC in 20 mL of 100 mg F^-/L solution in 40 mL glass vials and shaken in an end-over-end shaker for 24 h). The fluoride saturated CAGAC was separated by decanting the bulk solution. The fluoride concentration of the bulk solution was measured to estimate the fluoride adsorbed by CAGAC. The decanted fluoride solution was replaced with DI water and the vials are shaken in the end-over-end shaker for 24 h. The CAGAC was separated again from the solution by decanting the water, and the fluoride concentration of the bulk solution was measured and mass balance was conducted to find out the amount of fluoride desorbed at the end of the time period. This process was continued for 6 months and fresh DI water was used each time.

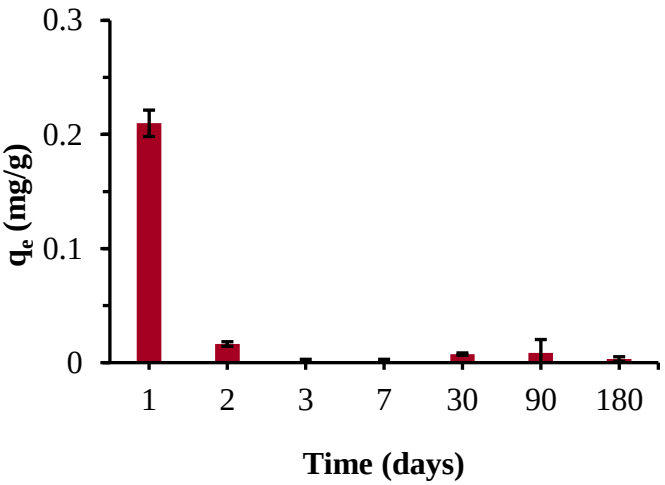

Figure 2.7. Desorption of fluoride from spent (fluoride saturated) CAGAC. The results indicated that fluoride was strongly bound to the surface of CAGAC.

The desorption study showed that ~12% of adsorbed fluoride got desorbed after the first day (Fig. 2.7). From the second day, only 0.05-0.1% adsorbed fluoride was found to desorb over each sampling interval over the 6-month period. The result indicates that fluoride is strongly bound to the surface of CAGAC. So, CAGAC is an effective and safe adsorbent for fluoride removal. CAGAC showed very poor desorption behavior, and materials with poor desorption behavior are difficult to be regenerated (Singh et al., 2017). However, poor desorption behavior is a positive

aspect of CAGAC as the adsorbed fluoride will not come out in the effluent from a filter even after its useful life is over (i.e., the adsorptive filter is exhausted) and, thus, will not aggravate the human health effect. This desorption study data should be taken with a caveat that the study was not aimed at evaluating the hazards of potential disposal of the used CAGAC medium, and for that separate studies have to be conducted.

Negligible desorption of the adsorbed fluoride is a requirement for an adsorption reaction to be pseudo-second-order kinetics (Xiao et al., 2018), and here we have met that requirement.

2.4. Conclusion

In this study, citric acid modified granular activated carbon (CAGAC) was prepared and its fluoride (fluoride) removal efficiency was evaluated. Additional functional groups were introduced on the GAC surface via citric acid (CA) incorporation and that increased the fluoride adsorption capacity of the activated carbon. The fluoride adsorption onto CAGAC followed the pseudo-second-order kinetics and Dubinin-Radushkevich (D-R isotherm). Over 70% of fluoride was removed in the first 60 min by CAGAC for all concentrations, whereas unmodified granular activated carbon (GAC) removed only 30%. The point-of-zero-charge (PZC) was 4.89 for CAGAC. However, CAGAC worked more or less the same over a wide range of pH which suggests that the removal mechanisms are controlled by both electrostatic interaction and surface adsorption. The fluoride removal efficiency by CAGAC remained the same in presence of interfering ions and organic matters at an environmentally significant concentration of co-existing ions. Thermodynamic data elucidate that the adsorption process is spontaneous and endothermic in nature. Desorption study over a 6-month period showed very negligible release of the adsorbed fluoride. The novelty of the work involves the use of commercial GAC and its modification with an easily available weak acid. Since fluoride is a health menace in many countries, the

development of such adsorbents using a weak acid will empower the affected people as they can potentially make this adsorptive medium in their own kitchen. Further, no or low interferences from other anions like chlorides, bicarbonates, and sulfates make it a suitable candidate for groundwater fluoride removal, while other available adsorbents are often adversely affected by these ions. The new medium has potential for immediate field applications.

2.5. References

Alagumuthu, G., Rajan, M. 2010a. Equilibrium and kinetics of adsorption of fluoride onto zirconium impregnated cashew nut shell carbon. Chemical Engineering Journal, 158(3), 451-457.

Alagumuthu, G., Rajan, M. 2010b. Kinetic and equilibrium studies on fluoride removal by zirconium (iv)-impregnated groundnut shell carbon. Hemijska Industrija, 64(4), 295-304.

Amalraj, A., Pius, A. 2017. Removal of fluoride from drinking water using aluminum hydroxide coated activated carbon prepared from bark of Morinda tinctoria. Applied Water Science, 7(6), 2653-2665.

Amini, M., Mueller, K., Abbaspour, K.C., Rosenberg, T., Afyuni, M., Moller, K.N., Sarr, M., Johnson, C.A. 2008. Statistical modeling of global geogenic fluoride contamination in groundwaters. Environmental Science & Technology, 42(10), 3662-3668.

Basar, C.A. 2006. Applicability of the various adsorption models of three dyes adsorption onto activated carbon prepared waste apricot. Journal of Hazardous Materials, 135(1-3), 232-241.

Belin, C., Quellec, C., Lamotte, M., Ewald, M., Simon, P. 1993. Characterization by fluorescence of the dissolved organic-matter in natural-water - application to fractions obtained by tangential ultrafiltration and xad resin isolation. Environmental Technology, 14(12), 1131-1144.

Bhagawan, D., Saritha, P., Shankaraiah, G., Himabindu, V. 2019. Fluoride Removal from Groundwater Using Hybrid Cylindrical Electrocoagulation Reactor. Journal of Water Chemistry and Technology, 41(3), 164-169.

Bhatnagar, A., Kumar, E., Sillanpaa, M. 2011. Fluoride removal from water by adsorption-A review. Chemical Engineering Journal, 171(3), 811-840.

Biswas, G., Kumari, M., Adhikari, K., Dutta, S. 2017. A Critical Review on Occurrence of Fluoride and Its Removal through Adsorption with an Emphasis on Natural Minerals. Current Pollution Reports, 3(2), 104-119.

Brunson, L.R., Sabatini, D.A. 2016. Methods for Optimizing Activated Materials for Removing Fluoride from Drinking Water Sources. Journal of Environmental Engineering, 142(2).

Chen, J.P., Wu, S.N., Chong, K.H. 2003. Surface modification of a granular activated carbon by citric acid for enhancement of copper adsorption. Carbon, 41(10), 1979-1986.

Chigondo, M., Paumo, H.K., Bhaumik, M., Pillay, K., Maity, A. 2018. Rapid high adsorption performance of hydrous cerium-magnesium oxides for removal of fluoride from water. Journal of Molecular Liquids, 265, 496-509.

Daifullah, A.A.M., Yakout, S.M., Elreefy, S.A. 2007. Adsorption of fluoride in aqueous solutions using KMnO4-modified activated carbon derived from steam pyrolysis of rice straw. Journal of Hazardous Materials, 147(1-2), 633-643.

Fan, X., Parker, D.J., Smith, M.D. 2003. Adsorption kinetics of fluoride on low cost materials. Water Research, 37(20), 4929-4937.

Gao, S., Cui, J., Wei, Z.G. 2009. Study on the fluoride adsorption of various apatite materials in aqueous solution. Journal of Fluorine Chemistry, 130(11), 1035-1041.

Gbadebo, A.M. 2012. Groundwater fluoride and dental fluorosis in southwestern Nigeria. Environmental Geochemistry and Health, 34(5), 597-604.

Getachew, T., Hussen, A., Rao, V.M. 2015. Defluoridation of water by activated carbon prepared from banana (Musa paradisiaca) peel and coffee (Coffea arabica) husk. International Journal of Environmental Science and Technology, 12(6), 1857-1866.

Gurgel, L.V.A., de Freitas, R.P., Gil, L.F. 2008. Adsorption of Cu(II), Cd(II), and Pb(II) from aqueous single metal solutions by sugarcane bagasse and mercerized sugarcane bagasse chemically modified with succinic anhydride. Carbohydrate Polymers, 74(4), 922-929.

Karnitz, O., Gurgel, L.V.A., de Melo, J.C.P., Botaro, V.R., Melo, T.M.S., Gil, R., Gil, L.F. 2007. Adsorption of heavy metal ion from aqueous single metal solution by chemically modified sugarcane bagasse. Bioresource Technology, 98(6), 1291-1297.

Li, L., Quinlivan, P.A., Knappe, D.R.U. 2002. Effects of activated carbon surface chemistry and pore structure on the adsorption of organic contaminants from aqueous solution. Carbon, 40(12), 2085-2100.

Ma, Y., Wang, S.-G., Fan, M., Gong, W.-X., Gao, B.-Y. 2009. Characteristics and defluoridation performance of granular activated carbons coated with manganese oxides. Journal of Hazardous Materials, 168(2-3), 1140-1146.

Meenakshi, Maheshwari, R.C. 2006. Fluoride in drinking water and its removal. Journal of Hazardous Materials, 137(1), 456-463.

Metsamuuronen, S., Sillanpaa, M., Bhatnagar, A., Manttari, M. 2014. Natural Organic Matter Removal from Drinking Water by Membrane Technology. Separation and Purification Reviews, 43(1), 1-61.

Mondal, P., George, S. 2015. A review on adsorbents used for defluoridation of drinking water. Reviews in Environmental Science and Bio-Technology, 14(2), 195-210.

Mugisidi, D., Ranaldo, A., Soedarsono, J.W., Hikam, M. 2007. Modification of activated carbon using sodium acetate and its regeneration using sodium hydroxide for the adsorption of copper from aqueous solution. Carbon, 45(5), 1081-1084.

Mullick, A., Neogi, S. 2018. Acoustic cavitation induced synthesis of zirconium impregnated activated carbon for effective fluoride scavenging from water by adsorption. Ultrasonics Sonochemistry, 45, 65-77.

Mumtaz, N., Pandey, G., Labhasetwar, P.K. 2015. Global Fluoride Occurrence, Available Technologies for Fluoride Removal, and Electrolytic Defluoridation: A Review. Critical Reviews in Environmental Science and Technology, 45(21), 2357-2389.

Onyango, M.S., Kojima, Y., Aoyi, O., Bernardo, E.C., Matsuda, H. 2004. Adsorption equilibrium modeling and solution chemistry dependence of fluoride removal from water by trivalent-cation-exchanged zeolite F-9. Journal of Colloid and Interface Science, 279(2), 341-350.

Rajan, M., Alagumuthu, G. 2013. Study of Fluoride Affinity by Zirconium Impregnated Walnut Shell Carbon in Aqueous Phase: Kinetic and Isotherm Evaluation. Journal of Chemistry.

Ramos, R.L., Ovalle-Turrubiartes, J., Sanchez-Castillo, M.A. 1999. Adsorption of fluoride from aqueous solution on aluminum-impregnated carbon. Carbon, 37(4), 609-617.

Ravulapalli, S., Kunta, R. 2017. Defluoridation studies using active carbon derived from the barks of Ficus racemosa plant. Journal of Fluorine Chemistry, 193, 58-66.

Sailo, L., Mahanta, C. 2014. Arsenic mobilization in the Brahmaputra plains of Assam: groundwater and sedimentary controls. Environmental Monitoring and Assessment, 186(10), 6805-6820.

Singh, K., Lataye, D.H., Wasewar, K.L. 2017. Removal of fluoride from aqueous solution by using bael (Aegle marmelos) shell activated carbon: Kinetic, equilibrium and thermodynamic study. Journal of Fluorine Chemistry, 194, 23-32.

Sun, L., Wan, S., Luo, W. 2013. Biochars prepared from anaerobic digestion residue, palm bark, and eucalyptus for adsorption of cationic methylene blue dye: Characterization, equilibrium, and kinetic studies. Bioresource Technology, 140, 406-413.

Tahir, S.S., Rauf, N. 2006. Removal of a cationic dye from aqueous solutions by adsorption onto bentonite clay. Chemosphere, 63(11), 1842-1848.

Thakur, L.S., Mondar, P. 2017. Simultaneous arsenic and fluoride removal from synthetic and real groundwater by electrocoagulation process: Parametric and cost evaluation. Journal of Environmental Management, 190, 102-112.

USEPA (U.S. Environmental Protection Agency), 2009. National Primary Drinking Water Regulations. Available at: https://www.epa.gov/ground-water-and-drinking-water/national-primary-drinking-water-regulations#Inorganic, Accessed date: November 2019.

Wang, M., Yu, X.L., Yang, C.L., Yang, X.Q., Lin, M.Y., Guan, L.T., Ge, M.F. 2017. Removal of fluoride from aqueous solution by Mg-Al-Zr triple-metal composite. Chemical Engineering Journal, 322, 246-253.

Wang, S.Y., Wang, L.P., Kong, W.Q., Ren, J.L., Liu, C.F., Wang, K., Sun, R.C., She, D. 2013. Preparation, characterization of carboxylated bamboo fibers and their adsorption for lead(II) ions in aqueous solution. Cellulose, 20(4), 2091-2100.

Wang, Y.X., Reardon, E.J. 2001. Activation and regeneration of a soil sorbent for defluoridation of drinking water. Applied Geochemistry, 16(5), 531-539.

Weber, W.J., Morris, J.C. 1963. Kinetics of adsorption on carbon from solution. Journal of the Sanitary Engineering Division, 89(2), 31-60.

WHO, 2004. Guidelines for drinking-water quality. Volume 1 recommendations, 3rd edn. World Health Organization, Geneva.

Xiao, Y., Azaiez, J., Hill, J.M. 2018. Erroneous Application of Pseudo-Second-Order Adsorption Kinetics Model: Ignored Assumptions and Spurious Correlations. Industrial & Engineering Chemistry Research, 57(7), 2705-2709.

Xu, Y., Liu, Y.G., Liu, S.B., Tan, X.F., Zeng, G.M., Zeng, W., Ding, Y., Cao, W.C., Zheng, B.H. 2016. Enhanced adsorption of methylene blue by citric acid modification of biochar derived from water hyacinth (Eichornia crassipes). Environmental Science and Pollution Research, 23(23), 23606-23618.

Yadav, A.K., Abbassi, R., Gupta, A., Dadashzadeh, M. 2013. Removal of fluoride from aqueous solution and groundwater by wheat straw, sawdust and activated bagasse carbon of sugarcane. Ecological Engineering, 52, 211-218.

Yadav, K.K., Gupta, N., Kumar, V., Khan, S.A., Kumar, A. 2018. A review of emerging adsorbents and current demand for defluoridation of water: Bright future in water sustainability. Environment International, 111, 80-108.

Zhao, X.L., Wang, J.M., Wu, F.C., Wang, T., Cai, Y.Q., Shi, Y.L., Jiang, G.B. 2010. Removal of fluoride from aqueous media by Fe3O4@Al(OH)(3) magnetic nanoparticles. Journal of Hazardous Materials, 173(1-3), 102-109.

Zhou, Y.B., Gu, X.C., Zhang, R.Z., Lu, J. 2014. Removal of Aniline from Aqueous Solution using Pine Sawdust Modified with Citric Acid and beta-Cyclodextrin. Industrial & Engineering Chemistry Research, 53(2), 887-894.

Zou, W.H., Zhao, L. 2012. Removal of uranium(VI) from aqueous solution using citric acid modified pine sawdust: batch and column studies. Journal of Radioanalytical and Nuclear Chemistry, 292(2), 585-595.

CHAPTER 3: *CITRUS AURANTIIFOLIA* JUICE AND ANALYTICAL GRADE CITRIC ACID MODIFIED GRANULAR ACTIVATED CARBON FOR DRINKING WATER DEFLUORIDATION: A COMPARISON STUDY

3.1. Introduction

The Millennium Development Goals (MDGs) targeted to reduce the number of people with lack of access to safe drinking water by half by 2015 (Clasen, 2012). Implementation of this target reduced the number of such people from 19% in 2000 to 11% in 2015 in the world (UN 2018, UNICEF 2015). The currently pursued Sustainable Development Goals (SDGs) adopted by the General Assembly of the United Nations call for action to ensure availability and sustainable management of water for all by the year 2030 (UN, 2015). More than 2.2 billion people around the world have no safely managed drinking water and about 663 million people are without basic drinking water (WHO & UNICEF, 2017). In developing countries, 1.5 million people die every year due to water-related diseases (WHO/UNICEF 2000). The availability of safe and accessible drinking water is a core criterion for improving the economic condition of a region. SDG 6.1 aims to achieve universal and equitable access to safe and affordable drinking water for all (UN 2015).

For most countries, the goal of achieving universal access to safe drinking water is a grand technological and economic challenge. The rural and remote communities are experiencing the worst situation in safe drinking water availability and supply, and they need special attention. Of the 663 million people in the world who do not have access to safe drinking water, 79% of them reside in rural areas (WHO & UNICEF, 2017). Implementation of water treatment technologies in rural and remote areas is a big challenge due to the dearth of resources, lack of organized community involvement, and high capital and maintenance cost of the units. A large percentage of water treatment projects in rural areas experience failure (Smith, 2011; Barnes et al., 2010). In

a 2009 survey of 28 villages by the UNICEF, only 4 out of 16 water treatment systems were found to be operating. The lack of locally available resources, non-availability of expertise for timely maintenance, and high operational and maintenance costs are cited reasons for such failures (Garfi et al., 2011). The development of sustainable water treatment systems has promoted the key to solve such inequity in rural areas (Behailu et al., 2017). Sustainability of water units can be achieved by adopting technologies that use locally available materials and the use of less complicated treatment processes to ensure affordable capital and maintenance costs and less or no major maintenance issues. The use of locally available resources would attract community involvement and also accrue direct and indirect economic benefits to the local people.

One of the major water contaminant affecting 260 million people in at least 27 countries with China, India, Kenya, South Africa, and Tanzania being worst affected (Table 3.1) (Amini et al., 2008; Yadav et al., 2019; Jagtap et al., 2012). In the USA, high fluoride level is found in New Mexico, Washington, Ohio, Iowa, and Virginia (Waterlogic, 2019). The World Health Organization advises a 1.5 mg/L limit for fluoride in drinking water (WHO, 2004). While the intake of fluoride within the permissible limit (1.5 mg/L) is beneficial for human bone and teeth health, prolonged or chronic exposure to excess fluoride leads to dental and skeletal fluorosis as well as cognitive impairment, muscle fiber degeneration, low hemoglobin level, excessive thirst, skin rashes, depression, growth retardation, and DNA structural changes (Biswas et al., 2017; Gbadebo, 2012; Meenakshi and Maheshwari, 2006; Yadav et al., 2019). In addition, kidney damage and low IQ levels have been reported in the affected areas (Yadav et al., 2019).

Table 3.1. Countries affected by high fluoride levels in groundwater used for drinking and cooking. The countries reported dental and skeletal fluorosis, cognitive impairment, and impacts on kidneys due to excess fluoride in drinking water (modified after Mumtaz et al. (Mumtaz et al., 2019).

Country	Population Affected	Reported Fluoride Level (mg/L)
India	66.64 million	0.5-69.7
Tanzania	49.25 million	8.0-12.7
Kenya	44.35 million	2.0-20.0
South Africa	41.9 million	13.0
China	26.68 million	21.5

Fluoride is a recalcitrant nucleophile and difficult to be completely remediated. Some current methods used for fluoride removal from drinking water include ion exchange, use of membranes, electrodialysis, and coagulation and precipitation (Yadav et al., 2018). The Nalgonda technique is one of the cost-effective defluoridation techniques and is used widely in India and neighboring countries for small community and household water treatment (Jagtap et al., 2012). It involves the addition of lime, alum, and bleaching powder to the water. However, this technique can remove only 18-33% of fluoride and convert a larger portion (67-82%) of ionic fluoride (F^-) to soluble aluminofluoride compounds (Al^{3+}-F^-) (Yadav et al., 2019). Aluminum ions and their fluoride complexes are known to be neurotoxins (Martyn et al., 1989; Strunecka and Patocka, 1999). Aluminum (alum) based fluoride removal techniques, though efficient, are not sustainable. Activated alumina (AA) is an excellent adsorbent of fluoride and is finding use in water treatment (Loganathan et al., 2013). However, AA is highly pH-dependent with the pH needed to be on the acidic side of 7 for effective fluoride removal (Bhatnagar et al., 2011). It is also reported that the dissolution of aluminum oxides/hydroxides from an AA system is unavoidable below pH 6 (Jagtap

et al., 2012) and therefore, poses a severe threat to human health (Martyn et al., 1989; Strunecka and Patocka, 1999).

The currently practiced methods can remove fluoride well but have drawbacks like high cost of installation and maintenance, need for technical supervision (e.g., pH adjustment and maintenance), and/or sludge generation (Yadav et al., 2019). These drawbacks (Table 3.2) make them unsuitable for adaption in rural, remote, and socio-economically challenged communities. A significant portion of people affected with highly fluoridated water are from rural and remote communities, and they do not have access to advanced defluoridation technologies due to techno-economic reasons. There is a need for the development of water treatment (defluoridation) technologies that are cost-effective and adaptable in such communities.

Table 3.2. Comparison of various methods for F^- removal (Yadav et al., 2018; Yadav et al., 2019).

Technique	Materials	Advantages	Disadvantages
Coagulation-Precipitation	CaO, MgO, Alum, Alum and Lime (CaO)	Affordable, Tested technique in actual field condition	Sludge generation, Chemical intensive, Concentration of Al^{3+} and SO_4^{2-} is high in treated water, High maintenance cost
Membrane Process	Reverse osmosis, Electrodialysis, and Nano filtration membranes	Effective method (Up to 98%), Good water quality, No chemicals are used (except to prevent membrane fouling), minimal interference	Expensive, Membrane fouling, Generation of concentrated brine solution, pH adjustment is needed after treatment
Ion-Exchange Process	Anionic exchanger	High removal efficiency (up to 95%), The taste of water does not change	Expensive, Interferences from other ions are common, Generates F^- concentrate, Chlorine level, and pH is high in treated water
Adsorption	Activated alumina, carbon, and fly ash, nano-based adsorbents	Effective method (removes up to 90%), Ease of operation, Local availability of adsorbent, Cost-effective	Interference from other ions, waste generation

Activated carbon (AC) is an effective adsorbent for removing a wide variety of organic contaminants due to its high porosity, large surface area, and catalytic behavior (Li et al., 2002). However, AC has a very low adsorption capacity for inorganic pollutants like fluoride (Mugisidi et al., 2007). Modification of the AC surface has improved its adsorption capacity for certain contaminants. Metal oxides and strong oxidants such as nitric acid, hydrogen peroxide, and potassium permanganate can be used to modify AC surface for enhanced fluoride adsorption (Ma et al., 2009; Getachew et al., 2015; Brunson and Sabatini, 2016; Ravulapalli and Kunta, 2017; Yadav et al., 2018). However, most of these modifiers (chemicals) are not locally available in rural and remote areas, the process is not easy to adopt, and is toxic and/or corrosive in nature (Mondal and George, 2015). The need to develop an alternative modifier for surface modification of AC for enhanced defluoridation has been felt necessary. Such modifiers should be locally available, less expensive, and easy to handle. Rashid and Bezbaruah (2020) used citric acid (CA, $C_6H_8O_7$) which is a weak organic acid to prepared CA modified granular activated carbon (CAGAC) for fluoride. This modification introduced more carboxyl groups on the GAC surface and increased its F^- adsorption capacity (Rashid and Bezbaruah, 2020). CA is a weak tricarboxylic acid commonly used as a food preservation and available even in a typical grocery store, and as such it easy to procure and its handling is easy. However, the use of CA does not necessarily close the loop completely specifically in remote communities as food preservation is not a traditional practice in these communities.

Citric acid is also found in citrus fruits (e.g., lemons and limes). Lime (*Citrus aurantiifolia*) juice contains citric acid, ascorbic acid, minerals, and sugars (Table B1, Appendix B) (Rangel et al., 2011). The citric acid concentration in lime juice varies from 0.2 M to 0.3 M and is ~8% of the dry fruit mass of lime (Penniston et al., 2008). Rashid and Bezbaruah (2020) optimized 0.3 M

analytical grade CA as a surface modifier for GAC and the molarity is in the range of typical CA concentration in lime juice. Citrus fruits are abundantly available in most tropical and subtropical countries with Brazil, China, India, Mexico, Spain and the United States, leading in their global production (Liu et al., 2012). The major lime and lemon exporters (with 1% of the more global share in 2019) included Argentina, Brazil, Chile, China, Colombia, Egypt, Italy, Mexico, Netherlands, South Africa, Spain, Turkey, and the United States (Workman, 2020). Citrus is a cash crop (Langgut, 2017) and is also cultivated in rural and remote areas across the globe. The relatively high CA content in lime juice and availability of lime (*Citrus aurantiifolia*) across the globe make lime an attractive sustainable alternative source for chemicals needed for AC modification for fluoride removal. In this study, the juice extracted from store-brought *Citrus aurantiifolia* was used to produce lime-modified granular activated carbon (LGAC), and the produced LGAC was evaluated its potential to remove aqueous fluoride. The fluoride adsorption behavior of LGAC, the removal kinetics, and the possible removal mechanisms as well as desorption of fluoride from the used LGAC were studied. The results from the LGAC studies were compared with those from CAGAC reported earlier by Rashid and Bezbaruah (2020). It was hypothesized that it would be possible to replace commercial CA with locally available lime juice for GAC surface modification and the produced LGAC would work as efficiently as or better than CAGAC for aqueous fluoride removal.

3.2. Experimental section

3.2.1. Materials

Granular activated carbon (Black Diamond®, Commercial Grade, Marineland, VA), sodium hydroxide (NaOH, BDH, ACS grade), hydrochloric acid (HCl, EMD Millipore, ACS), sodium sulfate (Na_2SO_4, Sigma-Aldrich, ACS), sodium fluoride (NaF, Spectrum, ACS), sodium

chloride (NaCl, EMD Millipore, ACS), potassium nitrate (KNO_3, Sigma-Aldrich, ≥99.0% pure), sodium bicarbonate ($NaHCO_3$, Sigma-Aldrich, ACS) and potassium dihydrogen phosphate (KH_2PO_4, EMD Millipore, ACS) were used as received unless otherwise specified. Limes (*citrus aurantiifolia*) were purchased from a local supermarket. The juice from the limes was extracted using a lime squeezer and used immediately for the experiments.

3.2.2. Citric acid content in lime juice

The CA content of fresh lime juice was determined through a titration for every batch of lime purchased from a local supermarket. Briefly, 25 mL of freshly squeezed and filtered (through 45 µm filter, VWR) lime juice was taken in a 250 mL Erlenmeyer flask and 75 mL of deionized (DI) water was added to it. A few drops (5-6 drops) of phenolphthalein indicator were added to the solution. After that, the solution was titrated with 1 M NaOH until the color of the solution turned into light pink color. The quantity of NaOH used was measured (V) and citric acid concentration was calculated using Eq. 3.1.

$$CCA = \left[\frac{(C_{NaOH}\ x\ V_{NaOH})}{3\ x\ V_{Lime}}\right] \tag{3.1}$$

In Eq. 1, C_{CA} is the concentration of citric acid (M), C_{NaOH} is the concentration of NaOH used in the titration (M), V_{NaOH} is the volume of NaOH used in the titration (L), and V_{Lime} is the volume of lime juice (L).

3.2.3. Preparation of lime modified granular activated carbon

The lime-modified GAC (LGAC) was prepared following the process described elsewhere for CA-modified GAC (CAGAC) (Rashid and Bezbaruah, 2020). Briefly, 4 g commercial-grade granular activated carbon (GAC) was mixed with 25 mL of fresh lime juice (filtered) in a 125 mL flask and shaken for 45 min using a magnetic stirrer to ensure that GAC is impregnated with the

lime juice. The impregnated GAC was dehydrated (50 °C, 24 h) and then dried in a hot air oven (100 °C, 24 h). When heated at 50 ^{o}C, the lime juice dehydrates and the citric acid (CA) in lime juice becomes a reactive anhydride that reacts with the hydroxyl groups present on the GAC surface to form carboxylated GAC (Rashid and Bezbaruah, 2020; Wang et al., 2013). The lime-modified granular activated carbon (LGAC) was then washed several times with DI water to remove excess juice and then dried again at 100 °C for 24 h. The dried LGAC was stored in glass bottles at room temperature (22±2 ^{o}C) for future use.

3.2.4. LGAC characterization

The concentration of carboxylic functional group (–COOH) on LGAC surface was determined as per Karnitz et al. 2007 (Karnitz et al., 2007) and Gurgel et al. 2008 (Gurgel et al., 2008). Briefly, 100 mg of LGAC (or GAC control) was treated with 100 mL of 0.01 M NaOH in a 250 mL beaker and stirred using a magnetic stirrer for 1 h. The content was then filtered and the filtrate (25 mL) was titrated with 0.01 M HCl to determine the –COOH concentration (Eq. 3.2).

$$C_{COOH} = \left[\frac{(C_{NaOH}\ x\ V_{NaOH}) - (4\ x\ C_{HCl}\ x\ V_{HCl})}{M}\right] \quad (3.2)$$

In Eq. 2, C_{COOH} is the concentration of carboxylic functional group in GAC (mM/g), C_{NaOH} is the concentration of NaOH (mM), C_{HCl} is the concentration of HCl (mM), V_{NaOH} is the volume of NaOH (L), V_{HCl} is the volume of HCl used in titration (L), and M is the mass (g) of LGAC.

Nitrogen adsorption-desorption isotherms experiments were performed at -196 ^{o}C using a Quantachrome Nova-e surface area analyzer. Before the measurements, the samples were outgassed at 120 ^{o}C in a vacuum for 6 h. The Brunauer-Emmett-Teller (BET) method was used to calculate the specific surface area of LGAC. The pore-size distributions were derived from the adsorption branch of the isotherms by the Barrett-Joyner-Halenda (BJH) method. The total pore volume was estimated from the amount nitrogen adsorbed at a relative pressure of $P/P_0 = 0.95$.

3.2.5. Fluoride adsorption experiments

Fluoride adsorption experiments were conducted to examine the adsorption isotherm, determine the kinetics of fluoride removal and investigate the fluoride removal efficiency of LGAC under different environmental conditions (pH, temperature, and the presence of coexisting ions). The sorption experiments were carried out in 40 mL glass vials (reactors) containing 20 mL of fluoride solution and 400 mg of the adsorbent (LGAC here), and the reactors were shaken in a custom-made end-over-end shaker at 28 rpm for 24 h. All experiments were conducted at room temperature at a pH of 6.5-7.0. The initial pH of the solution was adjusted using 0.1 M HCl or 0.1 M NaOH, and neither additional pH adjustments were made nor a pH buffer was used during the experiment. The reactors with the contents were centrifuged after 24 h, and the supernatant from each reactor was analyzed for fluoride using a UV-VIS spectrophotometer (Hach, Model DR 5000, Method 8029), and the fluoride removal efficiency was calculated (Eq. 3.3). Separate calibration for fluoride was done for each batch experiment.

$$\eta = \left[\frac{C_0 - C_e}{C_0}\right] X\ 100\% \tag{3.3}$$

In Eq. 3, η is the removal efficiency (%), and C_0 is the initial, and C_e is the equilibrium fluoride concentration (mg/L).

In the adsorption isotherm experiment, fluoride solution with different initial concentrations (5-150 mg/L) was used. The kinetic experiment was conducted using two different initial fluoride concentrations (5 and 20 mg/L). Sacrificial reactors were taken from the end-over-end shaker at fixed time intervals (0, 15, 30, 60, 120, 240, and 480 min) and the fluoride concentration in the bulk solution was measured. In isotherm and kinetic experiments, controls were run with unmodified GAC.

The effects of relevant environmental parameters on fluoride removal by LGAC were investigated at an initial fluoride concentration (C_0) of 10 mg/L. Each experiment was run for 24 h and the bulk solution fluoride concentration was measured at the end. The effect of pH on fluoride removal was evaluated using five different initial pH (2, 4, 6, 8, and 10). The influence of co-existing anions (sulfate (SO_4^{2-}), phosphate (PO_4^{3-}), bicarbonate (HCO_3^-), and nitrate (NO_3^-)) on fluoride adsorption was examined using individual co-existing anions (0, 10, and 100 mg/L). The fluoride removal efficiency of LGAC was also evaluated at different temperatures (4-45 ^oC) in an environmental chamber (Walk-in Environmental Chamber, Darwin Chambers Company, USA) to determine the thermodynamic parameters (Gibbs free energy (ΔG^o), change in enthalpy ($\Delta H°$) and change in entropy (ΔS^o)) of the adsorption process.

The fluoride adsorption behavior of LGAC was also compared with analytical grade citric acid modified granular activated carbon (CAGAC) using the results reported earlier (Rashid and Bezbaruah, 2020).

3.2.6. Quality control and statistical analysis

All experiments were conducted in triplicates and the average values are reported along with the standard deviations. One-way ANOVA analysis was used to determine statistically significant differences in the data sets, and Tukey's pairwise comparison was employed to identify the data that were significantly different.

3.3. Result and discussions

3.3.1. Citric acid content of lime juice

The citric acid concentration of lime juice was found to be in the range of 0.3 to 0.35 M (average values 0.31 ± 0.017 M, n = 24) and others reported similar (0.20 M−0.35 M) similar results (Penniston et al., 2008).

3.3.2. LGAC characterization

The amount of carboxyl group on the LGAC surface was 1.98 ± 0.12 mM carboxyl group /g of GAC) which is a 57% increase compared to unmodified GAC (1.26 ± 0.01 mM). This indicated the successful introduction of the carboxyl group on the GAC surface when treated with lime juice. Similar results were reported by Rashid and Bezbaruah. (Rashid and Bezbaruah, 2020) where carboxyl group content increased by 47% after the GAC was treated with citric acid.

The surface area of the materials was determined using the BET method and there was a 47% reduction in surface area when GAC was treated with lime (surface area in GAC = 359.1 m^2/g and LGAC = 187.89 m^2/g). Similarly, the BJH pore volume of LGAC (0.149 cm^3/g) was 42% lower than the unmodified GAC (0.255 cm^3/g). The BJH pore radius of LGAC (1.560 nm) was marginally reduced compared to the unmodified GAC (1.563 nm). The decrease in surface area, pore-volume, and BJH pore radius after modification can be attributed to the pore blockage by the constituents (ascorbic acid, malic acid, mineral, and sugar) of the lime juice as well as unreacted CA from lime that possibly did not get removed while washing with DI water. A similar observation was reported earlier for CAGAC and net reductions were 14% in surface area and 24% in pore volume (Rashid and Bezbaruah, 2020). While CAGAC was prepared with pure CA, LGAC was prepared with lime juice that contained constituents other than CA (Table B1, Appendix B), and so, there were more reductions in surface area and pore volume.

3.3.3. Adsorption isotherm

The maximum fluoride adsorption capacity (experimental) of LGAC was found to be 1.63 mg/g which is comparable with the maximum fluoride adsorption capacity of CAGAC (1.65 mg/g) but double that of unmodified GAC (0.88 mg/g) (Fig. 3.1). LGAC has better fluoride adsorption capacity compared to most of the other inorganic acid-modified activated carbon (Fig. 3.2). While

similar adsorption capacity can possibly be achieved with other acids, lime juice is non-toxic, non-corrosive, and the crop (lime) can be cultivated in most parts of the world or can be made available easily. Further, the CA modification process is very straightforward and simple and can be adopted by individual families and the LCAG production process can be completed in their kitchens.

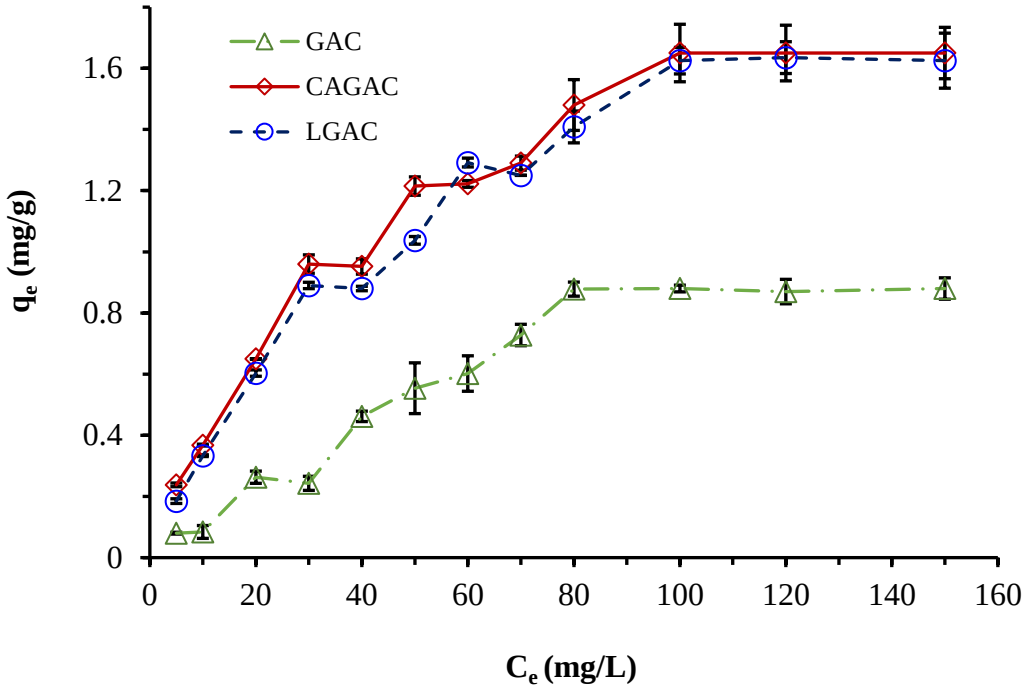

Figure 3.1. The maximum fluoride adsorption capacity of LGAC was found to be 1.63 mg/g that is almost the same as that of CAGAC (1.65 mg/g), but the unmodified GAC had a maximum adsorption capacity of 0.88 mg/g. The data points are joined by straight lines for ease of reading only and do not represent trendlines. The vertical error bars indicate ± standard deviations.

LGAC Fluoride adsorption isotherm data were fitted into three isotherm models (Freundlich, Langmuir, and Dubinin-Radushkevich). The R^2 values for Langmuir (0.952) and Freundlich (0.971) isotherms were very close (Fig. 3.3 and Table 3.3) and it was difficult to conclude which isotherm fits the data better. In Freundlich isotherm, the value of 1/n was found to be between 0 and 1 indicating that the fluoride adsorption onto LGAC is favorable (Table 3.3). However, neither Freundlich Langmuir nor isotherm can distinguish between physical and chemical adsorption, and so, Dubinin-Radushkevich (D-R) isotherm was used to further analyze

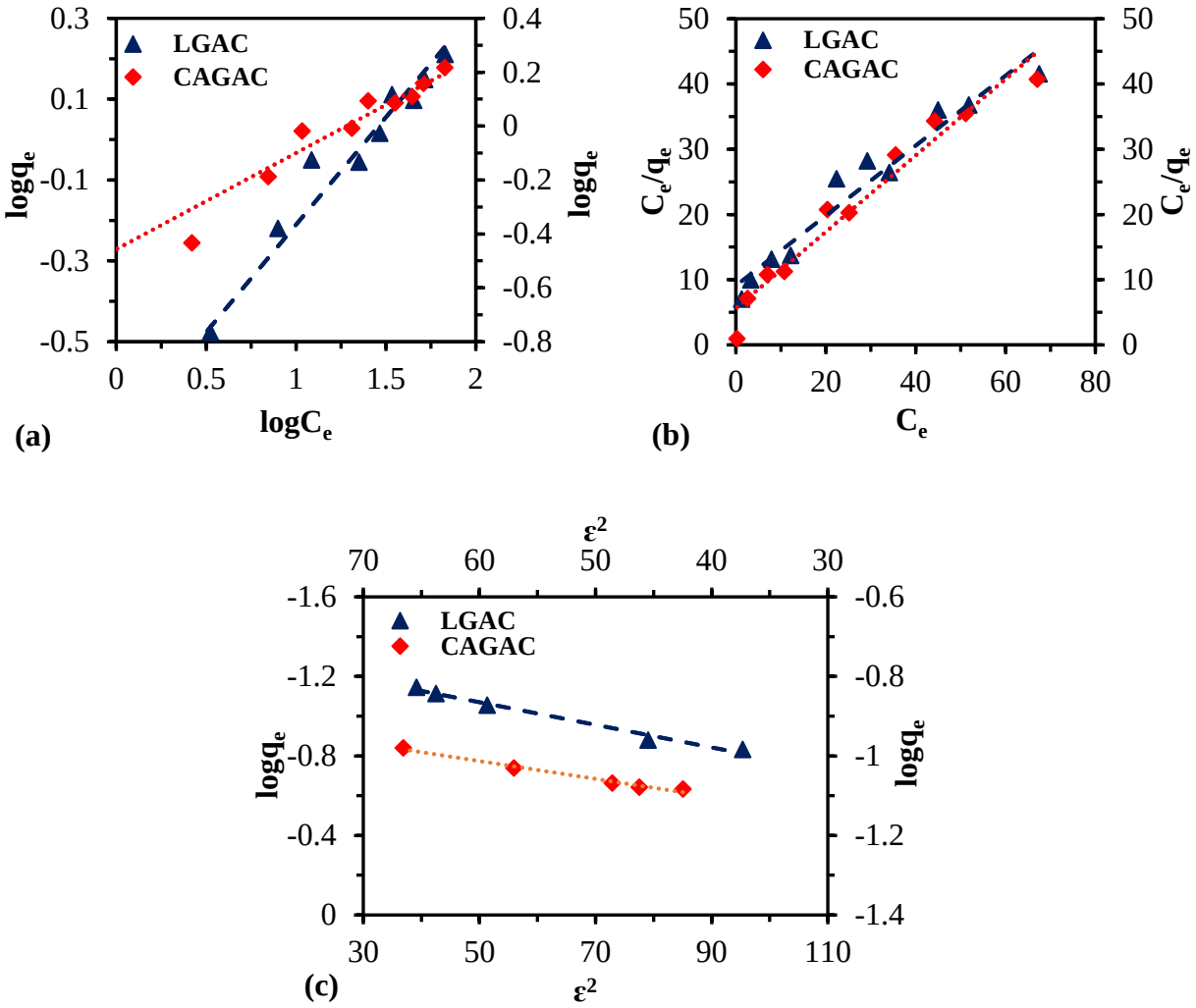

Figure 3.2. The experimental data were fitted into (a) Freundlich, (b) Langmuir, and (c) D-R isotherm models. The dotted lines in each plot represent the trendlines.

the adsorption data. The D-R plot of $\log_e(q_e)$ vs ε^2 (Fig. 3.3c) indicates a better R^2 value compared to Langmuir and Freundlich isotherms (Table 3.3). The value of the constant B obtained from the slope was used to calculate the mean free energy E (kJ mol^{-1}, $E = \frac{1}{\sqrt{2B}}$) and found to be 9.09 kJ mol^{-1} for LGAC indicating that the adsorption was governed by ion exchange (Rashid and Bezbaruah, 2020). The E value is useful to know the adsorption type. With E < 8 kJ mol^{-1}, the adsorption is "physisorption", for E > 16 kJ mol^{-1}, it is "chemisorption", and for 8 ≤ E ≤ 16 kJ $mole^{-1}$, the adsorption is ion-exchange (Basar, 2006; Daifullah et al., 2007; Ravulapalli and Kunta,

2017; Tahir and Rauf, 2006). The E value was 10.45 kJ mol^{-1} for CAGAC (Rashid and Bezbaruah, 2020) indicating same ion-exchange mechanism governs the process of fluoride removal in both LGAC and CAGAC.

Table 3.3. Adsorption isotherm parameters for fluoride adsorption onto LGAC and CAGAC.

Adsorbent	Langmuir model*				Freundlich model**			D-R model***	
	q_m (mg/g)	b	R^2	R_L	K_F	1/n	R^2	E (Kj mol^{-1})	R^2
LGAC	1.86	0.065	0.952	0.13-0.75	0.181	0.5316	0.972	9.09	0.984
CAGAC	1.71	0.104	0.959	0.09-0.66	0.349	0.357	0.956	10.45	0.983

* $q_e = K_F {C_e}^{1/n}$ ** $q_e = \frac{bQ_0C_e}{1+bC_e}$ *** $q_e = Q_0 \exp(-B\varepsilon^2)$ where q_e (mg/g) is the equilibrium adsorption capacity, C_e (mg/g) is the fluoride concentration at equilibrium, K_F (mg/g) is the Freundlich affinity coefficient, 1/n is the Freundlich linearity constant, Q_0 (mg/g) is the maximum adsorption capacity, b is the Langmuir constant, B a constant related to the adsorption energy (mol^2/kJ^2), and, ε the potential energy of the surface ($\varepsilon = RT \ln\left(1 + \frac{1}{C_e}\right)$; R is the universal gas constant (kJ mol^{-1} K^{-1}), and T is the absolute temperature).

3.3.4. Fluoride removal studies

Fluoride removal by LGAC was investigated with two different initial concentrations of F^- (5 and 20 mg/L) and the results showed that LGAC removed 88% (C_o = 5 mg/L) and 83% (C_o = 20 mg/L) F^- over an 8-h period while unmodified GAC removed <30% in the same time period (Fig. 3.4). When compared with the CAGAC data (Rashid and Bezbaruah, 2020), no significant difference (p = 0.263) between LGAC (88%) and CAGAC (83%) was found for fluoride removal when the initial fluoride concentration was 5 mg/L. However, a significant difference was observed when the initial fluoride concentration was 20 mg/L (83% for LGAC and 72% for CAGAC, p = 0.001). At high F^- concentration LGAC performed better and removed 11% more fluoride than CAGAC. Metals are known to facilitate fluoride removal (Yadav et al., 2018), and the presence of calcium, zinc, potassium, manganese, iron, and copper (Appendix B, Table B1) in lime juice might have helped in this study. These minerals might have been left in the pores of

LGAC even after washing. The bulk of the F^- removal (59-68%) happened rapidly in the first 30 min and then the process slowed down to reach a plateau (83-88%) at 4 h. While LGAC and CAGAC remained active till ~4 h, the unmodified GAC was exhausted in ~60 min.

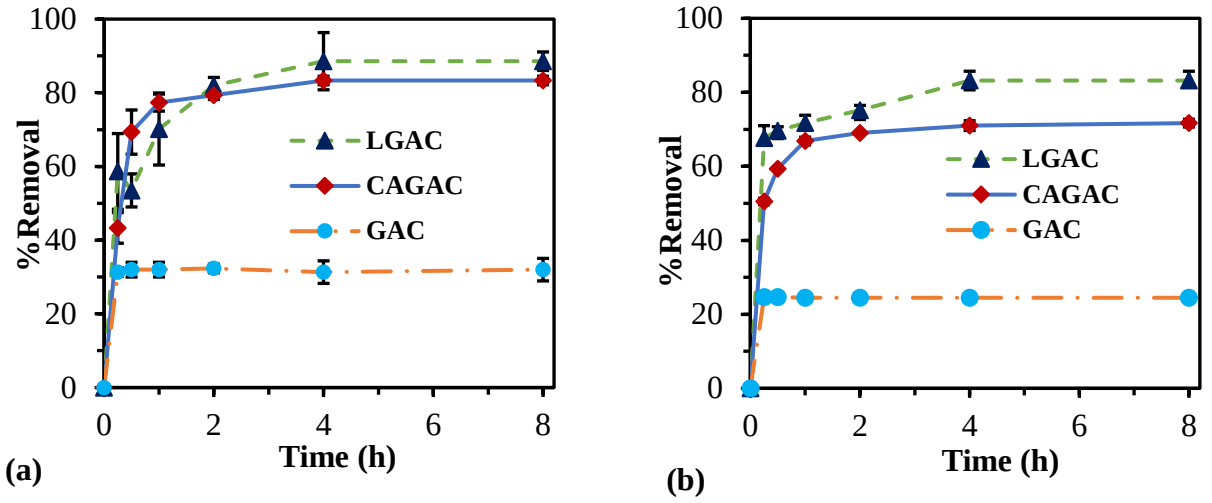

Figure 3.3. Removal of F^- by LGAC, CAGAC and GAC (a) Initial F^- concentration = 5 mg/L; (b) Initial F^- concentration = 20 mg/L. The fluoride removal by LGAC and CAGAC was rapid in the first 30 min, then slowed down and reached equilibrium in 4 h. The data points are connected with straight lines for ease of reading only and they do not represent trendlines. The vertical error bars indicate ± standard deviations.

The fluoride removal data fitted well to the pseudo-second-order model (Table 3.4). The experimental equilibrium adsorption capacities ($q_{e,exp}$, 0.221 mg/g for C_0 = 5 mg/L and 0.830 mg/g for C_0 = 20 mg/L) were found to be very close to the theoretical equilibrium adsorption capacities ($q_{e,cal}$) calculated from the pseudo-second-order model (0.228 mg/g for C_0 = 5 mg/L and 0.745 mg/g for C_0 = 20 mg/L). Given that the fluoride removal followed a pseudo-second-order reaction, the removal (adsorption) process was dominated by chemisorption involving ion exchange between the sorbate and adsorbent (Chi et al., 2017) which is in agreement with the results from CAGAC (Rashid and Bezbaruah, 2020).

To further investigate the rate-limiting step of the adsorption process, the intra-particle diffusion model (Eq. 3.4) was applied. The adsorption of fluoride onto porous solids usually

involves three essential steps (Fan et al., 2003): (1) external mass transfer (diffusion or transport of fluoride from the bulk solution to the external surface of adsorbent), (2) gradual uptake of fluoride onto the adsorbent (external) surface, and (3) intra-particle diffusion (transfer of adsorbed F^- into the internal surfaces of the porous solids).

$$\frac{t}{q_t} = \frac{1}{k_2 q_e^2} + \frac{t}{q_e} \tag{3.4}$$

Table 3.4. Comparison of kinetic parameters of fluoride adsorption onto LGAC and CAGAC(CAGAC data shown in parentheses*).

C_0 (mg/L)	Experimental	From the Models				
		Pseudo First-Order		Pseudo Second-Order		
	$q_{e,exp}$ (mg/g)	$q_{e,cal}$ (mg/g)	R^2	$q_{e,cal}$ (mg/g)	R^2	k ($mgL^{-1}s^{-1}$)
5	0.221 (CAGAC = 0.208*)	0.119 (CAGAC = 0.100*)	0.9316 (CAGAC = 0.793*)	0.239 (CAGAC = 0.218*)	0.995 (CAGAC = 0.994*)	0.00380
20	0.830 (CAGAC = 0.721*)	0.165 (CAGAC = 0.235*)	0.9841 (CAGAC = 0.868*)	0.753 (CAGAC = 0.730*)	0.999 (CAGAC = 0.999*)	0.00857

$q_{e,exp}$: Experimental equilibrium adsorption capacity; $q_{e,cal}$: Model predicted equilibrium adsorption capacity; *Data from Rashid and Bezbaruah, 2020.

The experimental data were fitted into the intra-particle diffusion model to find out whether diffusion was the rate-controlling step and also to elucidate the F^- removal mechanism by LGAC. If the plot of q_t vs $t^{0.5}$ passes through the origin, intra-particle diffusion is the only rate-determining step (Weber and Morris, 1963) and that was not observed here. In this work, the plot of q_t vs $t^{0.5}$ (from $q_t = K_p t^{0.5}$) have shown multi-linearity for both 5 and 20 mg/L of fluoride (Fig. B1, Appendix B) indicating that fluoride adsorption process happened in three distinct steps: (1) the external mass transport, (2) gradual adsorption (intra-particle diffusion being rate limiting here), (3) the equilibrium stage (intra-particle diffusion slowed down here) (Ma et al., 2009). We can infer that fluoride adsorption onto LGAC may involve both intra-particle diffusion and surface

adsorption. LGAC behaved exactly the same way as CAGAC reported earlier (Rashid and Bezbaruah, 2020).

3.3.5. Role of pH on fluoride removal

The point-of-zero-charge (PZC) of LGAC was determined to be 3.05 (Fig. B2, Appendix B) which is lower than CAGAC (PZC = 4.89, Rashid and Bezbaruah, 2020). This might have happened due to the presence of other compounds such as ascorbic acid, malic acid, minerals, and sugars in lime juice. The fluoride removal efficiency of LGAC increased from 56% (pH 2) to 98% (pH 4) as the pH was increased in the acidic range (Fig. 3.5) and then it decreased to 38% at pH 10. The LGAC behaved exactly the same way as CAGAC under different pH conditions except at the lowest pH. LGAC showed the maximum removal efficiency at pH = 4 (95%) and removal efficiency decreased at pH = 2 although the surface was positively charged at this pH (pH < PZC). This might have happened because of the formation of hydrofluoric acid (HF) at low pH ($H^+ + F^- \rightleftharpoons$ H-F) (Dash et al., 2015; Dhillon et al., 2016). When the pH was below 3.14, the dissociation of HF ($pK_a = 3.14$) decreased and thus less F^- was available in solution to get adsorbed by the LGAC. In the case of CAGAC, hydrofluoric acid might not have formed as the PZC of CAGAC is higher than the dissociation constant of hydrofluoric acid.

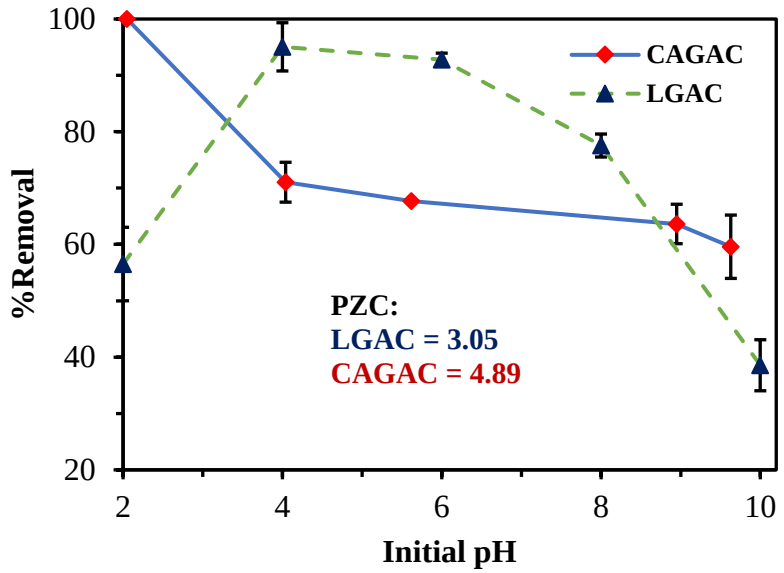

Figure 3.4. Effect of initial pH on fluoride adsorption onto LGAC and CAGAC. The Point-of-zero-charge (PZC) of LGAC was 3.05 and 4.89 for CAGAC. The highest removal was obtained at pH = 4. The data points are connected with straight lines for ease of reading only and they do not represent trendlines. The vertical error bars indicate ± standard deviations.

3.3.6. Effect of co-existing ions

For LGAC, the experiments reported for CAGAC (Rashid and Bezbaruah, 2020) were reproduced, and exactly the same patterns of interferences by NO_3^-, PO_4^{3-}, HCO_3^-, and SO_4^{2-} were observed. The anions had very little or no effect on fluoride adsorption when the interfering anions were present at low concentrations (10 mg/L, Fig. 3.6). While SO_4^{2-}, PO_4^{3-} and NO_3^- negatively affected the fluoride removal at high concentration (100 mg/L), HCO_3^- did not show any effect (additional discussion in Section B1, Appendix B). The inference by SO_4^{2-}, PO_4^{3-} and NO_3^- may not have a major impact as typical groundwater PO_4^{3-} concentration is ≤ 3 mg/L (Zhao et al., 2010; Thakur and Mondar, 2017), SO_4^{2-} concentration is ≤ 60 mg/L (Sailo and Mahanta, 2014; Bhagawan et al., 2019), and NO_3^- concentration is ≤ 42 mg/L (Sailo and Mahanta, 2014; Thakur and Mondar, 2017). There will be some decrease in fluoride removal by LGAC in some waters

where SO_4^{2-} and NO_3^- are present in high concentrations. Specifically, nitrate may be a concern where groundwater is excessively polluted by NO_3^- (Rezvani et al., 2019).

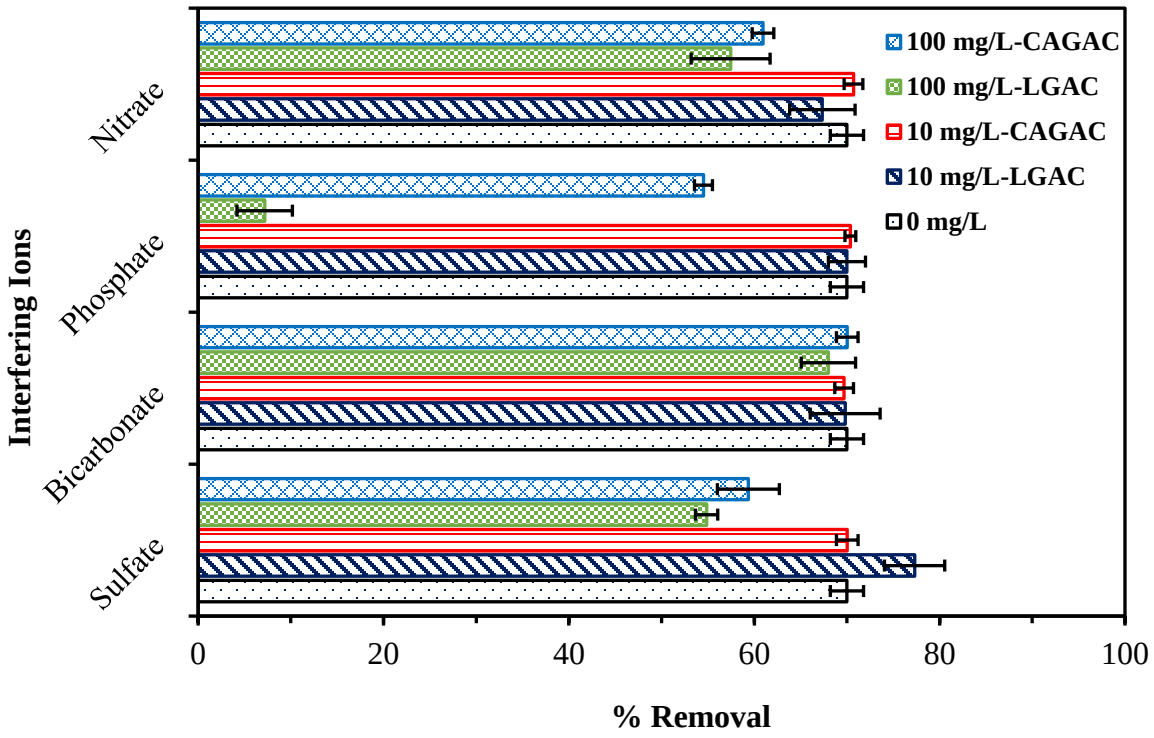

Figure 3.5. Effects of co-existing ions on fluoride adsorption onto LGAC and CAGAC. No significant interferences were observed by co-existing ions on fluoride adsorption onto both adsorbents (LGAC and CAGAC) at environmentally relevant concentrations of the interfering ions. While major interferences were observed at the highest concentration (100 mg/L) of the co-existing anions, such a high concentration is unlikely in typical groundwater. The initial fluoride concentration (C_0) was 10 mg/L and LGAC/CAGAC dose was 20 g/L. The horizontal error bars indicate ± standard deviations

3.3.7. Thermodynamic parameters

The comparison of the thermodynamic parameters for fluoride removal by LGAC (Section B2, Appendix B) indicated that LGAC performed better than CAGAC for fluoride removal. Fluoride adsorption onto both LGAC surface and CAGAC surface is endothermic in nature (standard enthalpy, ΔH^o = 25.704 kJ mol^{-1} for LGAC and 6.549 kJ mol^{-1} for CAGAC, Table 3.5) (Xu et al., 2016). Given that adsorption by LGAC has much higher standard enthalpy means that more heat energy is absorbed from the surrounding during the fluoride removal by LGAC

compared to CAGAC. The negative values of standard free energy (ΔG^o = –1.464 to –4.344 kJ mol^{-1} for LGAC) indicate the spontaneous nature of the fluoride adsorption onto LGAC (Mullick and Neogi, 2018). The higher values of ΔG^o for LGAC compared to CAGAC (–1.658 to –0.2.528 kJ mol^{-1}) indicate higher spontaneity of fluoride adsorption by LGAC. The positive value of standard entropy $\Delta S°$ (0.096 kJ mol^{-1}) is indicative of the affinity of LGAC for fluoride. The higher value (0.096 kJ mol^{-1}) of $\Delta S°$ for LGAC than CAGAC (and 0.029 kJ mol^{-1}) suggests a higher affinity for fluoride, and an increase in randomness at the interface of LGAC and fluoride solution during adsorption (Mullick and Neogi, 2018) (Xu et al., 2016).

Table 3.5. Thermodynamic parameters for the adsorption of fluoride onto LGAC and CAGAC.

Material	ΔH^o (kJ mol^{-1})	ΔS^o (kJ mol^{-1})	ΔG^o (kJ mol^{-1})			
			283 ^oK	293 ^oK	303 ^oK	313 ^oK
LGAC	25.704	0.096	-1.464	-2.424	-3.384	-4.344
CAGAC	6.549	0.029	-1.658	-1.948	-2.238	-2.528

3.3.8. Desorption study

A desorption study was conducted over a 6-month period to find out the stability of fluoride adsorbed onto LGAC (details in Section B3, Appendix B). After 24 h, there was ~18% desorption of the LGAC adsorbed fluoride compared to ~12% reported for CAGAC (Fig. 3.7). This desorption was observed possibly because of the detachment of the fluoride physically sorbed onto the LGAC. In the consecutive time points, fluoride desorption from LGAC always remained relatively high compared to CAGAC. In the 6-month period, a total ~37% of adsorbed fluoride came out from fluoride saturated LGAC and the corresponding number for CAGAC was 14%. It should be noted that in the first 3 days the desorption study was done in continuous shaking condition in an end-over-end shaker. Therefore, the chance of fluoride desorption is higher than the steady condition.

When used in a column, there will be steady flow with no shaking and apparent will have less desorption. Higher desorption by LGAC may be because of other elements/compounds present in the lime juice (Table B1, Appendix B). The unwashed/unreacted elements and compounds might have remained in the pores of GAC and might have adsorbed some fluoride. As the pure citric acid modified GAC showed poor desorption compared to LGAC, we can conclude that the fluoride attached to the other compound/elements of lime juice was loosely bound and came out during shaking. The F^- desorption behavior of LGAC can potentially be used as an advantage for the regeneration of the used LGAC. Additional research is needed to better understand this new adsorbent.

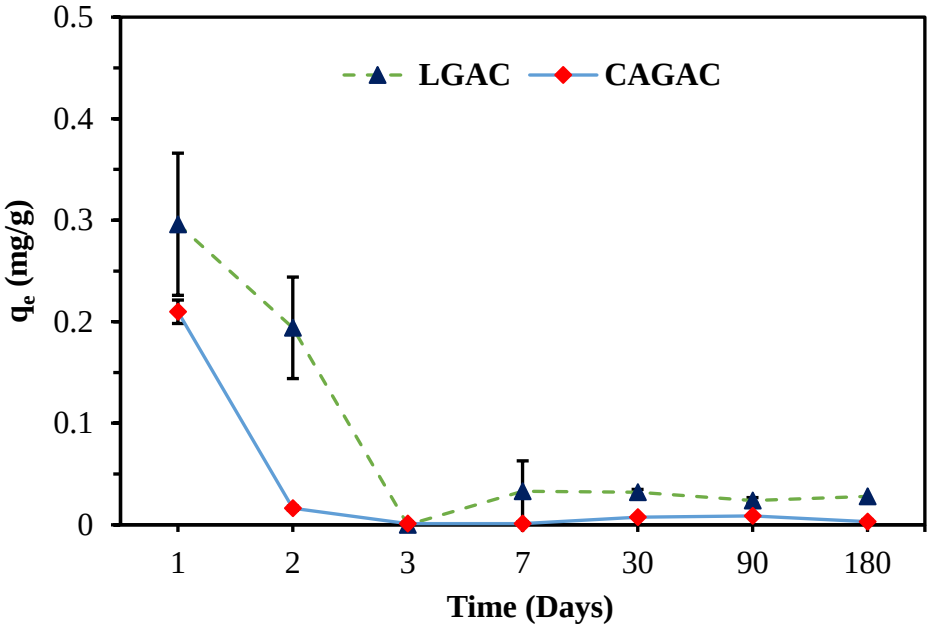

Figure 3.6. Desorption of fluoride from saturated LGAC and CAGAC over 6 months. A total of 37% of the adsorbed fluoride got desorbed from LGAC whereas CAGAC desorbed only 14% of adsorbed fluoride. The vertical error bars indicate ± standard deviations.

3.4. Conclusion

This study evaluated the fluoride removal efficiency of lime (*Citrus aurantiifolia*) juice modified granular activated carbon (LGAC). This study compared the performance of LGAC with

an analytical grade citric acid modified granular activated carbon (CAGAC). The maximum adsorption capacity of LGAC was found to be 1.63 mg/g and comparable to the adsorption capacity of CAGAC (1.65 mg/g). Kinetic study showed that both LGAC removed more than 70% fluoride and the equilibrium was achieved in 4 h as in the case of CAGAC and worked efficiency at environmentally relevant pH of 4-8. The co-existing anions present at environmentally relevant concentrations did not interfere in fluoride by LGAC. Both surface adsorption and intra-particle diffusion participated in the fluoride removal process. Lime is a locally available product in most rural and remote communities and that makes it an attractive surface modifier for GAC for enhanced fluoride removal. Further, lime is very safe to handle and easy to work with. Therefore, this material (LGAC) has the potential to be used in rural and remote communities for drinking water defluoridation with the caveat that there is a potential for the desorption of the adsorbed fluoride. The desorption problem can potentially be resolved by using additional adsorptive media (LGAC) in the adsorption columns (filters). The major contribution of this work is the development of a very simple activated carbon functionalization technique that can be easily adopted in remote, rural, and socio-economically challenged communities.

3.5. References

Amini, M., Mueller, K., Abbaspour, K.C., Rosenberg, T., Afyuni, M., Moller, K.N., Sarr, M., Johnson, C.A., 2008. Statistical modeling of global geogenic fluoride contamination in groundwaters. Environmental Science & Technology 42, 3662-3668.

Basar, C.A., 2006. Applicability of the various adsorption models of three dyes adsorption onto activated carbon prepared waste apricot. Journal of Hazardous Materials 135, 232-241.

Barnes, R.; Ashbolt, N., 2010. Development of a planning framework for sustainable rural water supply and sanitation: A case study of a Filipino NGO. *Int. Stud. Manag. Organ* 40, 78–98.

Behailu, B.M., Hukka, J.J., Katko, T.S., 2017. Service Failures of Rural Water Supply Systems in Ethiopia and Their Policy Implications. Public Works Management & Policy 22, 179-196.

Beltran-Aguilar, E.D., Barker, L., Dye, B.A., 2010. Prevalence and severity of dental fluorosis in the United States, 1999-2004. NCHS data brief, 1-8.

Bhagawan, D., Saritha, P., Shankaraiah, G., Himabindu, V., 2019. Fluoride Removal from Groundwater Using Hybrid Cylindrical Electrocoagulation Reactor. Journal of Water Chemistry and Technology 41, 164-169.

Bhatnagar, A., Kumar, E., Sillanpaa, M., 2011. Fluoride removal from water by adsorption-A review. Chemical Engineering Journal 171, 811-840.

Biswas, G., Kumari, M., Adhikari, K., Dutta, S., 2017. A Critical Review on Occurrence of Fluoride and Its Removal through Adsorption with an Emphasis on Natural Minerals. Current Pollution Reports 3, 104-119.

Brunson, L.R., Sabatini, D.A., 2016. Methods for Optimizing Activated Materials for Removing Fluoride from Drinking Water Sources. Journal of Environmental Engineering 142.

Chi, Y., Chen, Y., Hu, C., Wang, Y., Liu, C., 2017. Preparation of Mg-Al-Ce triple-metal composites for fluoride removal from aqueous solutions. Journal of Molecular Liquids 242, 416-422.

Clasen, T.F., 2012. Millennium Development Goals water target claim exaggerates achievement. Tropical Medicine & International Health 17, 1178-1180.

Daifullah, A.A.M., Yakout, S.M., Elreefy, S.A., 2007. Adsorption of fluoride in aqueous solutions using KMnO4-modified activated carbon derived from steam pyrolysis of rice straw. Journal of Hazardous Materials 147, 633-643.

Dash, S.S., Sahu, M.K., Sahu, E., Patel, R.K., 2015. Fluoride removal from aqueous solutions using cerium loaded mesoporous zirconium phosphate. New Journal of Chemistry 39, 7300-7308.

Dhillon, A., Sharma, T.K., Soni, S.K., Kumar, D., 2016. Fluoride adsorption on a cubical ceria nanoadsorbent: function of surface properties. Rsc Advances 6, 89198-89209.

Fan, X., Parker, D.J., Smith, M.D., 2003. Adsorption kinetics of fluoride on low cost materials. Water Research 37, 4929-4937.

Garfi, M., Ferrer-Marti, L., Bonoli, A., Tondelli, S., 2011. Multi-criteria analysis for improving strategic environmental assessment of water programmes. A case study in semi-arid region of Brazil. Journal of Environmental Management 92, 665-675.

Gbadebo, A.M., 2012. Groundwater fluoride and dental fluorosis in southwestern Nigeria. Environmental Geochemistry and Health 34, 597-604.

Getachew, T., Hussen, A., Rao, V.M., 2015. Defluoridation of water by activated carbon prepared from banana (Musa paradisiaca) peel and coffee (Coffea arabica) husk. International Journal of Environmental Science and Technology 12, 1857-1866.

Gurgel, L.V.A., de Freitas, R.P., Gil, L.F., 2008. Adsorption of Cu(II), Cd(II), and Pb(II) from aqueous single metal solutions by sugarcane bagasse and mercerized sugarcane bagasse chemically modified with succinic anhydride. Carbohydrate Polymers 74, 922-929.

Hutson, N.D., Yang, R.T., 1997. Theoretical basis for the Dubinin-Radushkevitch (D-R) adsorption isotherm equation. Adsorption-Journal of the International Adsorption Society 3, 189-195.

Jagtap, S., Yenkie, M.K., Labhsetwar, N., Rayalus, S., 2012. Fluoride in Drinking Water and Defluoridation of Water. Chemical Reviews 112, 2454-2466.

Karnitz, O., Gurgel, L.V.A., de Melo, J.C.P., Botaro, V.R., Melo, T.M.S., Gil, R., Gil, L.F., 2007. Adsorption of heavy metal ion from aqueous single metal solution by chemically modified sugarcane bagasse. Bioresource Technology 98, 1291-1297.

Langgut, D., 2017. The Citrus Route Revealed: From Southeast Asia into the Mediterranean. Hortscience 52, 814-822.

Li, L., Quinlivan, P.A., Knappe, D.R.U., 2002. Effects of activated carbon surface chemistry and pore structure on the adsorption of organic contaminants from aqueous solution. Carbon 40, 2085-2100.

Liu, Y.Q., Heying, E., Tanumihardjo, S.A., 2012. History, Global Distribution, and Nutritional Importance of Citrus Fruits. Comprehensive Reviews in Food Science and Food Safety 11, 530-545.

Loganathan, P., Vigneswaran, S., Kandasamy, J., Naidu, R., 2013. Defluoridation of drinking water using adsorption processes. Journal of Hazardous Materials 248, 1-19.

Ma, Y., Wang, S.-G., Fan, M., Gong, W.-X., Gao, B.-Y., 2009. Characteristics and defluoridation performance of granular activated carbons coated with manganese oxides. Journal of Hazardous Materials 168, 1140-1146.

Martyn, C.N., Osmond, C., Edwardson, J.A., Barker, DJP., Harris, E.C., Lacey, R.F., 1989. Geographical relation between alzheimers-disease and aluminum in drinking-water. Lancet; 1: 59-62.

Meenakshi, Maheshwari, R.C., 2006. Fluoride in drinking water and its removal. Journal of Hazardous Materials 137, 456-463.

Mondal, P., George, S., 2015. A review on adsorbents used for defluoridation of drinking water. Reviews in Environmental Science and Bio-Technology 14, 195-210.

Mugisidi, D., Ranaldo, A., Soedarsono, J.W., Hikam, M., 2007. Modification of activated carbon using sodium acetate and its regeneration using sodium hydroxide for the adsorption of copper from aqueous solution. Carbon 45, 1081-1084.

Mullick, A., Neogi, S., 2016. Synthesis of potential biosorbent from used stevia leaves and its application for malachite green removal from aqueous solution: kinetics, isotherm and regeneration studies. Rsc Advances 6, 65960-65975.

Mullick, A., Neogi, S., 2018. Acoustic cavitation induced synthesis of zirconium impregnated activated carbon for effective fluoride scavenging from water by adsorption. Ultrasonics Sonochemistry 45, 65-77.

Mumtaz, N., Pandey, G., Labhasetwar, P.K., 2015. Global Fluoride Occurrence, Available Technologies for Fluoride Removal, and Electrolytic Defluoridation: A Review. Critical Reviews in Environmental Science and Technology 45, 2357-2389.

Penniston, K.L., Nakada, S.Y., Holmes, R.P., Assimos, D.G., 2008. Quantitative assessment of citric acid in lemon juice, lime juice, and commercially-available fruit juice products. Journal of Endourology 22, 567-570.

Rangel, C.N., de Carvalho, L.M.J., Fonseca, R.B.F., Soares, A.G., de Jesus, E.O., 2011. Nutritional value of organic acid lime juice (Citrus latifolia T.), cv. Tahiti. Ciencia E Tecnologia De Alimentos 31, 918-922.

Rashid, U.S., Bezbaruah, A.N., 2020. Citric acid modified granular activated carbon for enhanced defluoridation. Chemosphere 252, 126639.

Ravulapalli, S., Kunta, R., 2017. Defluoridation studies using active carbon derived from the barks of Ficus racemosa plant. Journal of Fluorine Chemistry 193, 58-66.

Rezvani, F., Sarrafzadeh, M.-H., Ebrahimi, S., Oh, H.-M., 2019. Nitrate removal from drinking water with a focus on biological methods: a review. Environmental Science and Pollution Research 26, 1124-1141.

Sailo, L., Mahanta, C., 2014. Arsenic mobilization in the Brahmaputra plains of Assam: groundwater and sedimentary controls. Environmental Monitoring and Assessment 186, 6805-6820.

Smith, G., 2011. Rural Water System Sustainability: A Case Study of Community-Managed Water Systems in Saramaka Communities. Civil Engineering. Houghton, MI: Michigan Technological University. Master of Science: 58.

Strunecka, A., Patocka, J., 1999. Pharmacological and toxicological effects of aluminofluoride complexes. Fluoride 32, 230-242.

Tahir, S.S., Rauf, N. 2006. Removal of a cationic dye from aqueous solutions by adsorption onto bentonite clay. Chemosphere, **63**(11), 1842-1848.

Thakur, L.S., Mondar, P., 2017. Simultaneous arsenic and fluoride removal from synthetic and real groundwater by electrocoagulation process: Parametric and cost evaluation. Journal of Environmental Management 190, 102-112.

United Nations, General Assembly (Seventieth Session) Agenda Items 15 and 116 adopted on 25 September 2015, A/RES/70/1, Distributed on 21 October 2015 (available at https://undocs.org/A/RES/70/1).

United Nations Water (UN-Water), 2018. SDG 6 Synthesis Report 2018 on Water and Sanitation. Available online: http://www.unwater.org/publication_categories/sdg-6-synthesis-report-2018-on-waterand- sanitation/, Accessed Date: August 2020.

United Nations International Children's Emergency Fund (UNICEF), 2015. Progress on Sanitation and Drinking Water—2015 Update and MDG Assessment. Available online: http://files.unicef.org/publications/files/Progress_on_Sanitation_and_Drinking_Water_2015_Update_.pdf, Accessed Date: August 2020.

United Nation, 2015. Sustainable development goals: Clean water and Sanitation. Available at https://www.un.org/sustainabledevelopment/wp-content/uploads/2016/08/6_Why-It-Matters-2020.pdf, Accessed Date: March 2021.

UN. Transforming Our World, 2015. The 2030 Agenda for Sustainable Development; United Nations (UN): New York, NY, USA, Volume A/RES/70/1, p. 35.

USEPA (U.S. Environmental Protection Agency), 2009. National Primary Drinking Water Regulations. Available at: https://www.epa.gov/ground-water-and-drinking-

water/national-primary-drinking-water-regulations#Inorganic, Accessed date: November 2020.

Wang, J., Xu, W.H., Chen, L., Jia, Y., Wang, L., Huang, X.J., Liu, J.H., 2013a. Excellent fluoride removal performance by CeO2-ZrO2 nanocages in water environment. Chemical Engineering Journal 231, 198-205.

Waterlogic, 2019. Water Fluoridation in the USA. Avaialable at: https://www.waterlogic.com/en-us/resources/fluoride-level-map/, Accessed date: February 2021.

Weber, W.J., Morris, J.C., 1963. Kinetics of adsorption on carbon from solution. Journal of the Sanitary Engineering Division 89, 31-60.

Workman, Daniel. Lemon and Lime Exporters by Country, World's Top Exporters. Available at http://www.worldstopexports.com/lemons-exporters-by-country/, Accessed August 2020.

WHO, 2004. Guidelines for drinking-water quality. Volume 1 recommendations, 3rd edn. World Health Organization, Geneva.

WHO/UNICEF Joint Monitoring Program for Water Supply and Sanitation, 2000. Global Water Supply and Sanitation Assessment 2000 Report. Geneva, World Health Organization, Water Supply and Sanitation Collaborative Council and United Nations Children Fund.

WHO & UNICEF, 2017. Safely Managed Drinking Water-Thematic Report on Drinking Water. Geneva, Switzerland: World Health Organization. Licence: CC BY-NC-SA 3.0 IGO.

Xu, Y., Liu, Y.G., Liu, S.B., Tan, X.F., Zeng, G.M., Zeng, W., Ding, Y., Cao, W.C., Zheng, B.H., 2016. Enhanced adsorption of methylene blue by citric acid modification of biochar derived from water hyacinth (Eichornia crassipes). Environmental Science and Pollution Research 23, 23606-23618.

Yadav, A.K., Abbassi, R., Gupta, A., Dadashzadeh, M., 2013. Removal of fluoride from aqueous solution and groundwater by wheat straw, sawdust and activated bagasse carbon of sugarcane. Ecological Engineering 52, 211-218.

Yadav, K.K., Gupta, N., Kumar, V., Khan, S.A., Kumar, A., 2018. A review of emerging adsorbents and current demand for defluoridation of water: Bright future in water sustainability. Environment International 111, 80-108.

Yadav, K.K., Kumar, S., Pham, Q.B., Gupta, N., Rezania, S., Kamyab, H., Yadav, S., Vymazal, J., Kumar, V., Tri, D.Q., Talaiekhozani, A., Prasad, S., Reece, L.M., Singh, N., Maurya, P.K., Cho, J., 2019. Fluoride contamination, health problems and remediation methods in Asian groundwater: A comprehensive review. Ecotoxicology and Environmental Safety 182.

Zhao, X.L., Wang, J.M., Wu, F.C., Wang, T., Cai, Y.Q., Shi, Y.L., Jiang, G.B., 2010. Removal of fluoride from aqueous media by Fe3O4@Al(OH)(3) magnetic nanoparticles. Journal of Hazardous Materials 173, 102-109.

CHAPTER 4: FLUORIDE REMOVAL BY GO-CeO_2 NANOHYBRID

4.1. Introduction

Fluoride (F^-) is an essential trace element necessary for human teeth and skeletal health (Chouhan and Flora, 2010). However, excessive intake of fluoride can lead to fluorosis of teeth and bones (Gbadebo, 2012). Chronic intake of fluoride may also lead to muscle fiber degeneration, low hemoglobin level, excessive thirst, skin rashes, depression, growth retardation, and DNA structural changes (Gbadebo, 2012; Meenakshi and Maheshwari, 2006). Fluoride is mainly released into groundwater via slow dissolution of geogenic fluoride bearing minerals such as fluorite, fluorospar, cryolite, theorapatite, phosphorite, apatite, topaz, villiaumite, sepiolite, and palygorskite in rocks (Banerjee, 2015; Jagtap et al., 2012; Yadav et al., 2018). Fluoride is also generated by industries producing glass and ceramics, chemicals and metals with effluent from these industries having fluoride levels ranging from 10 to 10,000 mg/L (Bhatnagar et al., 2011). The world health organization (WHO) recommends a threshold of 1.5 mg F^-/L in drinking water (WHO, 2004). The United States Environmental Protection Agency (USEPA) has established a maximum contaminant level (MCL) of 4 mg/L to prevent skeletal fluorosis and a secondary maximum contaminant level (SMCL) of 2 mg/L to protect against dental fluorosis in human (USEPA, 2009). More than 260 million people worldwide use drinking water containing fluoride in excess of the WHO recommended limit of 1.5 mg/L (Amini et al., 2008; Jagtap et al., 2012).

While precipitation/coagulation, membrane processes, ion exchange, and adsorption are used for fluoride removal from drinking water (Meenakshi and Maheshwari, 2006; Mohapatra et al., 2009), adsorption is the most widely used because of its low cost, simple design, high removal efficiency, and economic viability (Bhatnagar et al., 2011). Activated carbon (Araga and Sharma, 2017; Araga et al., 2017; Chen et al., 2017; Rashid and Bezbaruah, 2020), carbon-based

composites (Di et al., 2007; Kuang et al., 2017; Ruan et al., 2017; Zhang et al., 2019a), metal oxides (Mukhopadhyay et al., 2017), alum sludge (Sujana et al., 1998), metal-organic frameworks (MOFs) (Karmakar et al., 2016), and layered double hydroxides (Lv et al., 2007) are the popular adsorbents for fluoride removal. Among them, rare earth metal oxides have shown high binding affinities for fluoride (Chigondo et al., 2018b; Li et al., 2010; Mukhopadhyay et al., 2017; Zhang et al., 2019b). The mechanism of fluoride removal by metal oxides involves the exchange between fluoride ions and surface hydroxyl groups of the adsorbents (Karmakar et al., 2016; Yu et al., 2018). The hydroxyl groups either exist on the metal hydroxide surface or can be formed through the hydroxylation of metal oxides and metal organic frameworks in aqueous environments (Wendt et al., 2006).

Among the rare earth metal oxides, cerium oxide (Ceria, CeO_2) has been used for aqueous arsenic (Sakthivel et al., 2017), chromium (Xiao et al., 2009), lead (Sharma et al., 2018), mercury (Sharma et al., 2018), and organic dyes (Yu et al., 2015) removal. Ceria exhibits facile transformation between +3 and +4 oxidation states depending on the redox environment making it a versatile adsorbent for various contaminants (Chigondo et al., 2018b; McCormack et al., 2014; Sakthivel et al., 2017). Cerium-loaded mesoporous zirconium phosphate (Dash et al., 2015), carbon nanotube supported ceria nanoparticles (Di et al., 2007), cubical ceria nanoparticles (Dhillon et al., 2016), CeO_2-ZrO_2 nanocages (Wang et al., 2013), hydrous cerium-magnesium oxides (Chigondo et al., 2018b), and cerium(IV)-incorporated hydrous iron(III) oxide (Mukhopadhyay et al., 2017) have been reported to remove fluoride. However, these ceria-based materials needed 40-2750 minute contact time to remove fluoride (Table 4.1 in Results and Discussions) (Chigondo et al., 2018b; Dash et al., 2015; Dhillon et al., 2016; Di et al., 2007; Mukhopadhyay et al., 2017; Wang et al., 2013; Zhang et al., 2019a), and that limits their use as a

high contact time translates to a large reactor (filter) volume. Other materials with high fluoride adsorption capacity such as MOFs (Karmakar et al., 2016), layered double oxides (Lv et al., 2007), and composites of different metal oxides (Liu et al., 2016) have also shown slow adsorption kinetics.

Additionally, typical ceria nanoparticles are 3-12 nm in size (Zhang et al., 2002) and they agglomerate quickly (Rohder et al., 2014; Safi et al., 2010) and which limits their use in the aqueous environment. The agglomeration problem can be addressed by embedding (decorating) ceria nanoparticles onto graphene oxide sheets (Sakthivel et al., 2017). Graphene oxide (GO) provides a unique two-dimensional (2-D) platform with high specific surface area (theoretical value = ~2400 m^2/g (Zhang et al., 2020)), low bulk density (0.06-0.3 g/cm^3 (Kovtun et al., 2019)), high oxygen-containing functional group density (C/O ratio: 2-4 (Perreault et al., 2015)), and unique physicochemical properties (Mkhoyan et al., 2009; Perreault et al., 2015). Further, its two available basal planes can support nanomaterials (Perreault et al., 2015).

This paper reports for the first time the use of a GO-CeO_2 nanohybrid (ceria nanoparticles supported on GO sheets, referred to as GO-CeO_2 in this paper) to remove aqueous fluoride. We hypothesized that the GO support will keep the ceria nanoparticles (CeO_2 NPs) as discrete entities (non or less agglomerated) and help in aqueous dispersion. Further, the GO sheets will also act as electron mediators and help in maintaining enough Ce^{3+} in the nanohybrid for effective adsorption of fluoride. Specifically, the role of the GO sheets as electron reservoirs and how that helps in fluoride removal have been explored. The fluoride adsorption capacity of GO-CeO_2 (nanohybrid) was tested under various experimental conditions of pH, the presence of co-existing anions, and ionic strength. A possible fluoride removal mechanism has been proposed based on experimental results and characterization data.

4.2. Materials and methods

4.2.1. Materials

All chemicals were used as received unless otherwise specified. A multi-layered graphene oxide (GO) was obtained from Garmor, Inc. (Orlando, FL) and used without further modification. The list of chemicals is in SI (Section C.1.1, Appendix C).

4.2.2. Synthesis of GO-CeO_2 nanohybrid

The GO-CeO_2 was synthesized in a one-pot hydrothermal synthesis process using GO and cerium(III) nitrate hexahydrate as the starting materials as per our previously published method (Sakthivel et al., 2017). Details in SI (Section C.1.2, Appendix C).

4.2.3. Characterization

High-resolution transmission electron microscopy (HRTEM), Scanning Electron Microscopy (SEM), X-ray photoelectron spectroscopy (XPS), and a Zetasizer were used for material characterization. Details in SI (Section C.1.3, Appendix C).

4.2.4. Batch studies

The batch kinetic, isotherm, and interference studies conducted with GO-CeO_2 and control experiments were run with GO or CeO_2 nanoparticles as needed. The kinetic studies were conducted at an initial fluoride concentration (C_0) of 10 mg/L over time. Isotherm studies were carried out by varying the C_0 from 5 to 40 mg/L. The effect of pH was evaluated in the pH range of 2 to 10. The interference study was conducted using different concentrations of sulfate (SO_4^{2-}), phosphate (PO_4^{3-}- P), bicarbonate (HCO_3^-), and nitrate (NO_3^-- N). Details in SI (Section C.1.4, Appendix C).

4.2.5. Quality control and statistical analysis

All experiments were conducted in triplicates and the average values are reported here along with the standard deviations. One-way ANOVA analysis was done using Minitab to determine statistically significant differences in the data sets and Tukey's pairwise comparison was used to identify the data that were significantly different.

4.3. Result and discussions

4.3.1. Characterization

The nanostructure and morphology of the GO-CeO_2 were observed by HRTEM. It shows that the CeO_2 NPs (dark particles) are randomly distributed on the GO sheet (gray sheet), and the CeO_2 NPs deposited on the GO sheets have a particle size of 10-20 nm (Fig. 4.1a). These findings are in agreement with others (Sakthivel et al., 2017). The morphology of GO-CeO_2 was also studied using SEM. SEM micrographs show that GO-CeO_2 has a flaky structure with irregular size and shape (Fig. 4.1b).

Zeta potentials (ζ) of GO, CeO_2 NPs, and GO-CeO_2 were measured in 0.01 M NaCl medium (solution pH ~7). The GO remained well dispersed in aqueous media due to its high ζ (–42.99 ± 1.73 mV). Particles with $\zeta > |\pm 25|$ mV are known to make a stable suspension (ISO, 2000). While CeO_2 NPs with their low ζ (3.18 ± 0.28 mV) agglomerated easily, the GO-CeO_2 with a high ζ (33.99 ±0.44 mV) made a stable dispersion.

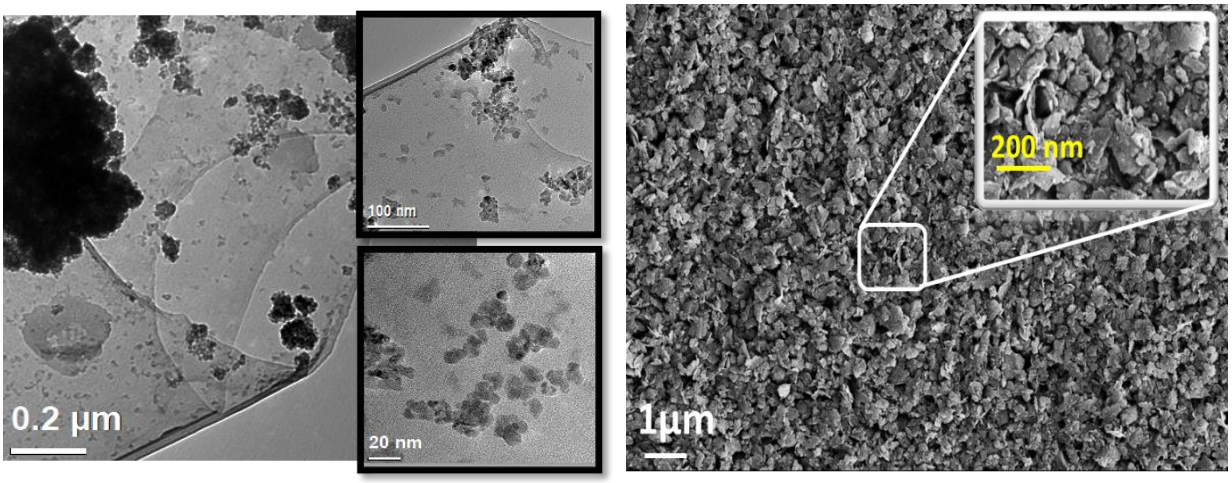

(a) **(b)**

Figure 4.1. (a) TEM micrographs of the GO-CeO_2 (nanohybrid). The micrograph at a lower magnification shows that the ceria particles (black dots) are present on the graphene oxide matrix (gray sheet). The micrographs at higher magnification (insets) show the CeO_2 NPs (10–20 nm), and (b) SEM micrographs of GO-CeO_2 show that it has a flaky structure.

4.3.2. Effectiveness of GO-CeO_2 nanohybrid

The comparison of fluoride removal efficiency of GO-CeO_2 and the controls (CeO_2 NPs and GO) showed that the GO-CeO_2 has a high removal efficiency (85%) which is significantly higher than that of CeO_2 NPs (12% fluoride removal, $p = 0.000$, $\alpha = 0.05$) or GO (1%, $p = 0.000$, $\alpha = 0.05$) used alone (Fig. 4.2a). The potential quick aggregation of CeO_2 NPs (when used alone) might have decreased their reactivity (Safi et al., 2010) and they exhibited poor fluoride removal efficiency (12%). However, the nanohybrid had an improved fluoride removal efficiency which was ~73% higher compared to only CeO_2 NPs. It is logical to infer that the use of GO as a platform for CeO_2 NPs increased the reactivity of the nanoparticles and enhanced fluoride removal was achieved. Enhanced dispersion (ζ of 33.99±0.44 mV) of the nanohybrid potentially influenced fluoride removal (also see Fluoride Removal Mechanisms).

4.3.3. Effect of adsorbent dose

At C_0 = 10 mg F^-/L, fluoride removal efficiency increased from 18% to 100% with the increase of adsorbent (GO-CeO_2) dosage from 0.2 to 1.5 g/L (Fig. 4.2b). Given, the recommended

WHO threshold of 1.5 mg F^-/L in drinking water, the optimal adsorbent dose was decided as 1 g/L (85% removal) in this study; this dosing was sufficient to achieve the recommended WHO limit for fluoride in drinking water and keeping some fluoride in the water for human nutritional requirements. Similar adsorbent doses were reported by others (Table 4.1). All experiments reported henceforth used 1 g/L of the nanohybrid.

4.3.4. Kinetics

The results of fluoride removal by GO-CeO_2 over time (till 120 min, C_0 = 10 mg F^-/L and adsorbent dose of 1 g/L) showed that the fluoride adsorption by GO-CeO_2 follows very fast kinetics (Fig. 4.2c) compared to the materials reported by others including MOFs, mesoporous ZrO_2, GO-Zr, and Ce-Zr composites (Chen et al., 2016a; Karmakar et al., 2016; Mohan et al., 2016; Wang et al., 2017; Yu et al., 2018; Zhang et al., 2017). GO-CeO_2 achieved 85% fluoride adsorption within 1 min and reached equilibrium at the same time (Fig. 4.2c inset). We have compared the results with other reported ceria-based materials (Table 4.1) and as well as other standard materials (activated carbon, activated alumina, and calcium-based adsorbents) (Table C1, Appendix C). Our material showed ultra-rapid kinetics which is 40-2750 times higher than other ceria-based materials (nano and non-nano) and 20-780 times higher than the typical (non-nano) fluoride adsorbents even when high adsorbent doses were used by others (Table C1, Appendix C). For example, cerium loaded mesoporous zirconium phosphate showed 84.7% fluoride removal in 60 min and cubical ceria nanosorbent took 120 min for 95% fluoride removal (at the same C_0 = 10 mg F^-/L as in this study). This makes GO-CeO_2 much superior to all previously reported fluoride adsorbents. To rule out the dose-effect (sorbent to sorbate ratio) on the observed fast kinetics,

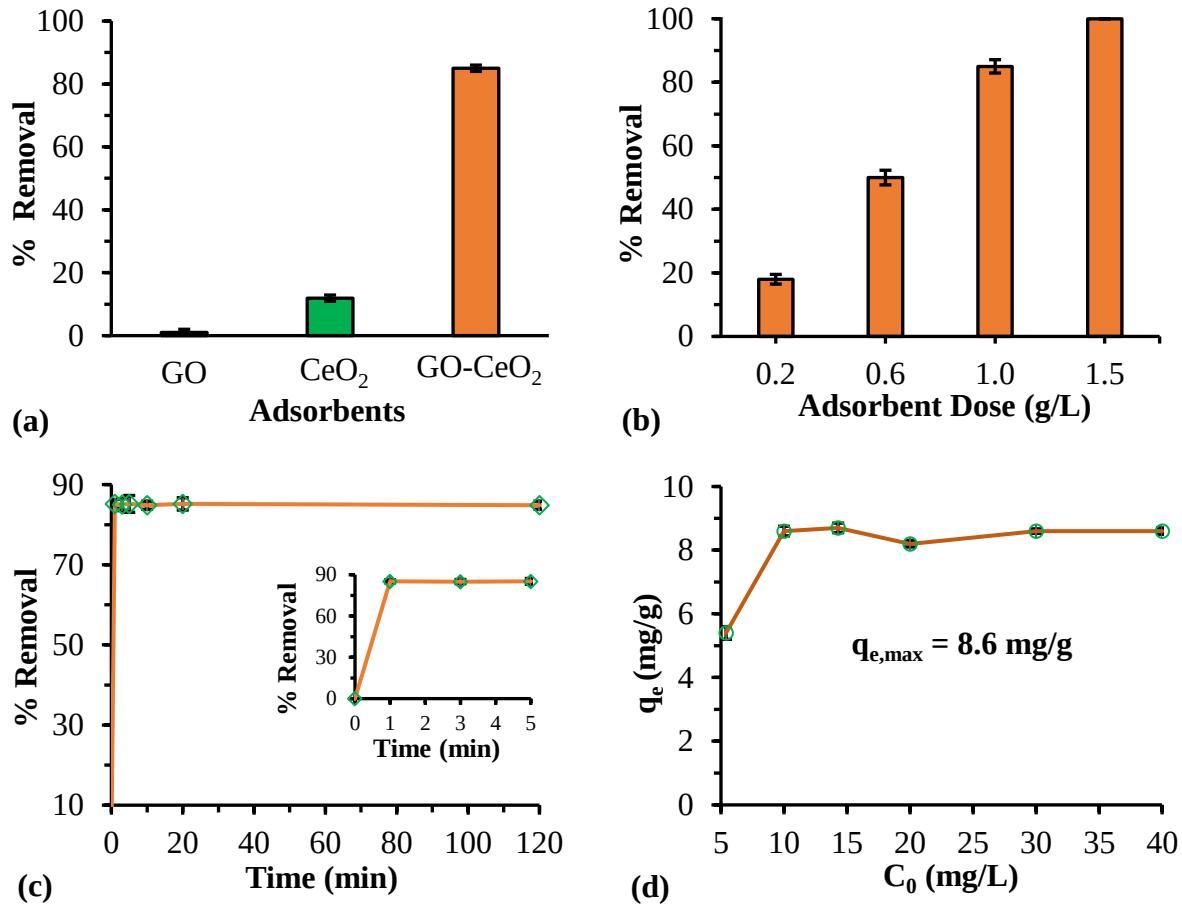

Figure 4.2. (a) Fluoride removal by GO-CeO_2 and the controls (CeO_2 NPs and GO); adsorbent dose = 1 g/L; C_0 = 10 mg F^-/L; (b) Effect of GO-CeO_2 dosing on fluoride removal. Dosing of 1 g/L yielded 85% fluoride removal (C_0 = 10 mg F^-/L) reducing bulk fluoride concentration to 1.5 mg F^-/L (WHO recommended limit for drinking water), and so 1 g/L was selected as the optimal dose; (c) Removal of fluoride by GO-CeO_2 over time (C_0 = 10 mg F^-/L) (Inset: Initial 5 min data zoomed in). The fluoride removal reached equilibrium within 1 min which is the fastest fluoride removal kinetics reported so far and (d) Fluoride adsorption capacity of GO-CeO_2 at different concentrations of fluoride. The maximum fluoride adsorption capacity was found to be 8.6 mg/g. GO-CeO_2 dose = 1 g/L and initial pH 6.5. The data points are connected with straight lines for ease of reading only and they do not represent trendlines, and the vertical error bars represent ± standard deviations.

additional kinetic studies were conducted with different GO-CeO_2 dosages (0.2 to 1.0 g/L). The rapid kinetics was observed irrespective of the sorbent to sorbate ratio used (Fig. C1, Appendix C) indicating that the rapid kinetics was not affected by the sorbent dose used and, hence, other factors

might have played roles. This rapid adsorption translates to a short detention time which will lead to a small reactor (treatment unit) volume and thus reduced infrastructure cost. With its fast reaction kinetics, GO-CeO_2 is a potential candidate for use in high throughput defluoridation systems for both point-of-use and centralized water treatment systems.

The kinetic study data were fitted into the Webber-Morris intra-particle diffusion model (Weber and Morris, 1963) (Eq. 4.1) to find out the potential rate-controlling steps such as film diffusion or intra-particle diffusion.

$$Q_t = K_p t^{0.5} \tag{4.1}$$

In Eq 1, K_p is the intra-particle diffusion rate in $mg/g/min^{0.5}$ and q_t is the adsorption capacity (mg/g) at time t. If the plot of q_t vs $t^{0.5}$ passes through the origin then intra-particle diffusion is the only rate-determining step. In this study, the plot showed bilinearity (Fig. C2, Appendix C) with the first section (solid line) representing the external mass transport across the boundary layer, and the second section (dashed line) being the equilibrium stage (Sadeghi et al., 2020). The equilibrium was reached within 1 min, we could not get any data points between 0 min and 1 min to investigate intra-particle diffusion which might have occurred during that time along with film diffusion. Sadeghi et al., while treating arsenic with graphene oxide nanoribbons achieved near-equilibrium within 2 min and reported that both intra-particle diffusion and film diffusion participated in the removal process (Sadeghi et al., 2020). While we cannot conclusively prove that intra-particle diffusion took place, it is highly likely given the structure of our nanohybrid. In the multi-layered GO we used, CeO_2 NPs were decorated on both faces of each GO sheet and a stacked GO-CeO_2 was formed. Others also reported similar nanoparticle deposition patterns (Wu et al., 2012). Fluoride ions might have interacted with the CeO_2 nanoparticles inside the staked layers via intra-particle diffusion. We can infer that both intra-particle diffusion and film diffusion were rate-

limiting in our experiment with the caveat that we did not have any experimental data points between 0 and 1 min.

Table 4.1. Comparison of fluoride removal by different ceria-based material.

Adsorbent	pH	Dosing (g/L)	Initial Conc (mg/L)	Contact Time (min)	Sorbent/ Sorbate (g/mg)	% Removal	Source
Hydrous CeO_2-Fe_3O_4 decorated polyaniline fibers	6.0	0.6	40	120	0.015	90	(Chigondo et al., 2018b)
CeO_2-Rod	3.5	0.5	50	2750	0.01	70	(Kang et al., 2017)
Mn–Ce oxide	6.0	0.1	10	180	0.01	73.5	(Deng et al., 2011)
Ce–Fe bimetal oxides	NR	0.5	10	40	0.05	90	(Tang and Zhang, 2016)
CeO_2–ZrO_2 nanocages	4.0	0.2	10	1440	0.02	70	(Wang et al., 2013)
Cerium(IV)-incorporated hydrous iron(III) oxide	7.0	0.5	10	120	0.05	85	(Mukhopadhyay et al., 2017)
Cerium loaded mesoporous zirconium phosphate	6.0	1.0	10	60	0.1	84.7	(Dash et al., 2015)
Cubical ceria nanosorbent	7.0	1.0	10	120	0.1	95	(Dhillon et al., 2016)
Mg-Al-Ce triple-metal composites	7.0	0.2	50	180	0.004	38	(Chi et al., 2017)
GO-CeO_2 nanohybrid	**6.5 4.0**	**1**	**10**	**1**	**0.1**	**85 100**	**This work**

NR = pH was not reported in the paper

4.3.5. Isotherm studies

The maximum fluoride adsorption capacity ($q_{e,max}$) of GO-CeO_2 was found to be 8.6 mg/g (initial pH 6.5) (Fig. 4.2d). We also conducted isotherm studies at pH 4 (Fig. C3, Appendix C) as maximum fluoride removal was achieved at pH 4 (see Effect of pH) and the maximum adsorption capacity increased to 16.07 mg/g. However, 8.61 mg/g at near-neutral pH is the more relevant value. We compared our result with two conventional adsorbents (acidic alumina and granular activated alumina) (Ghorai and Pant, 2005; Goswami and Purkait, 2012) typically used for

drinking water fluoride removal. Our nanohybrid recorded similar adsorption capacity as the acidic alumina (AA, adsorption capacity 8.4 mg/g) and acted 3.5 times better than the granular activated alumina (GAA, 2.41 mg/g). While GAA was tested at pH 7, AA was effective at pH 4.4 only. Dissolution of aluminum complexes from aluminum-based adsorbent poses a human health risk as aluminum ion and its aluminofluoride complexes are known neurotoxins (Martyn et al., 1989; Strunecka and Patocka, 1999), so the use of AA and GAA are increasingly being questioned (George et al., 2010). Further, our nanohybrid exhibited kinetics which is 90 times faster compared to AA and 360 times faster than GAA, and that too at near-neutral pH (6.5), making it a superior adsorbent for use in a high throughput defluoridation system.

To determine the relationship between adsorbent and adsorbate, and to understand the mechanism(s) of fluoride removal, the experimental adsorption data were fitted onto Freundlich and Langmuir isotherm models (Section C.2.4). The data fitted well onto Langmuir isotherm (R^2 = 0.9995) rather than Freundlich (R^2 = 0.0103) (Fig. C4, Appendix C) indicating that the adsorption of fluoride by GO-CeO_2 is a monolayer and homogenous phenomenon, and the maximum adsorption capacity calculated as 8.61 mg/g (Table C2, Appendix C) which tallies with our experimental value (8.6 mg/g). The dimensionless constant R_L values calculated for the fluoride concentrations (5, 10, 20, 30, and 40 mg/L) used in this study are in the range of 0.003-0.025 (between 0 and 1) (Table C2, Appendix C) suggesting that fluoride adsorption onto GO-CeO_2 is favorable.

4.3.6. Effect of pH

As the pH increased from 2 to 4, the fluoride removal increased from 98% to 100% (Fig. 4.3a). With a further increase to 6 a significant decrease (to 83%, $p = 0.000$, $\alpha = 0.05$) in fluoride removal was observed and the removal efficiency gradually decreased to 66% at pH 10. The point-

of-zero-charge (PZC) of GO-CeO_2 was measured as 2.7 (Fig. 4.3b). The surface of the nanohybrid remained positively charged below pH 2.7 and took up the fluoride ions electrostatically (Dash et al., 2015; Dhillon et al., 2016; Mukhopadhyay et al., 2017; Wang et al., 2013). We expected the highest fluoride removal at the lowest pH but our fluoride removal efficiency decreased at pH = 2, possibly because of the formation of hydrofluoric acid ($H^+ + F^- \rightleftharpoons HF$) at low pH (Dash et al., 2015; Dhillon et al., 2016). Hydrofluoric acid does not completely dissociate in the water below pH 3.14 (dissociation constant, pK_a = 3.14), and less ionic fluoride would be available for electrostatic adsorption by GO-CeO_2. With F^- increasing at pH > 3.14, maximum fluoride removal was achieved at pH 4. At pH >> PZC, the F^- removal efficiency decreased significantly (Fig. 4.3a) due to the generation of negative charges on the adsorbent surface engendering repulsion for the fluoride ions. Further, at higher pH, more OH^- were available near the GO-CeO_2 surface competing for available adsorption/ion-exchange sites (Chai et al., 2013; Dash et al., 2015). However, the efficiency of fluoride removal did not go down below 66% even at pH 10 indicating that the fluoride removal by GO-CeO_2 was not dominated by electrostatic interaction only but chemisorption was also possibly involved.

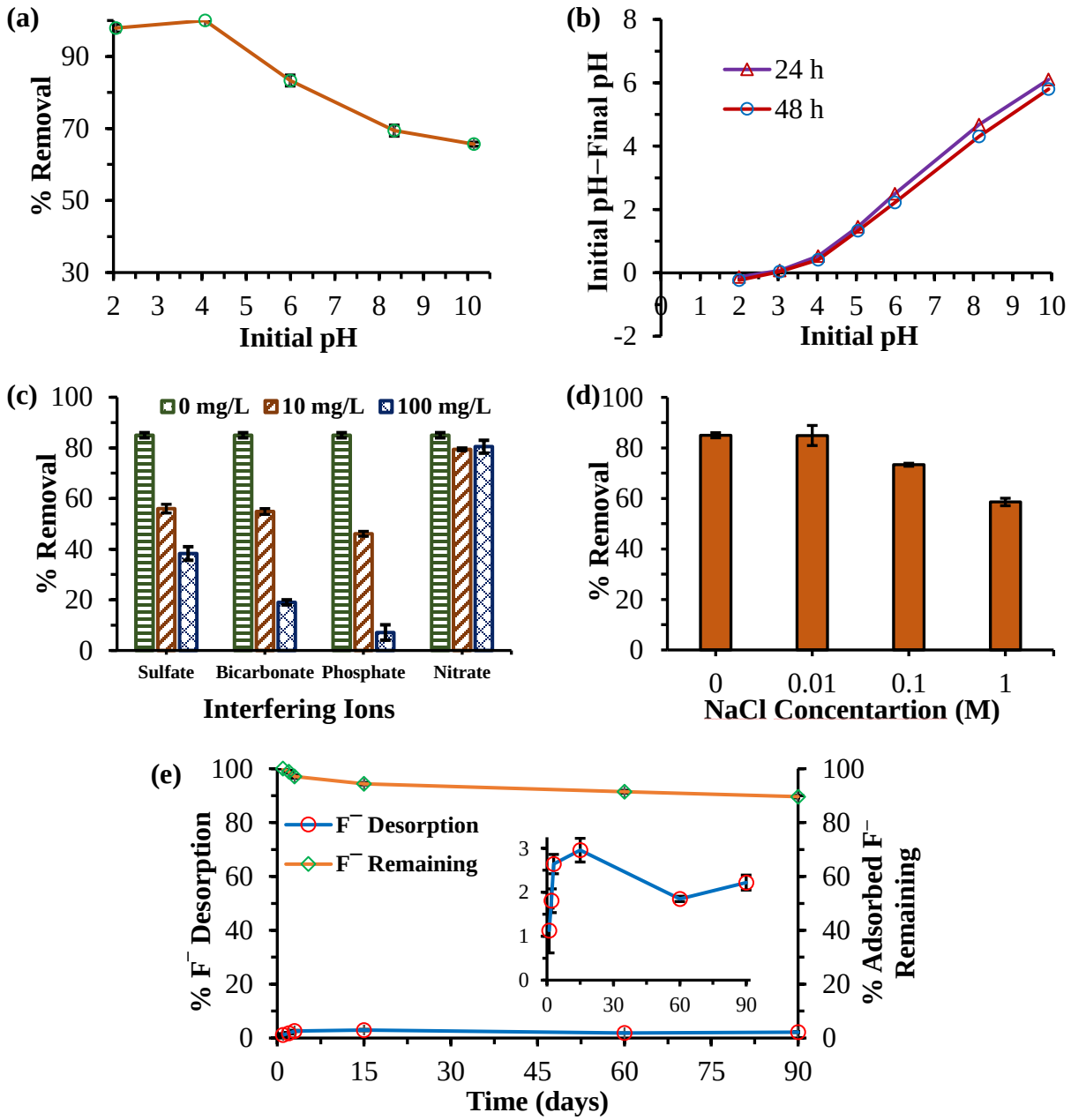

Figure 4.3. (a) Effect of initial pH on fluoride adsorption onto GO-CeO_2; (b) Point-of-Zero-Charge (PZC) of GO-CeO_2 was found to be 2.7; (c) Effect of co-existing ions on fluoride adsorption onto GO-CeO_2. The order of interference is $PO_4^{3-} > HCO_3^- > SO_4^{2-} > NO_3^-$. The concentration of nitrate is in mg NO_3^-N/L and phosphate concentration is in mg PO_4^{3-}P/L; and (d) Effect of ionic strength on fluoride removal by GO-CeO_2. While there was no significant change at 0.01 M NaCl (compared to 0 M NaCl), the fluoride removal efficiency decreased with the increase of ionic strength beyond 0.01 M. The findings indicated that the outer-sphere complexation also contributed to fluoride removal by GO-CeO_2; and I Desorption of fluoride from the used GO-CeO_2 (Inset: percent desorption in 90 days with the Y-axis limited to 3.25%). The secondary axis shows fluoride adsorbed onto GO-CeO_2. Note: The data points are connected with straight lines for ease of reading only and they do not represent trendlines, and the vertical error bars represent ± standard deviations.

4.3.7. Effect of co-existing ions

Groundwater contains anions such as sulfate (SO_4^{2-}), bicarbonate (HCO_3^-), phosphate (PO_4^{3-}), and nitrate (NO_3^-) in addition to fluoride in contaminated waters. The potential interferences by co-existing ions were examined by adding individual interfering anions (NO_3^-, PO_4^{3-}, HCO_3^-, and SO_4^{2-}; 0, 10, and 100 mg/L) to the bulk fluoride solution (C_0 = 10 mg/L and adsorbent dose = 1 g/L). Significant interferences (p = 0.000-0.037, $\alpha = 0.05$) in fluoride adsorption was observed in the presence of all anions (Fig. 4.3c). However, NO_3^- showed the least effect (85% fluoride removal with no NO_3^-—N, and 80% at 100 mg NO_3^-—N/L); NO_3^- being a low-affinity ligand did not compete for the fluoride adsorption sites (Chen et al., 2016b; Mohanty et al., 2005). The presence of PO_4^{3-} significantly decreased fluoride removal from 85% (no PO_4^{3-}—P) to 46% (10 mg PO_4^{3-}—P/L) and then to ~7% (100 mg PO_4^{3-}—P/L). The presence of SO_4^{2-} also significantly decreased fluoride removal from 85% (no SO_4^{2-}) to 56% (10 mg/L) and then to ~38% (100 mg/L). HCO_3^- also showed a significant negative effect on fluoride removal (dropped to 19% at 100 mg/L) possibly because of hydrolysis of HCO_3^- ($HCO_3^- + H_2O \rightleftharpoons H_2CO_3 + OH^-$) leading to more OH^- being present to compete with fluoride for the adsorption sites (Deng et al., 2011; Wang et al., 2013). The order of interference of the co-existing anions was $PO_4^{3-} > HCO_3^- > SO_4^{2-} > NO_3^-$. The order of interference is related to the charge/radius (Z/R) values of the competing anions (except HCO_3^-): PO_4^{3-} (3/3.40) > SO_4^{2-} (2/2.40) > NO_3^- (1/2.81). The greater the Z/R, the more likely it that the specific anion was attracted to the adsorbent surface leading to more interference with fluoride adsorption (Liu et al., 2016; Zhao et al., 2010). Working with cubical ceria (Dhillon et al., 2016), ceria-iron bimetal oxides (Tang and Zhang, 2016), and CeO_2-Fe_3O_4 decorated polyaniline fibers nanocomposite (Chigondo et al., 2018a), others have observed interferences from PO_4^{3-} (Chigondo et al., 2018a), HCO_3^- (Tang and Zhang, 2016), SO_4^{2-} (Dhillon et al., 2016),

and NO_3^- (Dhillon et al., 2016) (Table C3, Appendix C). The typical concentration of phosphate in groundwater is < 100 µg/L, and therefore, will have minimal effect on fluoride removal by GO-CeO_2. The interference by bicarbonate can be minimized by adjusting the pH (≤ 7.0). Pretreatments may be necessary to reduce the interferences of some of the ions. Narsimha and Sudarshan (2017) (Narsimha and Sudarshan, 2017) reported that SO_4^{2-} concentration in groundwater in one of the worst fluoride affected areas in India varied from 21 to 137 mg/L; we expect GO-CeO_2 to work reasonably well with low sulfate concentration but more adsorbent may be need to treat water with high sulfate levels.

4.3.8. Effect of ionic strength

The effect of ionic strength on fluoride adsorption by GO-CeO_2 was evaluated (C_0 = 10 mg F^-/L) to find out whether the outer-sphere complexation (electrostatic interaction) was participating in fluoride removal. The fluoride removal efficiency decreased from 85% to 59% with the increase of ionic strength from 0 M to 1 M (Fig. 4.3d) indicating that the electrostatic interaction significantly impacted the overall fluoride adsorption onto GO-CeO_2. The outer-sphere complexes were suppressed when ionic strength increased due to the competition between the electrolyte ions (i.e., Cl^-) and adsorbing anions (F^- here) for available surface sites (Liu et al., 2015). The electrolyte concentration might have also affected the interfacial potentials and that led to a decrease in adsorption activity as suggested by Hayes et al. (1988) (Hayes et al., 1988). The electrolyte ions and outer-sphere complexes are present in the same plane (β-plane of the diffuse double layer around the adsorbent surface) in a bulk solution (Hayes et al., 1988). Therefore, outer-sphere complexes are expected to be more sensitive than the inner-sphere complexes to ionic strength variation. We can infer that outer-sphere complexation (electrostatic interaction) was contributing to fluoride removal in this study.

4.3.9. Desorption study

A desorption study was conducted over a 3-month period to find out the stability of fluoride adsorbed onto the GO-CeO_2. Batches of GO-CeO_2 (20 mg) were saturated with fluoride by putting the nanohybrid in 20 mL of fluoride solution (10 mg/L) in 40 mL glass vials and shaking the vials end-over-end for 24 h. The saturated GO-CeO_2 were then separated and the bulk solution fluoride concentration was measured to determine the amount of fluoride adsorbed by GO-CeO_2. The decanted solution was then replaced with DI water and the contents (fluoride saturated GO-CeO_2 and DI water) were shook for another 24 h. After that, the GO-CeO_2 was separated again from the solution by centrifugation and the bulk solution was analyzed to estimate the amount of desorbed fluoride in the elapsed time. This process was continued at regular intervals for 3 months, and each time fresh DI water was used to replace the bulk solution. Results showed that the adsorbed fluoride remained strongly bound to GO-CeO_2 over the study period (Fig. 4.3e). About 1% of adsorbed fluoride got desorbed after the first day. After that only 1-2.8% of adsorbed fluoride got desorbed after each time period. After the 3-month time period, total fluoride desorbed was found to be 1.19 mg/g (11.9%). During fluoride removal by GO-CeO_2, fluoride complexed with Ce^{3+} to form insoluble CeF_3 in the ceria lattice (Menon et al., 1986; Valicsek et al., 2019) (see Fluoride Removal Mechanisms), and for that reason desorption was not that high. The ~12% desorption observed in this study was possibly from the fluoride adsorbed onto GO-CeO_2 via outer-sphere complexation (electrostatic interaction).

4.3.10. Fluoride removal mechanisms

Mechanisms involved: In the pH studies (Fig. 4.3a), the maximum fluoride removal was recorded at pH 4 (>> PZC, 2.7) and substantial removal occurred (~66%) even at pH 10. These

observations indicate that not only electrostatic interaction was responsible for fluoride removal by GO-CeO_2 but chemisorption was also potentially playing a role.

The fluoride removal by GO-CeO_2 decreased with the increase of ionic strength (Fig. 4.3d) indicating outer-sphere complex formation and electrostatic interaction of fluoride with GO-CeO_2. However, the presence of PO_4^{3-} and SO_4^{2-} significantly decreased fluoride adsorption onto GO-CeO_2 (Fig. 4.3c). Inner-sphere complexation governs the adsorption of PO_4^{3-} (Dhillon et al., 2016; McCormack et al., 2014), and SO_4^{2-} (Kuang et al., 2017) onto CeO_2. Given that PO_4^{3-} and SO_4^{2-} interfered with fluoride adsorption in our study, it is safe to assume that PO_4^{3-} and SO_4^{2-} were targeting the same inner-sphere sites that fluoride would have otherwise occupied. So, we can infer that fluoride adsorption by GO-CeO_2 might have occurred due to the formation of inner-sphere complexes as well. Others have reported similar phenomena where fluoride adsorption by ceria-based material was governed by inner-sphere complexation, and the presence of PO_4^{3-} and SO_4^{2-} significantly decreased the fluoride removal efficiency (Chigondo et al., 2018b; Dhillon et al., 2016; Kuang et al., 2017). While both outer-sphere and inner-sphere complexations played a significant role in fluoride removal by GO-CeO_2, the substantial removal (~66%) at high pH (pH 10 >> PZC) (Fig. 4.3a) and low desorption (~12%) from adsorbed phase during the desorption experiment (Fig. 4.3e) indicate that inner-sphere complexation (chemisorption) was more dominant than outer-sphere complexation.

To investigate the fluoride removal mechanism further, samples of the GO-CeO_2 before and after fluoride adsorption were characterized using XPS (Fig. 4.4). The peaks from the deconvoluted XPS Ce 3d spectra before and after fluoride adsorption (Fig. 4.4a) can be distinguished and ascribed to unique oxidation states. Peaks at ~880, 885, 898, and 903 eV belong to Ce^{3+} oxidation state and peaks at ~882, 888, 899, 901, 908, and 917 eV belong to Ce^{4+} oxidation

state (Seal et al., 2020). The XPS data have confirmed that the GO-CeO_2 used in this study contained both Ce^{3+} and Ce^{4+} before and after fluoride adsorption. We synthesized GO-CeO_2 via a hydrothermal process at a high temperature (140 ^oC) in a closed reaction vessel. Exposure to high temperature and/or reducing gas conditions (i.e., low oxygen partial pressures) led to the loss of oxygen from ceria crystal surface to the gas phase, generating intrinsic oxygen vacancies (defects) (Dutta et al., 2006; Schmitt et al., 2020). In ceria lattice, when an oxygen vacancy is created, two electrons are released and those electrons reduce Ce^{4+} to Ce^{3+} oxidation state (Campbell and Peden, 2005; Schmitt et al., 2020).

The concentration of Ce^{3+} before fluoride adsorption was 16% but increased to 34% after adsorption (Fig. 4.4a). The changes to the surface Ce^{3+} (or Ce^{4+}) oxidation state after fluoride adsorption was also highly visible in the deconvoluted Ce 3d XPS spectrum. The increase of Ce^{3+} after fluoride adsorption indicates that additional oxygen vacancies were created in the ceria lattice (Ahmad et al., 2014). The chemical shifts and changes in valence state concentrations (Fig. 4.4a) of cerium on the surface of GO-CeO_2 after fluoride adsorption reveal that charge transfer interaction occurred between the GO-CeO_2 (adsorbent) and F^- ions. The C 1s spectral lines in the XPS spectra for the nanohybrid before and after fluoride adsorption (Fig. 4.4c) show that the peaks belonging to GO (C-C/C=C, C-O-C, and O-C=O) have shifted (change in binding energies) after the adsorption of fluoride which also confirms the charge transfer interaction between GO-CeO_2 and F^- ions.

In addition, the O 1s envelops were analyzed and deconvoluted into four peaks (C=O, C-O, Ce^{3+}-O^{2-}, and Ce^{4+}-O^{2-}, Fig. 4.4b) (Kang et al., 2017). The major peak at a binding energy of ~529 eV represents the lattice oxygen of Ce^{4+}-O^{2-} and the peak at a binding energy of ~530 eV can be ascribed to the Ce^{3+}-O^{2-} lattice oxygen (Ahmad et al., 2014; Kumar et al., 2009). Because

the ionic radii of F^- (0.133 nm) and O^{2-} (0.140 nm) are almost of the same size (Slater, 1964), the added fluoride in this study might have replaced the O^{2-} ions in the ceria lattice via ion exchange (Fig. 4.5c, ii). This in turn led to a charge imbalance promoting conversion of Ce^{4+} to Ce^{3+} which is reflected in our XPS data (Ce^{3+} concentration increased after adsorption, Fig. 4.4a). The reduced Ce^{3+} continuously adsorbed fluoride and made fluorine (CeF_3) complex in the ceria lattice(Ahmad et al., 2014). The presence of a strong F 1s peak at binding energy ~684.5eV (Fig. 4.5a) in our used (i.e., after fluoride adsorption) nanohybrid confirms the presence of the chemically bound fluoride in ceria lattice (CeF_3) indicating that fluoride was effectively adsorbed by the GO-CeO_2. A similar phenomenon was reported by Ahmad et al. (2014) (Ahmad et al., 2014) where a fluoride-doped ceria nanocrystal was used for oxidative coupling of benzylamines, and they observed that the doped fluoride can occupy the oxygen sites of CeO_2 lattice and reported that Ce^{3+} forms CeF_3 with F^- ions. Further, they found a higher concentration of Ce^{3+} upon fluoride doping because of charge compensation due to F^- incorporation onto the O^{2-} sites which is in line with our observation of reduction of Ce^{4+} to Ce^{3+}.

From the adsorption behavior and XPS data, we can propose that the removal of fluoride by GO-CeO_2 happened in two steps (Fig. 4.5c): (1) first, fluoride was taken up by the nanohybrid electrostatically (outer-sphere complexation), and then (2) fluoride replaced O^{2-} and incorporated itself into the ceria lattice (inner-sphere complexation) releasing two electrons in the process. The released electrons reduced Ce^{4+} to Ce^{3+}, and the Ce^{3+} complexed with fluoride in the form of lattice fluorine (CeF_3).

Rapid kinetics and role of graphene oxide: To understand the rapid kinetics, we conducted a separate kinetic study with pristine CeO_2 NPs alone (not hybridized with GO), and observed that even though CeO_2 NPs exhibited poor removal of fluoride (13.4%), they exhibited fast kinetics till

1 min (Fig. 4.5b, Fig. C5, Appendix C). It can be inferred that the rapid removal (adsorption/capture) of fluoride by GO-CeO_2 was mostly because of the CeO_2 NPs. When only CeO_2 NPs (not hybridized with GO) showed poor fluoride removal of only 13.4% compared to 85% with GO-CeO_2 which indicates that GO might have played a major role in achieving the ~72% increase in fluoride removal (Fig. 4.2a). While effective dispersion of the CeO_2 NPs on the GO sheets (See TEM micrograph in Fig. 4.1a) possibly helped in enhanced fluoride removal, the GO-CeO_2 hybrid configuration might have also played additional roles. It is also worth noting that we used a dose of 1 g/L of CeO_2 NPs and GO-CeO_2 where the amount (mass) of CeO_2 was not the same (while CeO_2 was pure, GO-CeO_2 was a hybrid of GO and CeO_2 and 1 g of the nanohybrid contained less than 1 g of CeO_2). The role of GO is worth investigating.

When an oxygen vacancy is created in CeO_2 NPs, two electrons are released and left at the vacancy site of CeO_2 NPs, and these electrons remain localized in the f level of two cerium atoms and eventually help to reduce Ce^{4+} to Ce^{3+} (Joung et al., 2011; Pirmohamed et al., 2010; Skorodumova et al., 2002). GO sheets have both mobile holes and mobile electrons (Yeh et al., 2013). When CeO_2 nanoparticles are decorated onto GO sheets (in GO-CeO_2), the electrons in CeO_2 (localized in the f level) interact with the mobile holes of GO sheets via electrostatic interaction (Joung et al., 2011) (Fig. 4.5c, iii). Therefore, the mobile holes of GO sheets get trapped at the oxygen vacancy sites of CeO_2 NPs, and as a result, the mobile electrons present in GO sheets now face less resistance and can move along the GO sheets easily (Fig. 4.5c,iii). The mobile electrons present in the GO sheet move to the CeO_2 lattice (in GO-CeO_2) and reduce more Ce^{4+} to Ce^{3+} at the CeO_2 NPs-GO interface (Wang et al., 2018; Xia et al., 2017) (Fig. 4.5c,iii). The new Ce^{3+} also interacts with F^- ions to form CeF_3 complex, and that creates more oxygen vacancies. The GO sheets in this study might have facilitated the adsorption of fluoride onto GO-CeO_2 by

serving as an effective electron carrier. Others also reported electron transfer between metal oxide nanoparticles and GO sheets while reporting aqueous arsenic (Das et al., 2020) and methylene blue (Mohamadi and Ghorbanali, 2020) removal by other types of GO-based nanohybrids.

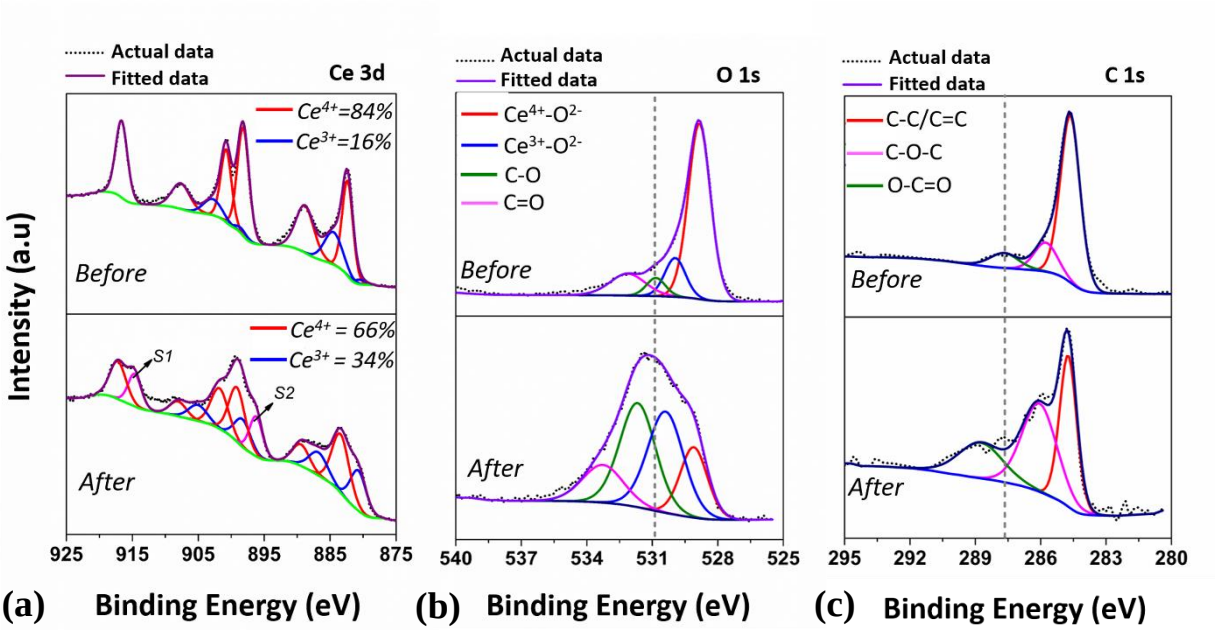

Figure 4.4. XPS spectra of GO-CeO_2 nanohybrid (a) Ce3d; (b) O1s; and (c) C1s before and after fluoride adsorption. The red line in Ce3d belongs to the Ce^{4+} oxidation state and the blue line is for Ce^{3+}. There are two additional peaks identified after fluoride adsorption, e.g., S1 and S2, and they belong to the satellite peaks of Ce^{3+}. The vertical dotted lines in O1s and C1s are to identify the chemical shift that occurred after fluoride adsorption.

Our claim that GO was playing a major role in achieving high fluoride removal needed additional validation by ruling out major CeO_2 NP surface area impact on fluoride removal. We conducted two sets of experiments (details in Section C.2.7, Appendix C) with only CeO_2 NPs (no GO) where we sonicated the nanoparticles in one experiment (Fig. C6a, Appendix C) and used Tween 20 surfactant (Fig. C6b, Appendix C) in another to disperse the nanoparticles. Increased dispersion (reduced agglomeration) enhanced the removal performance slightly (from 9% to 12% with sonication and 9% to 25% with Tween 20) but did not match the removal performance of

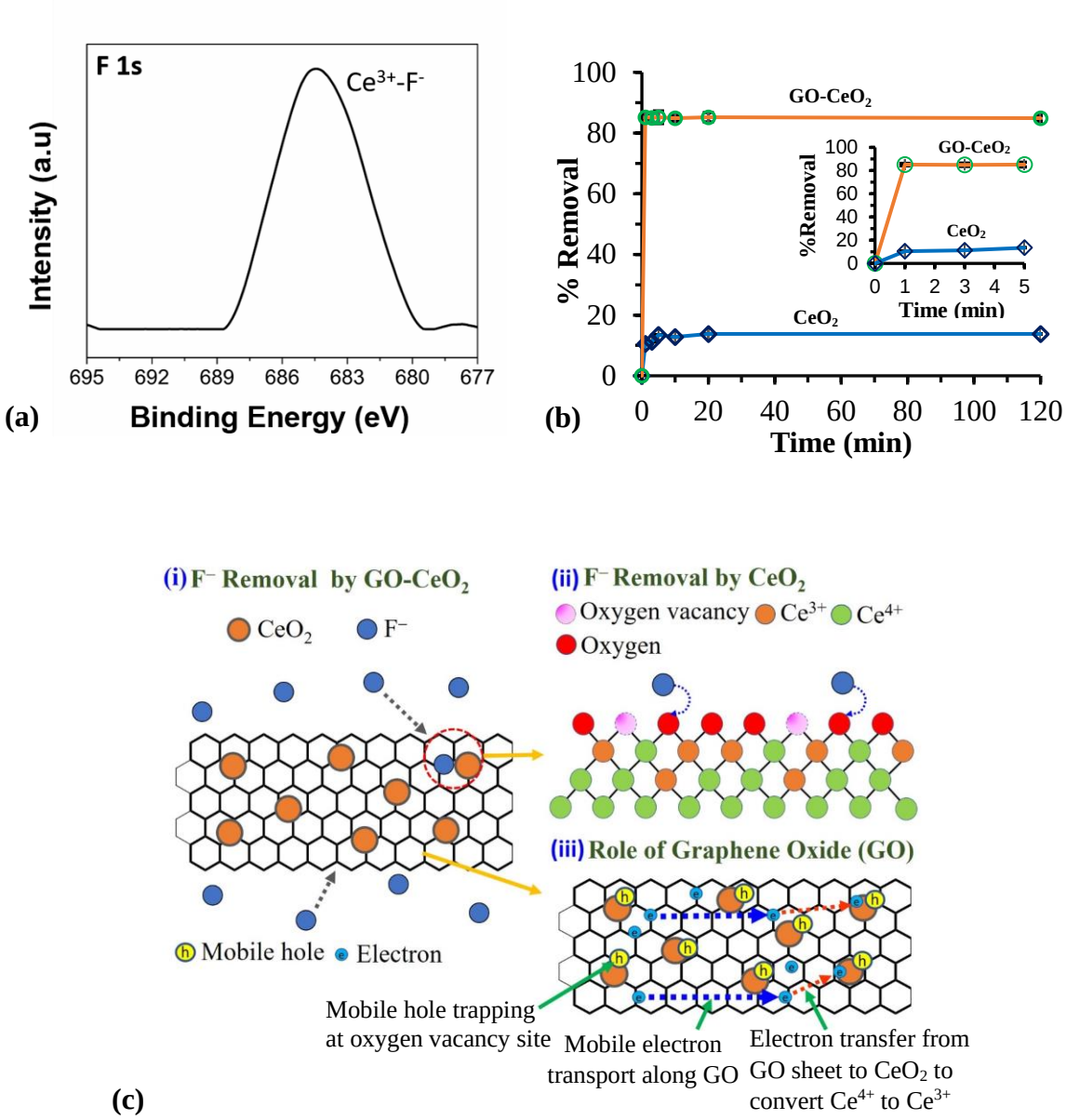

Figure 4.5. High-resolution XPS of F 1s spectrum after fluoride adsorption; (b) Fluoride removal by only CeO_2 NPs; the plot for fluoride removal by GO-CeO_2 is also shown for ease of comparison (Inset: Initial 5 min data zoomed in). The data points are connected with straight lines for ease of reading only and they do not represent trendlines, and the vertical error bars represent ± standard deviations; and (c) Schematic of the proposed mechanisms of fluoride removal by the GO-CeO_2 (i) the negatively charged fluoride ions move towards positively charged GO-CeO_2 and get adsorbed through electrostatic attraction; (ii) a ceria lattice with both Ce^{3+} and Ce^{4+} and surface oxygen vacancies, two ceria atoms coordinated with one oxygen atom. Fluoride replaces the surface O^{2-} by ion exchange process; and (iii) mobile holes of GO sheet trapped by the oxygen vacancy sites in the ceria lattice which facilitate the mobile electron transport in the GO sheet. The mobile electrons can transfer to CeO_2 at the CeO_2 NP-GO interface and reduce Ce^{4+} to Ce^{3+}.

GO-CeO_2 (85%). These results indicate that the reactive surface area is not the only factor that playing a role in the increase of fluoride removal efficiency. While the dispersion of CeO_2 NPs in the GO sheet reduces nanoparticle agglomeration to make them more reactive, the GO-CeO_2 hybrid configuration drastically enhances the reactivity of the ceria by possibly mediating an electron transfer process between the GO sheet and ceria.

4.3.11. Environmental application

The synthesis of graphene oxide ceria nanohybrid (GO-CeO_2) is a simple and scalable process. The fluoride removal capacity of GO-CeO_2 is comparable or better than commercially available adsorbents (Table C1, Appendix C). GO-CeO_2 is effective in a wide range of pH (2-10) (Fig. 4.3a) and the inferences by coexisting ions are comparable to the commercially available adsorbents (Table C3, Appendix C). GO-CeO_2 can potentially be used for point-of-use and community treatment units. Assuming 5 mg/L raw water fluoride and a 1.5 mg F^-/L limit as per WHO guidelines, we calculated the amount of GO-CeO_2 needed for a household treatment unit (filter) to treat 30 liters of water per family per day and compared that with two conventional fluoride adsorbents (detailed calculations in Section C.2.8, and Table C4, Appendix C). If the unit is run in near-neutral pH, 4.45 kg of GO-CeO_2 will be needed per year, but the running unit with adjusted raw water pH of 4 would reduce the amount to 2.38 kg per year. The corresponding amount of acidic alumina (AA) is 4.56 kg (pH 4.4) and granular activated alumina (GAA) is 15.90 kg (pH 7). The amount of GO-CeO_2 is needed in less amount respective of raw water pH and provide a distinct advantage. Further, minimal desorption of the adsorbed fluoride from the used GO-CeO_2 (Fig. 4.3e) makes it even more attractive. Before any field application, further studies are needed to optimize the material performance under continuous flow conditions and with actual F^- contaminated groundwater.

4.4. Conclusions

This study has evaluated the performance of a GO-CeO_2 nanohybrid for the fast capture of fluoride from water and investigated the mechanisms involved. The GO-CeO_2 nanohybrid exhibited ultra-rapid kinetics for fluoride removal by reaching the equilibrium within 1 minute which is at least 40 times faster than other ceria-based materials reported for fluoride removal and at least 20 times faster than all other materials reported including typical aluminum-based adsorbents. The adsorption capacity of GO-CeO_2 was found to be 8.61 mg/g which is comparable with the two conventionally used fluoride adsorbents, acidic alumina (AA), and granular activated alumina (GAA). The GO-CeO_2 exhibited effective fluoride removal over a wide range of pH (2-10). This novel material contains highly effective Ce^{3+}-O^{2-} in the lattice which plays a major role in the fast capture of aqueous fluoride via ion exchange. The GO sheet facilitated the fluoride removal process by serving as an effective electron mediator to reduce Ce^{4+} to Ce^{3+}, and Ce^{3+} continuously adsorbed more fluoride to make a stable CeF_3 complex. Because of its extremely rapid kinetics, the nanohybrid has the potential for use in high throughput defluoridation systems. To the best of our knowledge, this is the first time that fluoride removal by GO-CeO_2 nanohybrid and the possible mechanisms involved are reported.

4.5. References

Ahmad, S., Gopalaiah, K., Chandrudu, S.N., Nagarajan, R., 2014. Anion (Fluoride)-Doped Ceria Nanocrystals: Synthesis, Characterization, and Its Catalytic Application to Oxidative Coupling of Benzylamines. Inorganic Chemistry 53, 2030-2039.

Amini, M., Mueller, K., Abbaspour, K.C., Rosenberg, T., Afyuni, M., Moller, K.N., Sarr, M., Johnson, C.A., 2008. Statistical modeling of global geogenic fluoride contamination in groundwaters. Environmental Science & Technology 42, 3662-3668.

Araga, R., Sharma, C.S., 2017. Adsorption of fluoride in aqueous solution using Jamun (Syzygium cumini) seed derived activated carbon. Abstracts of Papers of the American Chemical Society 253.

Araga, R., Soni, S., Sharma, C.S., 2017. Fluoride adsorption from aqueous solution using activated carbon obtained from KOH-treated jamun (Syzygium cumini) seed. Journal of Environmental Chemical Engineering 5, 5608-5616.

Banerjee, A., 2015. Groundwater fluoride contamination: A reappraisal. Geoscience Frontiers 6, 277-284.

Bhatnagar, A., Kumar, E., Sillanpaa, M., 2011. Fluoride removal from water by adsorption-A review. Chemical Engineering Journal 171, 811-840.

Campbell, C.T., Peden, C.H.F., 2005. Chemistry - Oxygen vacancies and catalysis on ceria surfaces. Science 309, 713-714.

Chai, L.Y., Wang, Y.Y., Zhao, N., Yang, W.C., You, X.Y., 2013. Sulfate-doped Fe3O4/Al2O3 nanoparticles as a novel adsorbent for fluoride removal from drinking water. Water Research 47, 4040-4049.

Chen, C.L., Park, S.W., Huang, C.P., 2017. Functionalized activated carbons for enhancing fluoride removal capacity from water. Abstracts of Papers of the American Chemical Society 254.

Chen, L., Zhang, K.S., He, J.Y., Cai, X.G., Xu, W.H., Liu, J.H., 2016a. Performance and mechanism of hierarchically porous Ce-Zr oxide nanospheres encapsulated calcium alginate beads for fluoride removal from water. Rsc Advances 6, 36296-36306.

Chen, L., Zhang, K.S., He, J.Y., Xu, W.H., Huang, X.J., Liu, J.H., 2016b. Enhanced fluoride removal from water by sulfate-doped hydroxyapatite hierarchical hollow microspheres. Chemical Engineering Journal 285, 616-624.

Chigondo, M., Paumo, H.K., Bhaumik, M., Pillay, K., Maity, A., 2018a. Hydrous CeO2-Fe3O4 decorated polyaniline fibers nanocomposite for effective defluoridation of drinking water. Journal of Colloid and Interface Science 532, 500-516.

Chigondo, M., Paumo, H.K., Bhaumik, M., Pillay, K., Maity, A., 2018b. Rapid high adsorption performance of hydrous cerium-magnesium oxides for removal of fluoride from water. Journal of Molecular Liquids 265, 496-509.

Chouhan, S., Flora, S.J.S., 2010. Arsenic and fluoride: Two major groundwater pollutants. Indian Journal of Experimental Biology 48, 666-678.

Das, T.K., Sakthivel, T.S., Jeyaranjan, A., Seal, S., Bezbaruah, A.N., 2020. Ultra-high arsenic adsorption by graphene oxide iron nanohybrid: Removal mechanisms and potential applications. Chemosphere 253.

Dash, S.S., Sahu, M.K., Sahu, E., Patel, R.K., 2015. Fluoride removal from aqueous solutions using cerium loaded mesoporous zirconium phosphate. New Journal of Chemistry 39, 7300-7308.

Deng, S.B., Liu, H., Zhou, W., Huang, J., Yu, G., 2011. Mn-Ce oxide as a high-capacity adsorbent for fluoride removal from water. Journal of Hazardous Materials 186, 1360-1366.

Dhillon, A., Sharma, T.K., Soni, S.K., Kumar, D., 2016. Fluoride adsorption on a cubical ceria nanoadsorbent: function of surface properties. Rsc Advances 6, 89198-89209.

Di, Z.C., Li, Y.H., Peng, X.J., Luan, Z.K., Liang, J., 2007. Adsorption of fluoride by aligned carbon nanotubes supported ceria nanoparticles. pp. 1221-1224.

Dutta, P., Pal, S., Seehra, M.S., Shi, Y., Eyring, E.M., Ernst, R.D., 2006. Concentration of Ce3+ and oxygen vacancies in cerium oxide nanoparticles. Chemistry of Materials 18, 5144-5146.

Gbadebo, A.M., 2012. Groundwater fluoride and dental fluorosis in southwestern Nigeria. Environmental Geochemistry and Health 34, 597-604.

George, S., Pandit, P., Gupta, A.B., 2010. Residual aluminium in water defluoridated using activated alumina adsorption - Modeling and simulation studies. Water Research 44, 3055-3064.

Ghorai, S., Pant, K.K., 2005. Equilibrium, kinetics and breakthrough studies for adsorption of fluoride on activated alumina. Separation and Purification Technology 42, 265-271.

Goswami, A., Purkait, M.K., 2012. The defluoridation of water by acidic alumina. Chemical Engineering Research & Design 90, 2316-2324.

Hayes, K.F., Papelis, C., Leckie, J.O., 1988. Modeling Ionic-Strength Effects On Anion Adsorption At Hydrous Oxide Solution Interfaces. Journal Of Colloid And Interface Science 125, 717-726.

International Organization for Standardization(ISO)., 2000. Sample preparation-dispersing procedures for powders in liquids. International Organization for Standardization, Geneva, Switzerland.

Jagtap, S., Yenkie, M.K., Labhsetwar, N., Rayalus, S., 2012. Fluoride in Drinking Water and Defluoridation of Water. Chemical Reviews 112, 2454-2466.

Joung, D., Singh, V., Park, S., Schulte, A., Seal, S., Khondaker, S.I., 2011. Anchoring Ceria Nanoparticles on Reduced Graphene Oxide and Their Electronic Transport Properties. Journal of Physical Chemistry C 115, 24494-24500.

Kang, D., Yu, X., Ge, M., 2017. Morphology-dependent properties and adsorption performance of CeO2 for fluoride removal. Chemical Engineering Journal 330, 36-43.

Karmakar, S., Dechnik, J., Janiak, C., De, S., 2016. Aluminium fumarate metal-organic framework: A super adsorbent for fluoride from water. Journal of Hazardous Materials 303, 10-20.

Kovtun, A., Treossi, E., Mirotta, N., Scida, A., Liscio, A., Christian, M., Valorosi, F., Boschi, A., Young, R.J., Galiotis, C., Kinloch, I.A., Morandi, V., Palermo, V., 2019. Benchmarking of graphene-based materials: real commercial products versus ideal graphene. 2d Materials 6.

Kuang, L.Y., Liu, Y.Y., Fu, D.D., Zhao, Y.P., 2017. FeOOH-graphene oxide nanocomposites for fluoride removal from water: Acetate mediated nano FeOOH growth and adsorption mechanism. Journal of Colloid and Interface Science 490, 259-269.

Kumar, A., Babu, S., Karakoti, A.S., Schulte, A., Seal, S., 2009. Luminescence Properties of Europium-Doped Cerium Oxide Nanoparticles: Role of Vacancy and Oxidation States. Langmuir 25, 10998-11007.

Li, Z.J., Deng, S.B., Zhang, X.Y., Zhou, W., Huang, J., Yu, G., 2010. Removal of fluoride from water using titanium-based adsorbents. Frontiers of Environmental Science & Engineering in China 4, 414-420.

Liu, C.H., Chuang, Y.H., Chen, T.Y., Tian, Y., Li, H., Wang, M.K., Zhang, W., 2015. Mechanism of Arsenic Adsorption on Magnetite Nanoparticles from Water: Thermodynamic and Spectroscopic Studies. Environmental Science & Technology 49, 7726-7734.

Liu, L., Cui, Z.J., Ma, Q.C., Cui, W., Zhang, X., 2016. One-step synthesis of magnetic iron-aluminum oxide/graphene oxide nanoparticles as a selective adsorbent for fluoride removal from aqueous solution. Rsc Advances 6, 10783-10791.

Lv, L., He, J., Wei, M., Evans, D.G., Zhou, Z.L., 2007. Treatment of high fluoride concentration water by MgAl-CO3 layered double hydroxides: Kinetic and equilibrium studies. Water Research 41, 1534-1542.

Martyn, C.N., Osmond, C., Edwardson, J.A., Barker, D.J.P., Harris, E.C., Lacey, R.F., 1989. Geographical Relation Between Alzheimers-Disease And Aluminum In Drinking-Water. Lancet 1, 59-62.

McCormack, R.N., Mendez, P., Barkam, S., Neal, C.J., Das, S., Seal, S., 2014. Inhibition of Nanoceria's Catalytic Activity due to Ce3+ Site-Specific Interaction with Phosphate Ions. Journal of Physical Chemistry C 118, 18992-19006.

Meenakshi, Maheshwari, R.C., 2006. Fluoride in drinking water and its removal. Journal of Hazardous Materials 137, 456-463.

Menon, M.P., James, J., Jackson, J.D., 1986. Complexation, Solubilities And Thermodynamic Functions For Cerium(Iii) Fluoride-Water System. Journal of Radioanalytical and Nuclear Chemistry-Articles 102, 419-428.

Mkhoyan, K.A., Contryman, A.W., Silcox, J., Stewart, D.A., Eda, G., Mattevi, C., Miller, S., Chhowalla, M., 2009. Atomic and Electronic Structure of Graphene-Oxide. Nano Letters 9, 1058-1063.

Mohamadi, S., Ghorbanali, M., Adsorption and UV-assisted photodegradation of methylene blue by CeO2-decorated graphene sponge. Separation Science and Technology, 1-11.

Mohan, S., Kumar, V., Singh, D.K., Hasan, S.H., 2016. Synthesis and characterization of rGO/ZrO2 nanocomposite for enhanced removal of fluoride from water: kinetics, isotherm, and thermodynamic modeling and its adsorption mechanism. Rsc Advances 6, 87523-87538.

Mohanty, K., Jha, M., Meikap, B.C., Biswas, M.N., 2005. Removal of chromium(VI) from dilute aqueous solutions by activated carbon developed from Terminalia arjuna nuts activated with zinc chloride. Chemical Engineering Science 60, 3049-3059.

Mohapatra, M., Anand, S., Mishra, B.K., Giles, D.E., Singh, P., 2009. Review of fluoride removal from drinking water. Journal of Environmental Management 91, 67-77.

Mukhopadhyay, K., Ghosh, A., Das, S.K., Show, B., Sasikumar, P., Ghosh, U.C., 2017. Synthesis and characterisation of cerium(IV)-incorporated hydrous iron(III) oxide as an adsorbent for fluoride removal from water. Rsc Advances 7, 26037-26051.

Narsimha, A., Sudarshan, V., 2017. Contamination of fluoride in groundwater and its effect on human health: a case study in hard rock aquifers of Siddipet, Telangana State, India. Applied Water Science 7, 2501-2512.

Perreault, F., de Faria, A.F., Elimelech, M., 2015. Environmental applications of graphene-based nanomaterials. Chemical Society Reviews 44, 5861-5896.

Pirmohamed, T., Dowding, J.M., Singh, S., Wasserman, B., Heckert, E., Karakoti, A.S., King, J.E.S., Seal, S., Self, W.T., 2010. Nanoceria exhibit redox state-dependent catalase mimetic activity. Chemical Communications 46, 2736-2738.

Rashid, U.S., Bezbaruah, A.N., 2020. Citric acid modified granular activated carbon for enhanced defluoridation. Chemosphere 252.

Rohder, L.A., Brandt, T., Sigg, L., Behra, R., 2014. Influence of agglomeration of cerium oxide nanoparticles and speciation of cerium(III) on short term effects to the green algae Chlamydomonas reinhardtii. Aquatic Toxicology 152, 121-130.

Ruan, Z.Y., Tian, Y.X., Ruan, J.F., Cui, G.J., Iqbal, K., Iqbal, A., Ye, H.R., Yang, Z.Z., Yan, S.Q., 2018. Synthesis of hydroxyapatite/multi-walled carbon nanotubes for the removal of fluoride ions from solution (vol 412, pg 578, 2017). Applied Surface Science 437, 451-452.

Sadeghi, M.H., Tofighy, M.A., Mohammadi, T., 2020. One-dimensional graphene for efficient aqueous heavy metal adsorption: Rapid removal of arsenic and mercury ions by graphene oxide nanoribbons (GONRs). Chemosphere 253.

Safi, M., Sarrouj, H., Sandre, O., Mignet, N., Berret, J.F., 2010. Interactions between sub-10-nm iron and cerium oxide nanoparticles and 3T3 fibroblasts: the role of the coating and aggregation state. Nanotechnology 21.

Sakthivel, T.S., Das, S., Pratt, C.J., Seal, S., 2017. One-pot synthesis of a ceria-graphene oxide composite for the efficient removal of arsenic species. Nanoscale 9, 3367-3374.

Schmitt, R., Nenning, A., Kraynis, O., Korobko, R., Frenkel, A.I., Lubomirsky, I., Haile, S.M., Rupp, J.L.M., 2020. A review of defect structure and chemistry in ceria and its solid solutions. Chemical Society Reviews 49, 554-592.

Seal, S., Jeyaranjan, A., Neal, C.J., Kumar, U., Sakthivel, T.S., Sayle, D.C., 2020. Engineered defects in cerium oxides: tuning chemical reactivity for biomedical, environmental, & energy applications. Nanoscale 12, 6879-6899.

Sharma, R., Raghav, S., Nair, M., Kumar, D., 2018. Kinetics and Adsorption Studies of Mercury and Lead by Ceria Nanoparticles Entrapped in Tamarind Powder. Acs Omega 3, 14606-14619.

Skorodumova, N.V., Simak, S.I., Lundqvist, B.I., Abrikosov, I.A., Johansson, B., 2002. Quantum origin of the oxygen storage capability of ceria. Physical Review Letters 89.

Slater, J.C., 1964. ATOMIC RADII IN CRYSTALS. Journal of Chemical Physics 41, 3199-&.

Strunecka, A., Patocka, J., 1999. Pharmacological and toxicological effects of aluminofluoride complexes. Fluoride 32, 230-242.

Sujana, M.G., Thakur, R.S., Rao, S.B., 1998. Removal of fluoride from aqueous solution by using alum sludge. Journal of Colloid and Interface Science 206, 94-101.

Tang, D., Zhang, G., 2016. Efficient removal of fluoride by hierarchical Ce-Fe bimetal oxides adsorbent: Thermodynamics, kinetics and mechanism. Chemical Engineering Journal 283, 721-729.

USEPA (U.S. Environmental Protection Agency), 2009. National Primary Drinking Water Regulations. Available at: https://www.epa.gov/ground-water-and-drinking-water/national-primary-drinking-water-regulations#Inorganic, Accessed date: March, 2021.

Valicsek, Z., Kovacs, M., Horvath, O., 2019. Explanation for the Multi-Component Scintillation of Cerium Fluoride Through the Equilibrium and Photophysical Investigation of Cerium(III)-Fluoro Complexes. Nanomaterials 9.

Wang, H., Feng, Q.M., Liu, K., Li, Z.S., Tang, X.K., Li, G.Z., 2017. Highly efficient fluoride adsorption from aqueous solution by nepheline prepared from kaolinite through alkali-hydrothermal process. Journal of Environmental Management 196, 72-79.

Wang, J., Xu, W.H., Chen, L., Jia, Y., Wang, L., Huang, X.J., Liu, J.H., 2013. Excellent fluoride removal performance by CeO2-ZrO2 nanocages in water environment. Chemical Engineering Journal 231, 198-205.

Wang, Z.Q., Zhao, P.F., He, D.N., Cheng, Y., Liao, L.S., Li, S.D., Luo, Y.Y., Peng, Z., Li, P.W., 2018. Cerium oxide immobilized reduced graphene oxide hybrids with excellent microwave absorbing performance. Physical Chemistry Chemical Physics 20, 14155-14165.

Weber, W.J., Morris, J.C., 1963. Kinetics of adsorption on carbon from solution. Journal of the Sanitary Engineering Division 89, 31-60.

Wendt, S., Matthiesen, J., Schaub, R., Vestergaard, E.K., Laegsgaard, E., Besenbacher, F., Hammer, B., 2006. Formation and splitting of paired hydroxyl groups on reduced TiO2(110). Physical Review Letters 96.

WHO, 2004. Guidelines for drinking-water quality. Volume 1 recommendations, 3rd edn. World Health Organization, Geneva.

Wu, Z.S., Yang, S.B., Sun, Y., Parvez, K., Feng, X.L., Mullen, K., 2012. 3D Nitrogen-Doped Graphene Aerogel-Supported Fe3O4 Nanoparticles as Efficient Eletrocatalysts for the Oxygen Reduction Reaction. Journal of the American Chemical Society 134, 9082-9085.

Xia, W., Zhao, J., Wang, T., Song, L., Gong, H., Guo, H., Gao, B., Fan, X.L., He, J.P., 2017. Anchoring ceria nanoparticles on graphene oxide and their radical scavenge properties under gamma irradiation environment. Physical Chemistry Chemical Physics 19, 16785-16794.

Xiao, H., Ai, Z., Zhang, L., 2009. Nonaqueous Sol-Gel Synthesized Hierarchical CeO2 Nanocrystal Microspheres as Novel Adsorbents for Wastewater Treatment. Journal of Physical Chemistry C 113, 16625-16630.

Yadav, K.K., Gupta, N., Kumar, V., Khan, S.A., Kumar, A., 2018. A review of emerging adsorbents and current demand for defluoridation of water: Bright future in water sustainability. Environment International 111, 80-108.

Yeh, T.F., Cihlar, J., Chang, C.Y., Cheng, C., Teng, H.S., 2013. Roles of graphene oxide in photocatalytic water splitting. Materials Today 16, 78-84.

Yu, X.F., Liu, J.W., Cong, H.P., Xue, L., Arshad, M.N., Albar, H.A., Sobahi, T.R., Gao, Q., Yu, S.H., 2015. Template- and surfactant-free synthesis of ultrathin CeO2 nanowires in a mixed solvent and their superior adsorption capability for water treatment. Chemical Science 6, 2511-2515.

Yu, Z.C., Xu, C.H., Yuan, K.K., Gan, X.Z., Feng, C., Wang, X.Q., Zhu, L.Y., Zhang, G.H., Xu, D., 2018. Characterization and adsorption mechanism of ZrO2 mesoporous fibers for health-hazardous fluoride removal. Journal of Hazardous Materials 346, 82-92.

Zhang, F., Chan, S.W., Spanier, J.E., Apak, E., Jin, Q., Robinson, R.D., Herman, I.P., 2002. Cerium oxide nanoparticles: Size-selective formation and structure analysis. Applied Physics Letters 80, 127-129.

Zhang, J., Chen, N., Su, P.Y., Li, M., Feng, C.P., 2017. Fluoride removal from aqueous solution by Zirconium-Chitosan/Graphene Oxide Membrane. Reactive & Functional Polymers 114, 127-135.

Zhang, J., Kong, Y.Q., Yang, Y., Chen, N., Feng, C.P., Huang, X.D., Yu, C.Z., 2019a. Fast Capture of Fluoride by Anion-Exchange Zirconium-Graphene Hybrid Adsorbent. Langmuir 35, 6861-6869.

Zhang, S., Wang, H., Liu, J., Bao, C., 2020. Measuring the specific surface area of monolayer graphene oxide in water. Materials Letters 261.

Zhang, Y.Y., Qian, Y., Li, W., Gao, X., Pan, B., 2019b. Fluoride uptake by three lanthanum based nanomaterials: Behavior and mechanism dependent upon lanthanum species. Science of the Total Environment 683, 609-616.

Zhao, X.L., Wang, J.M., Wu, F.C., Wang, T., Cai, Y.Q., Shi, Y.L., Jiang, G.B., 2010. Removal of fluoride from aqueous media by Fe3O4@Al(OH)(3) magnetic nanoparticles. Journal of Hazardous Materials 173, 102-109.

CHAPTER 5: CONCLUSIONS

5.1. Conclusions

In this research, two activated carbon-based adsorbents and a metal-based adsorbent were developed and evaluated for defluoridation. In the first phase of this research, a commercial-grade granular activated carbon (GAC) was successfully modified by a weak organic acid (citric acid), and the fluoride removal efficiency and mechanisms were investigated with the citric acid modified granular activated carbon (CAGAC). The citric acid (CA) modification introduced additional functional groups on the GAC surface and that increased the fluoride adsorption capacity of the activated carbon. More than 70% of fluoride was removed by CAGAC for all fluoride concentrations tested (5-20 mg F^-/L) compared to only 30% by unmodified GAC. The maximum adsorption capacity of CAGAC was almost two times higher (1.65 mg/g) than unmodified GAC (0.88 mg/g). The adsorption capacity of CAGAC is comparable with other activated carbon-based adsorbents modified with strong inorganic acids (H_2SO_4 and HNO_3) reported by others (Ravulapalli & Kunta, 2017; Yadav et al., 2013). Pseudo-first-order and Dubinin-Radushkevich (D-R) isotherm described the experimental data well indicating that ion exchange was involved in fluoride removal by CAGAC. The kinetic data were fitted into the intraparticle diffusion model and results indicated that both surface adsorption and intra-particle diffusion were participating in the fluoride removal process. CAGAC worked effectively over a wide range of pH (2-10) even though the point-of-zero-charge (PZC) was 4.89 suggesting that the removal was not controlled by only electrostatic interaction, but the ion-exchange process was also involved in the removal process. There were negligible interferences by co-existing ions (NO_3^-, Cl^-, HCO_3^-, SO_4^{2-}, PO_4^{3-}) and organic matters at environmentally relevant concentrations. Desorption studies were carried out to find out the stability of the adsorbed fluoride, and the

adsorbed fluoride was minimally leaching out of adsorbed fluoride from the CAGAC making the adsorbent a reliable one. In Phase I of this research, we have developed a fluoride adsorbent that did not involve the use of any toxic chemicals or strong acid.

In the second phase of this research, a lime-modified granular activated carbon (LGAC) was prepared and its fluoride removal capacity was investigated. Lime juice was selected as an alternative to citric acid given lime and similar citrus fruits contain 0.2 to 0.3 M citric acid. The performance of LGAC with the citric acid modified granular activated carbon (CAGAC) prepared in the first phase of this research was compared. Over 70% fluoride was removed by both LGAC and CAGAC at all initial fluoride concentrations and the equilibrium was achieved within 4 hours. The maximum fluoride adsorption capacity of LGAC was found to be 1.63 mg/g which is very close to the maximum adsorption capacity of CAGAC (1.65 mg/g). The point-of-zero-charge (PZC) was 3.09 for LGAC. However, LGAC exhibited good fluoride removal efficiency at environmentally relevant pH (4-8). The presence of interfering ions did not significantly impact the fluoride removal efficiency when the co-existing anions were present at environmentally relevant concentrations. Within this study, the surface of granular activated carbon was modified with a locally available material (i.e., lime). Lime is very safe to handle and easy to work with. There is no possibility of leaching of toxic complexes like in an activated alumina-based adsorbent. This new material (LGAC) has the potential to be used in socio-economically challenged and remote communities to remove fluoride from groundwater. The major contribution of this work was the development of a very simple activated carbon functionalization technique that can be adopted easily by communities across the globe.

The third phase of this research evaluated the performance of graphene oxide-ceria (GO-CeO_2) nanohybrid for the removal of fluoride from water. This nanohybrid achieved the fastest

fluoride removal by reaching the equilibrium in less than 1 minute (85% fluoride removal) which is at least 40 times faster than other ceria-based adsorbents reported for fluoride removal (Table 4.1). This material showed the fastest kinetics reported so far in literature for any types of materials for fluoride removal (Table C1). The maximum fluoride adsorption capacity of the GO-CeO_2 nanohybrid was found to be 8.61 mg/g (at pH = 6.5) which is comparable with the most commonly used adsorbent, activated alumina (AA). The absorption capacity was further improved (to 16.07 mg/g) by lowering pH to 4.0. This novel material contains Ce^{3+}-O^{2-} in the lattice which plays an important role in the fast capture of fluoride from the water via ion exchange. The GO sheets also might have facilitated the fast capture of fluoride by serving as an effective electron mediator to reduce Ce^{4+} to Ce^{3+}, and Ce^{3+} continuously adsorbs more fluoride to make CeF_3 and/or CeF_3-like complexes. Because of its extremely rapid kinetics, the nanohybrid has the potential for use in high throughput (high flow) defluoridation system.

5.2. Future direction

Two activated carbon-based (CAGAC and LGAC) and a metal-based nanohybrid (GO-CeO_2) were prepared in the laboratory and used for fluoride removal from an aqueous solution. The behavior of these three adsorbents was investigated under relevant environmental conditions. However, the applicability of these adsorbents for *in situ* conditions still needs to be validated. Therefore, column studies and pilot-scale studies should be conducted with these adsorbents to make the processes adaptable in different situations, and that will help in establishing the viability of these technologies. In addition, the fluoride removal capacity of these adsorbents needs to be tested with real groundwater contaminated with fluoride. Further, the economics and social acceptability of the developed technology should be evaluated.

To increase the effectiveness of an adsorbent for fluoride removal, the regeneration and reuse of the spent adsorbent must be possible. The successful regeneration not only increases the efficacy of the adsorbent but also reduces the amount of used adsorbent that needs to be disposed of. Detailed and exhaustive regeneration studies should be conducted to find out the best solvents for regenerating CAGAC, LGAC, and GO-CeO_2. The solvents for CAGAC and LGAC regeneration should be locally available and should not be toxic as these new materials are targeted for use in rural, remote, and socio-economically challenged communities. After a certain number of regenerations cycles, the adsorbents need to be disposed of safely. A detailed study needs to be conducted to find out the proper handling, disposal, and stabilization of fluoride saturated CAGAC, LGAC, and GO-CeO_2.

While the surface of activated carbon was successfully modified using citric acid and lime juice (as a source of citric acid) for enhanced defluoridation, other citrus fruits should be used as a source of citric acid to modify the surface of activated carbon for fluoride removal.

5.3. References

Ravulapalli, S., Kunta, R., 2017. Defluoridation studies using active carbon derived from the barks of Ficus racemosa plant. Journal of Fluorine Chemistry 193, 58-66.

Yadav, A.K., Abbassi, R., Gupta, A., Dadashzadeh, M., 2013. Removal of fluoride from aqueous solution and groundwater by wheat straw, sawdust and activated bagasse carbon of sugarcane. Ecological Engineering 52, 211-218.

APPENDIX A

Table A1. Kinetic parameters associated with F^- adsorption onto CAGAC.

C_0 F^- (mg/L)	Experimental	From the Models				
		Pseudo First-Order		Pseudo Second-Order		
	$q_{e,exp}$ (mg/g)	$q_{e,cal}$ (mg/g)	R^2	$q_{e,cal}$ (mg/g)	R^2	k ($mgL^{-1}s^{-1}$)
5	0.208	0.100	0.793	0.218	0.994	0.00347
10	0.355	0.199	0.908	0.376	0.999	0.00262
20	0.721	0.235	0.868	0.730	0.999	0.00719

$q_{e,exp}$: Experimental equilibrium adsorption capacities, $q_{e,cal}$: Model predicted equilibrium adsorption capacities, R^2: Correlation coefficient, k: Reaction rate constant.

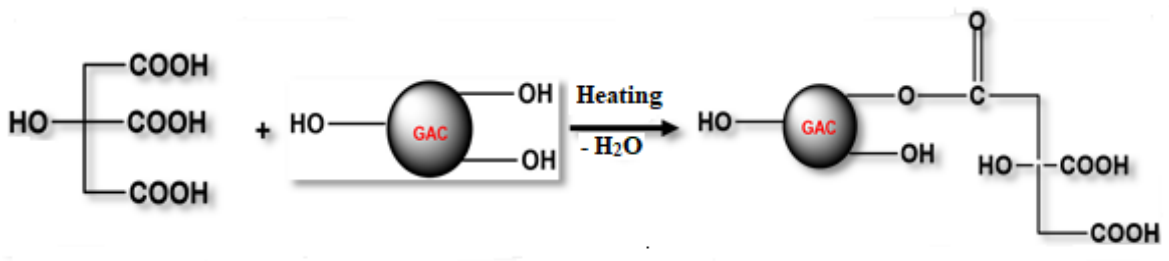

Figure A1. Citric acid modification of granular activated carbon (GAC)

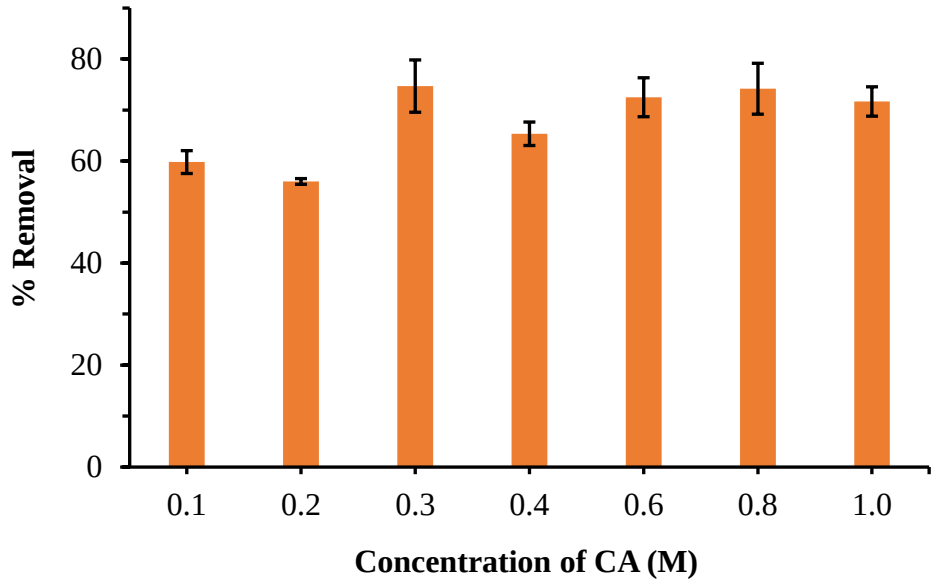

Figure A2. Effect of citric acid (CA) concentration (used for GAC surface modification) on F^- adsorption by CAGAC. No significant differences were observed in removal efficiency beyond 0.3 M CA ($p = 0.000$ for 0.1 M and 0.3 M also $p = 0.909$-1.000 for 0.3 M and other higher CA concentrations, $\alpha = 0.05$). The vertical error bars indicate ± standard deviations.

APPENDIX B

B.1. Effect of co-existing ions

Fluoride contaminated groundwater contains other anions which can potentially compete with F^- during adsorption onto LGAC. The effect of co-existing ions on fluoride removal by LGAC was carried out in presence of potential interfering anions (NO_3^-, PO_4^{3-}, HCO_3^-, and SO_4^{2-}). The presence of SO_4^{2-}, PO_4^{3-} and NO_3^- negatively affected the fluoride removal at high concentrations (100 mg/L). In the presence of high PO_4^{3-} concentration (100 mg/L), the fluoride removal efficiency decreasing from 70% (0 mg/L PO_4^{3-}) to 7% (100 mg PO_4^{3-}P/L). It is highly unlikely to have PO_4^{3-} concentrations of 100 mg/L in groundwater. The typical concentration of PO_4^{3-} in groundwater is 0.001-3 mg/L (Zhao et al., 2010; Thakur and Mondar, 2017) and will not affect fluoride removal by LGAC. Similarly, in the presence of high SO_4^{2-} concentration (100 mg/L) the fluoride removal efficiency decreased by 15%. Typically reported concentration of SO_4^{2-} in groundwater is 0.81-60 mg/L (Sailo and Mahanta, 2014; Bhagawan et al., 2019) and thus will have minimal effect on fluoride removal efficiency. The presence of NO_3^- at a high concentration (100 mg/L) decreased the fluoride removal efficiency by 14%. It is important to note that the typical NO_3^- concentration in groundwater is 0.01-42 mg/L (Sailo and Mahanta, 2014; Thakur and Mondar, 2017). So, NO_3^- will not affect the fluoride removal efficiency. A similar interference pattern was also observed in fluoride removal by CAGAC. Both LGAC and CAGAC exhibited the same order of interference as $PO_4^{3-} > SO_4^{2-} > NO_3^-$. The degree of interference is consistent with the charge/radius (z/r) ratio of the anions which have the following order: PO_4^{3-} (3/3.40) > SO_4^{2-} (2/2.40) > NO_3^- (1/2.81) (Chigondo et al., 2018). The higher the ratio, the stronger will be the competition between the anions and fluoride for the active adsorption sites (Zhao et al., 2010).

B.2. Thermodynamic parameters

A thermodynamic study was conducted to understand the feasibility and spontaneity of the fluoride adsorption process. Three major thermodynamic parameters, changes in (1) standard free energy (ΔG^o), (2) standard enthalpy (ΔH^o), and (3) standard entropy (ΔS^o) were used to find out the nature of the fluoride adsorption process onto LGAC. These parameters were obtained from the slope and intercept of Van't Hoff plot of $\ln K_0$ vs reciprocal temperature 1/T. The Van't Hoff plot was developed based on the following thermodynamic equations (Eq. B1-B2) (Wang et al., 2017):

$$lnK_0 = \frac{\Delta S^0}{R} - \frac{\Delta H^0}{RT} \qquad (B1)$$

$$\Delta G^o = RTlnK_0 \qquad (B2)$$

where K_0 is the thermodynamic equilibrium constant, T is the absolute temperature in Kelvin (K) and R is the universal gas constant (8.314 J/mol K). The endothermic nature of fluoride adsorption onto both LGAC surface and CAGAC surface is indicated by the positive value of ΔH^0 **(**25.704 kJ mol^{-1} for LGAC and 6.549 kJ mol^{-1} for CAGAC, Table 4) (Xu et al., 2016). The negative values of ΔG^o (–1.464 - –4.344 k $Jmol^{-1}$ for LGAC and –1.658 - –0.2.528 kJ mol^{-1} for CAGAC) at all temperatures suggested the feasibility and spontaneous nature of the fluoride adsorption onto LGAC and CAGAC (Mullick and Neogi, 2018). Furthermore, with the increase of temperature, the value of $\Delta G°$ decreased indicating that the fluoride adsorption onto both LGAC and CAGAC is more spontaneous at high temperature (Amalraj and Pius, 2017). The positive value of $\Delta S°$ (0.096 kJ mol^{-1} for LGAC and 0.029 for CAGAC) verifies the affinity of the adsorbents (LGAC and CAGAC) for fluoride and also suggests the increase in randomness at the interface of solid (LGAC and CAGAC) and solution (containing fluoride) during adsorption (Mullick and Neogi, 2018) (Xu et al., 2016).

B.3. Desorption study

A desorption study was conducted over a 6-month period to find out the stability of fluoride adsorbed onto LGAC. Several batches of LGAC saturated with adsorbed fluoride were prepared (400 mg of LGAC in 20 mL of 100 mg F^-/L solution in 40 mL glass vials and shaken in an end-over-end shaker for 24 h). The saturated LGAC was then separated by centrifuging the vials and decanting the supernatant. The fluoride concentration in the supernatant was measured to determine the amount of fluoride adsorbed by LGAC. The decanted solution was then replaced with DI water and the contents (fluoride saturated LGAC and DI water) were shaken in an end-over-end shaker for another 24 h. After that, the LGAC was separated again from the solution by centrifugation and the supernatant was analyzed to estimate the amount of desorbed fluoride. This process was continued at regular intervals for 6 months and each time fresh DI water was used to replace the supernatant. Mass balance was conducted each time to determine the exact amount of fluoride desorbed after the elapsed time.

Table B1. Composition of conventional lime juice (after Rangel et al., 2011).

Parameter	Amount
pH	2.81
Citric acid (Titratable Acidity)	6.05
Soluble Solids	8.42
Ascorbic Acid (mg/100 mL)	22.86
Glucose (g/100 g)	0.89
Fructose (g/100 g)	0.98
Sucrose (g/100 g)	0.07
K (µg/g)	376.79
Ca (µg/g)	23.24
Mn (µg/g)	0.08
Fe (µg/g)	1.71
Cu (µg/g)	0.35
Zn (µg/g)	0.29

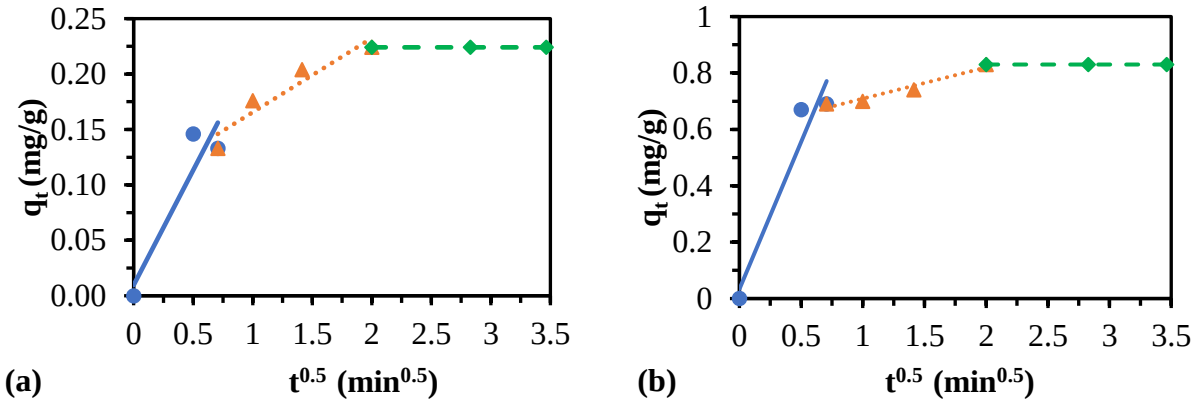

Figure B1. Plots of the intra-particle diffusion kinetics equation for adsorption of fluoride ions onto LGAC (a)) Initial fluoride concentration, C_0 = 5 mg F/L; (b) C_0 = 20 mg/L. The presence of multi-linearity in the plots for both the concentrations indicates that intra-particle diffusion is not the only rate-determining step for fluoride removal.

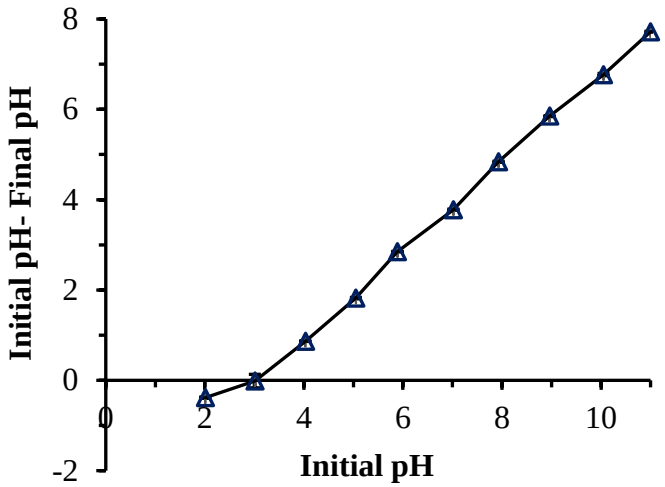

Figure B2. The Point-of-zero-charge of LGAC was found to be 3.05. The data points are connected with straight lines for ease of reading only and they do not represent trendlines. The vertical error bars indicate ± standard deviations.

APPENDIX C

C.1. Materials and methods

C.1.1. Materials

Cerium(III) nitrate hexahydrate ($Ce(NO_3)_3 \cdot 6H_2O$, ACS grade, Sigma Aldrich), ammonium hydroxide (NH_4OH, ACS, Sigma Aldrich), sodium hydroxide (NaOH, ACS, BDH), hydrochloric acid (HCl, ACS, EMD Millipore), sodium sulfate (Na_2SO_4, ACS, Sigma-Aldrich), sodium fluoride (NaF, ACS, Spectrum), sodium chloride (NaCl, ACS, EMD Millipore), potassium nitrate (KNO_3, ACS, Sigma-Aldrich), sodium bicarbonate ($NaHCO_3$, ACS, Sigma-Aldrich), Tween 20 (Reagent Grade, VWR) and potassium dihydrogen phosphate (KH_2PO_4, 99% pure, EMD Millipore) were used as received unless otherwise specified. The graphene oxide (GO, multi-layered) was obtained from Garmor, Inc. (Orlando, FL), and used without further modification.

C.1.2. Synthesis of GO-CeO_2 nanohybrid

The GO-CeO_2 nanohybrid was synthesized by following a one-pot synthesis process as described by Sakthivel et al. (2017) (Sakthivel et al., 2017). First, an appropriate amount of GO was sonicated in DI water for 60-90 min. Then cerium(III) nitrate hexahydrate was added to the GO solution and the mixture was stirred in a magnetic stirrer. After then, the pH of the solution was raised to 10 by drop-wise addition of ammonium hydroxide and was stirred for 15–30 min. The solution was then transferred to an acid digestion vessel followed by heating up to 140 °C for 2-5 hours with proper precautions. When the vessel cooled down to room temperature (22±2 ^oC), the solution was washed with DI water several times to remove the excess ammonium hydroxide and then dried. The yield of GO-CeO_2 nanohybrid was 97% in this process.

C.1.3. Characterization

High-resolution transmission electron microscopy (HRTEM) was performed using an FEI Tecnai F30 operating at 300 keV. Scanning Electron Microscopy (SEM) was carried out with a ZEISS ultra-55 FEG SEM. X-ray photoelectron spectroscopy (XPS) analysis was conducted using an ESCALAB-250Xi spectrometer in an ultra-high vacuum chamber (below 7 x 10^{-9} mbar) using an Al-Kα monochromatic radiation source, operating at a power of 300 W (15 kV, 20 mA). The spot size of the electron beam was 650 µm. Liquid CNP samples were dropped cast on Gold foil (Au) for measuring the XPS spectrum which helped in avoiding the substrate chemical effect. Binding energies were calibrated based on C 1s peak at 284.8 eV ± 0.2. Thermo Scientific Avantage software was used for the data processing and peak fitting. The Ce (3d) spectra are fitted with sets of spin-orbit split doublets of Ce 3d (3d5/2 and 3d3/2) with a Gaussian-Lorentzian peak shape after applying smart background in Avantage software. To ensure proper peak fitting, the area ratio of 3d spin-orbit split doublets, their splits, as well as peak positions, and their FWHMs from the reference spectra were considered. Spectra were analyzed using an automated incremental peak deconvolution program which varied the peak height within an envelope over a complete range to determine the best fit and checked using the X-squared value to the actual data. The percent concentration of surface Ce^{3+} (or Ce^{4+}) ions in the nanohybrid were calculated from the ratio of the sum of the integrated areas of the XPS 3d peaks related to Ce^{3+} (or Ce^{4+}) to the total integral area for the whole Ce 3d region. A Zetasizer Nano ZS (Malvern Panalytical Ltd, Malvern, UK) was used to measure zeta potential.

C.1.4. Batch studies

The batch study experiments for fluoride removal were carried out in 40 mL glass vials fitted with a plastic cap and a silicon septum. Each reactor was filled with 20 mL of fluoride

solutions and a measured amount of adsorbent (GO-CeO_2 nanohybrid, GO, or CeO_2 nanoparticles) was added. The reactors were rotated in a custom-made end-over-end shaker (28 rpm) and withdrawn at predetermined time intervals. The adsorbent in the withdrawn sample was filtered out from bulk solution using a 0.2 µm syringe filter. The filtrate was analyzed for fluoride using SPADNS Method in a UV-VIS spectrophotometer (Hach, Model DR 5000, Method 8029, detection range: 0.02-2.00 mg/L). Separate calibration for fluoride was done for each batch experiment. The removal efficiency (% removal) of fluoride was calculated as $(C_0 - C_e)/C_e*100\%$ (where C_0 is the initial and C_e is equilibrium F^- concentration). The fluoride removal efficiency of GO-CeO_2 nanohybrid was compared with the controls (GO and CeO_2 nanoparticles alone in batches). All experiments were performed at room temperature (22 ± 2 ^oC) and pH of 6.5-7.0 in batch reactors. The initial pH of the solution was adjusted using 0.1 M HCl or 0.1 M NaOH with no buffering or additional pH adjustment during the experiment. The initial fluoride concentration (C_0) was 10 mg/L and the duration of the batch study was 2 h. In preliminary studies, different adsorbent dosages (0.2, 0.6, 1.0, and 1.5 g/L of GO-CeO_2) were used and it was determined that 1 g/L adsorbent dosing was sufficient to bring down the fluoride concentration to 1.5 mg/L (WHO recommended level). All experiments henceforth were conducted with 1 g/L adsorbent (nanohybrid). The batch kinetic experiments for fluoride adsorption onto the GO-CeO_2 nanohybrid were conducted at an initial fluoride concentration (C_0) of 10 mg/L by varying the reaction times (0, 1, 3, 5, 15, 30, and 120 min). Isotherm studies were carried out by varying the initial fluoride concentration from 5 to 40 mg/L. Isotherm data were fitted onto Freundlich and Langmuir models, and the maximum adsorption capacity of the GO-CeO_2 nanohybrid was determined. The effect of pH was evaluated in the pH range of 2 to 10 (initial pH adjusted with 0.1 M HCl or 0.1 M NaOH, C_0 = 10 mg/L), and the bulk solution fluoride concentration was measured at 24 h. The possible

interferences by the co-existing ions and compounds on fluoride removal by the nanohybrid were investigated using different concentrations (0, 10, 100 mg/L) of sulfate (SO_4^{2-}), phosphate (PO_4^{3-}-P), bicarbonate (HCO_3^-) and nitrate (NO_3^-- N). The effect of ionic strength was evaluated using different concentrations (0, 0.01 M, 0.1 M, and 1.0 M) of NaCl.

C.2. Results and discussions

C.2.1. Comparison of GO-CeO_2 with existing fluoride adsorbents.

Table C1 lists the relevant existing fluoride adsorbents and their characteristics.

Table C1. Comparison of fluoride removal by different ceria-based and other conventional materials.

Adsorbent	pH	Adsorbent Dose (g/L)	Initial F^- Conc (mg/L)	Sorbent/ Sorbate (g/mg)	Contact Time (min)	% Removal	Adsorption Capacity (mg/g)	Source
Literature reported ceria-based materials								
Hydrous CeO_2-Fe_3O_4 decorated polyaniline fibers	6.0	0.6	40	0.015	120	90	93.46-117.64	(Chigondo et al., 2018)
CeO_2-Rod	3.5	0.5	50	0.01	2750	70	71.5	(Kang et al., 2017)
Mn–Ce oxide	6.0	0.1	10	0.01	180	73.5	45.5-79.5	(Deng et al., 2011)
Ce–Fe bimetal oxides	NR	0.5	10	0.05	40	90	60.97	(Tang and Zhang, 2016)
CeO_2–ZrO_2 nanocages	4.0	0.2	10	0.02	1440	70	175	(Wang et al., 2013)
Ce(IV) incorporated hydrous iron (III) oxide	7.0	0.5	10	0.05	120	85	24.8	(Mukhopadhyay et al., 2017)
Cerium loaded mesoporous zirconium phosphate	6.0	1.0	10	0.1	60	84.7	20.5	(Dash et al., 2015)
Cubical ceria nanosorbent	7.0	1.0	10	0.1	120	95	80.64	(Dhillon et al., 2016)
Mg-Al-Ce triple-metal composite	7.0	0.2	50	0.004	180	38	124.9	(Chi et al., 2017)
GO-CeO_2 nanohybrid	**6.5**	**1.0**	**10**	**0.1**	**1**	**85**	**8.61**	**This work**
	4.0					**100**	**16.07***	*see Fig. S3
Literature reported other conventional materials								
Acidic Alumina	4.4	4.5	15	0.3	90	94	8.4	(Goswami and Purkait, 2012)
Granular Activated Alumina	7.0	4.0	13.8	0.3	360	69.5	2.41	(Ghorai and Pant, 2005)
H_2SO_4 treated activated carbon	2.0	36.0-96.0	10	3.6-9.6	180-780	85	0.39-0.45	(Getachew et al., 2015)
HNO_3 treated activated carbon	7.0	4.0	5	0.8	60	88	1.65	(Ravulapalli and Kunta, 2017)
Citric acid modified activated carbon	6.5	20.0	10	2.0	240	70	1.65	(Rashid and Bezbaruah, 2020)
MnO_2 coated activated carbon	5.2	5.0	10	0.5	180	42	2.24	(Ma et al., 2009)
$KMnO_4$ coated activated carbon	2.0	NR	20	NR	180	NR	15.5	(Daifullah et al., 2007)
Alum impregnated activated alumina	6.5	8.0	20	0.4	180	99	40.65	(Tripathy et al., 2006)
La-modified activated alumina	7.0	1.25	10	0.125	120	-	6.7	(Cheng et al., 2014)
Chalk powder	5.0	0.6	2	0.3	20	90	3.65	(Gandhi and Sirisha, 2013)
Hydroxyapatite	5-7.3	4.0	NR	NR	960	96	4.7	(Jimenez-Reyes and Solache-Rios, 2010)
Quick lime	12.71	5.0	50	0.1	75	80.6	16.67	(Islam and Patel, 2007)

C.2.2. Impact of adsorbent dose (sorbent to sorbate ratio) on fluoride removal

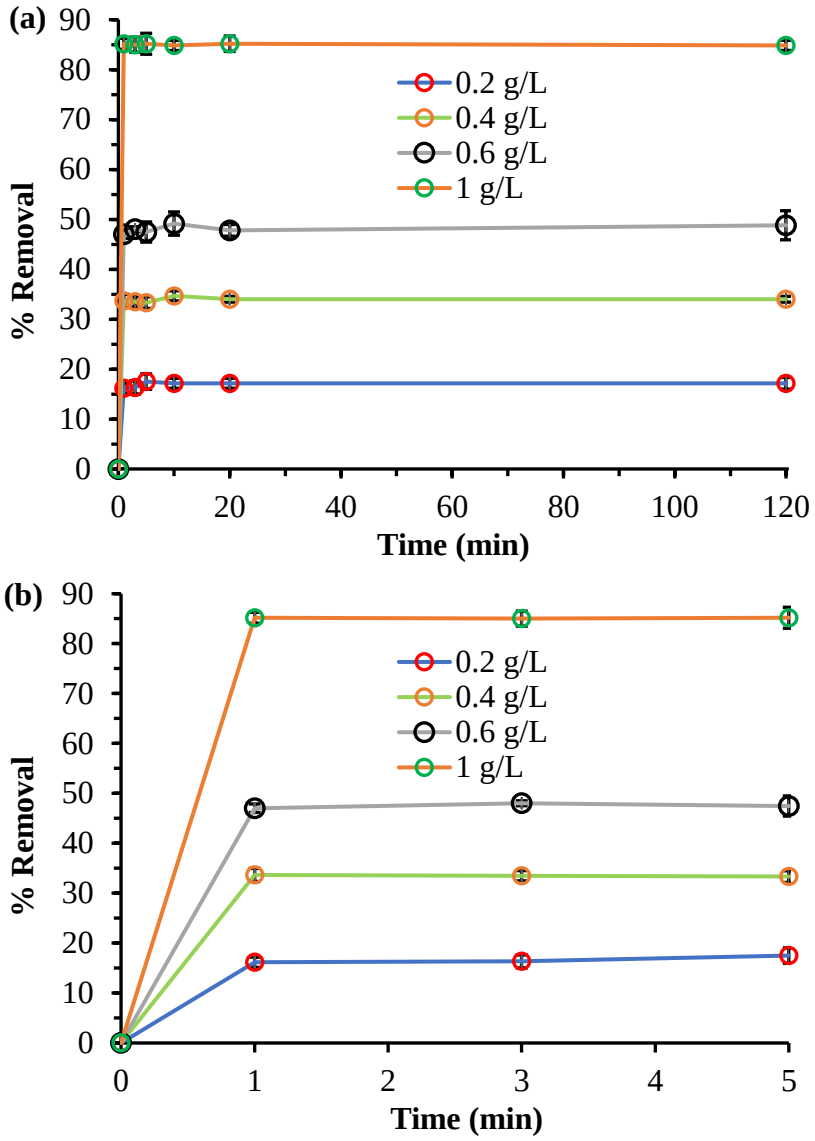

Figure C1. Removal of fluoride by GO-CeO_2 nanohybrid over time with different dosages of GO-CeO_2 nanohybrid (initial fluoride concentration = 10 mg/L). A rapid removal of fluoride was observed irrespective of the adsorbent dose (i.e., sorbent to sorbate ratio), and equilibrium was achieved within 1 minute of reaction in all cases. (a) All data points are shown (up to 120 min); (b) The plots are truncated at 5 min to zoom into the early-stage data sets. The data points are connected with straight lines for ease of reading only and they do not represent trendlines, and the vertical error bars represent ± standard deviations.

C.2.3. Intra-particle diffusion analysis

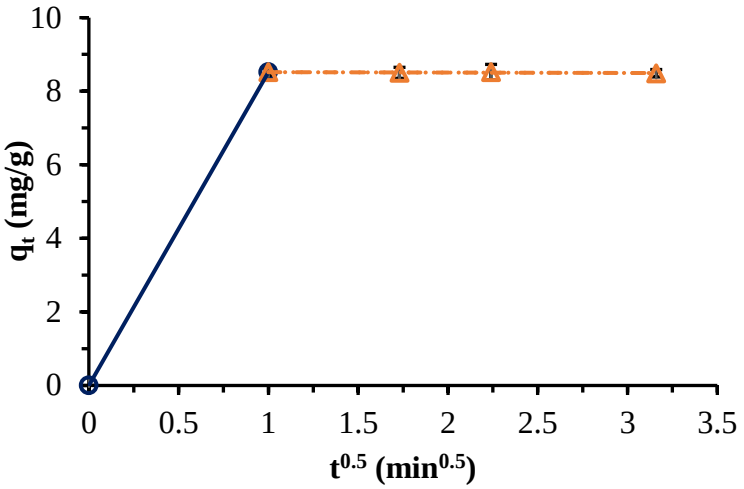

Figure C2. Plot to investigate fluoride adsorption via the intra-particle diffusion onto GO-CeO_2. Two linear sections were observed in the plots which indicate that intra-particle diffusion was not the only rate-determining step for fluoride removal by GO-CeO_2 (initial fluoride concentration = 10 mg/L, GO-CeO_2 dose = 1 g/L). The data points are connected with straight lines for ease of reading only and they do not represent trendlines, and the vertical error bars represent ± standard deviations.

C.2.4. Isotherm analyses

While the Freundlich model (Eq. C1) is applicable to heterogeneous sorption where sorption is a multi-layer phenomenon, the Langmuir isotherm (Eq. C2) assumes a homogenous surface, monolayer coverage, and each sorbate molecule to have equal sorption activation energy to be sorbed onto the adsorbent surface.

$$q_e = K_F C_e^{\frac{1}{n}} \qquad (C1)$$

$$q_e = \frac{b q_m C_e}{1 + b C_e} \qquad (C2)$$

In Eq. C1, q_e (mg/g) is the equilibrium adsorption capacity, K_F (mg/g) is the Freundlich affinity coefficient, C_e is the fluoride concentration at equilibrium and 1/n is Freundlich linearity constant. In Eq. C2, q_e (mg/g) is the equilibrium adsorption capacity, C_e (mg/L) is equilibrium concentration fluoride ions in solution, q_m (mg/g) is the maximum adsorption capacity, b is the Langmuir constant related to the affinity of the binding sites for fluoride ions. The dimensionless

constant R_L (Eq. C3) is another very important parameter associated with Langmuir isotherm to further investigate the adsorption intensity. Here, C_0 is the initial fluoride concentration. If R_L is between 0 and 1 then the adsorption process is favorable but $R_L > 1$ indicates unfavorable adsorption(Dash et al., 2015).

$$R_L = \frac{1}{1 + bC_0} \qquad (C3)$$

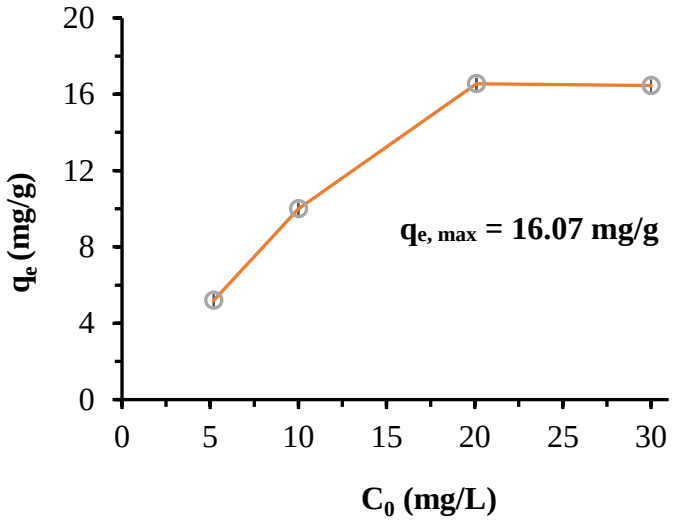

Figure C3. The Fluoride adsorption capacity of GO-CeO_2 nanohybrid at different initial concentrations (C_0) of fluoride when initial solution pH was 4 with no pH adjustment or buffering (GO-CeO_2 dose = 1 g/L). The maximum fluoride adsorption capacity was found to be 16.07 mg/g. The data points are connected with straight lines for ease of reading only and they do not represent trendlines, and the vertical error bars represent ± standard deviations.

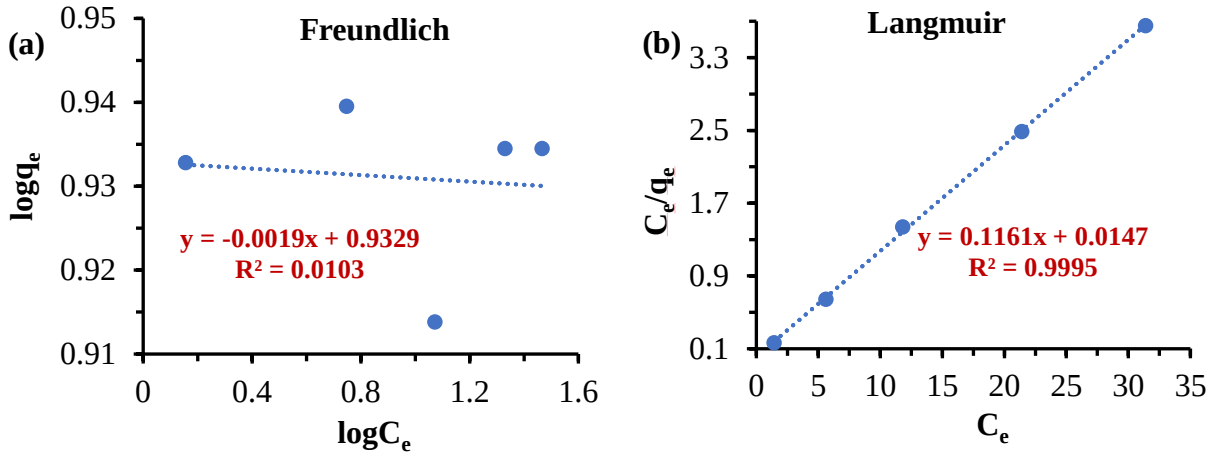

Figure C4. (a) Freundlich; and (b) Langmuir isotherms models for fluoride removal by GO-CeO_2 nanohybrid. It can be seen that the Langmuir isotherm fitted the data better than the Freundlich isotherm (based on the R^2 values). The dotted lines represent the best-fit or trend lines.

Table C2. Adsorption isotherm parameters for fluoride adsorption onto GO-CeO_2 nanohybrid.

Langmuir Isotherm				**Freundlich Isotherm**			
q_m (mg/g)	b (L/mg)	R^2	R_L	q_m (mg/g)	K_f (mg/g)	n	R^2
8.61	7.9	0.9995	0.003-0.025	8.50	8.56	-52.63	0.0103

C.2.5. Interferences by co-existing ions in fluoride removal by the various adsorbents

Table C3. Effect of the presence of environmentally relevant anions in raw water on fluoride removal efficiency (% removal) of different types of aluminum- and ceria-based materials. The first number in each cell of the table represents the % fluoride removal and the number within the parentheses represents the concentration of the specific anion used in the interference study.

Material	**Control (no interfering ions)**	**Sulphate (mg/L)**	**Bicarbonate (mg/L)**	**Phosphate- (mg PO_4^{3-}-P/L)**	**Nitrate (mg NO_3^--N /L)**	**Source**
GO-CeO_2	85	38.3 (100)	19 (100)	46 (10)	80 (100)	**This Work**
Acidic alumina	93	87 (100)	38 (100)	NR	86 (113)	(Goswami and Purkait, 2012)
Activated alumina	76	70 (100)	66 (100)	67 (16)	NR	(Tang et al., 2009)
Ce–Fe bimetal oxide	95	88 (100)	15 (100)	NR	85 (113)	(Tang and Zhang, 2016)
Cubical ceria	95	76 (50)	83 (50)	79 (13)	86 (11)	(Dhillon et al., 2016)
Hydrous CeO_2-Fe_3O_4 decorated polyaniline fibers	85	80 (40)	55 (40)	35 (13)	85 (9)	(Chigondo et al., 2018)

NR = Not reported

C.2.6. Role of CeO_2 in the fluoride removal process

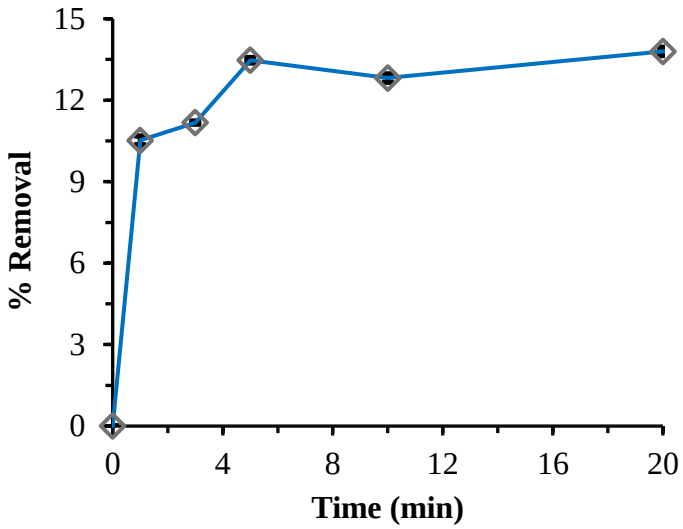

Figure C5. Fluoride removal by only CeO_2 NPs (no GO). Fluoride removal was rapid in the first 1 min, then slowed down and reached equilibrium within 5 min. There was no data point between 0 and 1 min due to experimental limitations. The data points are connected with straight lines for ease of reading only and they do not represent trendlines, and the vertical error bars represent ± standard deviations. C_0 = 10 mg F^- /L and CeO_2 NPs dose = 1 g/L.

C.2.7. Dispersion studies

We conducted two separate dispersion experiments with sonication and surface modification of the CeO_2 NPs to reduce agglomeration and increase their available reactive surface area for fluoride removal. In the sonication method, we used two different approaches: (1) Approach 1: CeO_2 NPs (1 g/L) and fluoride solution (10 mg/L) were first put together in reactors and then sonicated for 45 min, and (2) Approach 2: CeO_2 NPs were put in water first and sonicated for 45 min, and then fluoride solution was added to get an initial fluoride concentration of 10 mg/L. The reactors were shaken end-over-end for 2 h, CeO_2 NPs were filtered out from bulk solution using a 0.2 µm syringe filter, and bulk solution fluoride concentration was measured. Controls were run without any sonication. No significant improvement in fluoride removal was observed between the controls and the sonicated treatments (Fig. C6a).

We also used Tween 20 (standard neutral non-toxic surfactant) to improve the dispersion (reduce agglomeration) of CeO_2 NPs. We observed an improvement in the fluoride removal efficiency up to 25% depending on Tween 20 concentration (Fig. C6b). Reduced agglomeration (increased surface area) had an effect on enhancing the removal performance but did not match the removal performance of our graphene oxide ceria nanohybrid (85%).

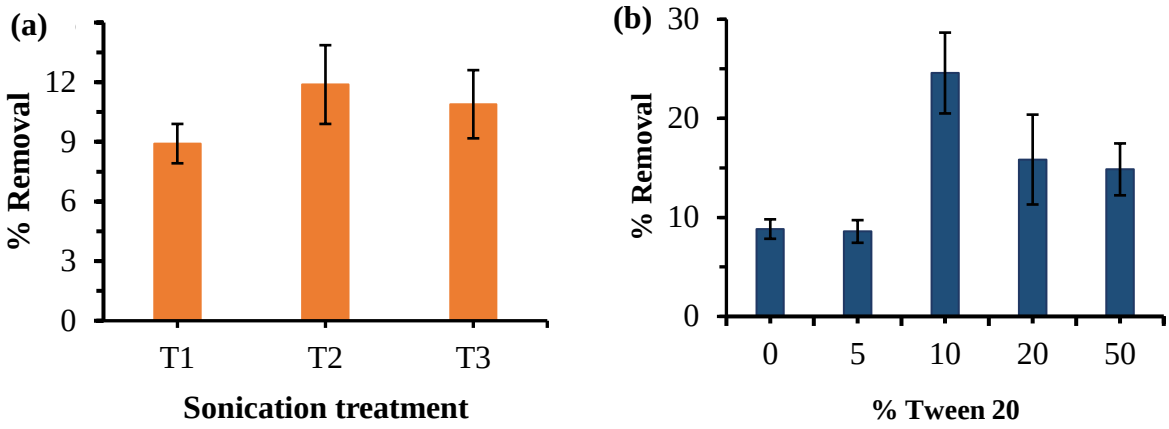

Figure C6. (a) Effects of sonication on fluoride removal by CeO_2 NPs, T1: control with means no sonication, T2: CeO_2 NPs and fluoride solution (10 mg/L) were first put together and then sonicated for 45 min, T3: First sonicated CeO_2 NPs in DI water for 45 minutes and then fluoride solution was added to get an initial fluoride concentration of 10 mg/L; (b) Fluoride removal by Tween 20 modified CeO_2 NPs, we used variable amount of Tween 20 (5-50%) to improve the dispersion and evaluated the fluoride removal efficiency. C_0 = 10 mg F^-/L and GO-CeO_2 dose = 1 g/L.

C.2.8. Environmental significance material requirements for a Point-of-Use (POU) treatment unit

The amounts of GO-CeO_2 (nanohybrid), acidic alumina (AA), and granular activated alumina (GAA) needed to treat drinking and cooking water for a typical household were calculated. The following assumptions were made.

(1) Influent (raw water) fluoride concentration = 5 mg/L (typical in many places)

(2) Target fluoride limit in treated water = 1.5 mg/L (as per WHO guidelines)

(3) Drinking and cooking water requirement for a 4-member family = 30 L/d

The following experimental data were used:

(4) Adsorption capacity of GO-CeO_2 = 8.61 mg/g (at pH 6.5) (from this study)

(5) Adsorption capacity of GO-CeO_2 = 16.07 mg/g (at pH 4.4) (from this study)

(6) Adsorption capacity of AA = 8.4 mg/g (at pH 4.4) (after Goswami and Purkait, 2012[16])

(7) Adsorption capacity of GAA = 2.41 mg/g (at pH 7) (after Ghorai and Pant, 2005[19])

The amount of materials needed for a single unit was calculated as per Eq. C4 and presented in Table C4.

$$Material\ \left(\frac{g}{year}\right) = \frac{(Initial\ F - Target\ F) \times \frac{water\ requirment}{d} \times 365\,\frac{d}{year}}{adsorption\ capacity} \qquad (C4)$$

For example, in the case of GO-CeO_2

$$\mathrm{GO-CeO_2}\ \left(\frac{\mathrm{g}}{\mathrm{year}}\right) = \frac{(\mathrm{Initial\ F - Target\ F}) \times \frac{\mathrm{water\ requirement}}{\mathrm{d}} \times 365\ \mathrm{d/year}}{\mathrm{adsorption\ capacity}}$$

$$= \frac{(5 - 1.5)\,\frac{\mathrm{mg}}{\mathrm{L}} \times 30\,\frac{\mathrm{L}}{\mathrm{d}} \times 365\ \mathrm{d/year}}{8.61\ \mathrm{mg/g}}$$

= 4452 g/year (= 4.452 kg/year)

Table C4. Amount of adsorbents needed for a Point-of-Use (POU) treatment system to supply treated water for drinking and cooking (30 L/d for a 4-member family).

Fluoride in raw water (mg/L)	Fluoride in treated water (mg/L)	Drinking/ cooking water demand per family (L/d)	Adsorbent used	Adsorption capacity (mg/g)	Material needed/family/year (g)
5	1.5	30	$GO\text{-}CeO_2$	8.61 (pH 6.5)	4452
				16.07 (pH 4)	2385
			AA*(Goswami and Purkait, 2012)	8.4 (pH 4.4)	4563
			GAA**(Ghorai and Pant, 2005)	2.41 (pH 7)	15903

*AA = acidic alumina; **GAA = Granular activated alumina.

C.3. References

Cheng, J., Meng, X., Jing, C., Hao, J., 2014. La3+-modified activated alumina for fluoride removal from water. Journal of Hazardous Materials 278, 343-349.

Chi, Y., Chen, Y., Hu, C., Wang, Y., Liu, C., 2017. Preparation of Mg-Al-Ce triple-metal composites for fluoride removal from aqueous solutions. Journal of Molecular Liquids 242, 416-422.

Chigondo, M., Paumo, H.K., Bhaumik, M., Pillay, K., Maity, A., 2018. Hydrous CeO2-Fe3O4 decorated polyaniline fibers nanocomposite for effective defluoridation of drinking water. Journal of Colloid and Interface Science 532, 500-516.

Daifullah, A.A.M., Yakout, S.M., Elreefy, S.A., 2007. Adsorption of fluoride in aqueous solutions using KMnO4-modified activated carbon derived from steam pyrolysis of rice straw. Journal of Hazardous Materials 147, 633-643.

Dash, S.S., Sahu, M.K., Sahu, E., Patel, R.K., 2015. Fluoride removal from aqueous solutions using cerium loaded mesoporous zirconium phosphate. New Journal of Chemistry 39, 7300-7308.

Deng, S.B., Liu, H., Zhou, W., Huang, J., Yu, G., 2011. Mn-Ce oxide as a high-capacity adsorbent for fluoride removal from water. Journal of Hazardous Materials 186, 1360-1366.

Dhillon, A., Sharma, T.K., Soni, S.K., Kumar, D., 2016. Fluoride adsorption on a cubical ceria nanoadsorbent: function of surface properties. Rsc Advances 6, 89198-89209.

Gandhi, N., Sirisha, D., 2013. Adsorption Of Fluoride From Aqueous Solution By Using Chalk Powder.

Getachew, T., Hussen, A., Rao, V.M., 2015. Defluoridation of water by activated carbon prepared from banana (Musa paradisiaca) peel and coffee (Coffea arabica) husk. International Journal of Environmental Science and Technology 12, 1857-1866.

Ghorai, S., Pant, K.K., 2005. Equilibrium, kinetics and breakthrough studies for adsorption of fluoride on activated alumina. Separation and Purification Technology 42, 265-271.

Goswami, A., Purkait, M.K., 2012. The defluoridation of water by acidic alumina. Chemical Engineering Research & Design 90, 2316-2324.

Islam, M., Patel, R.K., 2007. Evaluation of removal efficiency of fluoride from aqueous solution using quick lime. Journal of Hazardous Materials 143, 303-310.

Jimenez-Reyes, M., Solache-Rios, M., 2010. Sorption behavior of fluoride ions from aqueous solutions by hydroxyapatite. Journal of Hazardous Materials 180, 297-302.

Kang, D., Yu, X., Ge, M., 2017. Morphology-dependent properties and adsorption performance of CeO2 for fluoride removal. Chemical Engineering Journal 330, 36-43.

Ma, Y., Wang, S.-G., Fan, M., Gong, W.-X., Gao, B.-Y., 2009. Characteristics and defluoridation performance of granular activated carbons coated with manganese oxides. Journal of Hazardous Materials 168, 1140-1146.

Mukhopadhyay, K., Ghosh, A., Das, S.K., Show, B., Sasikumar, P., Ghosh, U.C., 2017. Synthesis and characterisation of cerium(IV)-incorporated hydrous iron(III) oxide as an adsorbent for fluoride removal from water. Rsc Advances 7, 26037-26051.

Rashid, U.S., Bezbaruah, A.N., 2020. Citric acid modified granular activated carbon for enhanced defluoridation. Chemosphere 252.

Ravulapalli, S., Kunta, R., 2017. Defluoridation studies using active carbon derived from the barks of Ficus racemosa plant. Journal of Fluorine Chemistry 193, 58-66.

Sakthivel, T.S., Das, S., Pratt, C.J., Seal, S., 2017. One-pot synthesis of a ceria-graphene oxide composite for the efficient removal of arsenic species. Nanoscale 9, 3367-3374.

Tang, D., Zhang, G., 2016. Efficient removal of fluoride by hierarchical Ce-Fe bimetal oxides adsorbent: Thermodynamics, kinetics and mechanism. Chemical Engineering Journal 283, 721-729.

Tang, Y.L., Guan, X.H., Su, T.Z., Gao, N.Y., Wang, J.M., 2009. Fluoride adsorption onto activated alumina: Modeling the effects of pH and some competing ions. Colloids and Surfaces a-Physicochemical and Engineering Aspects 337, 33-38.

Tripathy, S.S., Bersillon, J.-L., Gopal, K., 2006. Removal of fluoride from drinking water by adsorption onto alum-impregnated activated alumina. Separation and Purification Technology 50, 310-317.

Wang, J., Xu, W.H., Chen, L., Jia, Y., Wang, L., Huang, X.J., Liu, J.H., 2013. Excellent fluoride removal performance by CeO2-ZrO2 nanocages in water environment. Chemical Engineering Journal 231, 198-205.